UNIVERSIDAD CATÓLICA DEL NORTE

FACULTY OF SCIENCE

Physics Department

STUDYING THE VACUUM STABILITY OF A POTENTIAL WITH TWO REAL SCALAR FIELDS

Thesis submitted in fulfillment of the requirements for the degree of Magíster en Ciencias con Mención en Física,
from Universidad Católica del Norte

MATÍAS TOLEDO CALDERÓN

Advisor: PhD. Roberto Lineros (UCN).

Comittee: PhD. Alfonso Zerwekh (USM), PhD. Cesar Bonilla (UCN), PhD. Juan Rojas (UCN)

Antofagasta, Chile.
March, 2025

This thesis is dedicated to my entire family, both in Osorno and Antofagasta, for their unwavering love and support. To my friends, who have always stood by my side. And to God, for giving me the strength to get here.

Acknowledgements

Thanks to the computers in room 300 of the Physics Department at UCN, the DNA 10 server, and, above all, to PhD. Roberto Lineros, whose invaluable guidance and support have been fundamental throughout this journey. I am also deeply grateful to the other professors who taught me during my master's program. Their advice, though sometimes tough to hear, has pushed me into a constant process of awakening, reevaluating, and reinventing myself. Lastly, to my friends from Physics at UCN, who have always provided me with practical advice.

Content

List of Figures

Index tables

Resumen

Esta tesis es un intento de estudiar las condiciones de estabilidad del vacío a través de la inspección de las restricciones de acotado por abajo de un potencial escalar con dos campos escalares reales (ϕ_1, ϕ_2), identificando posteriormente las regiones que garantizan la estabilidad del vacío y caracterizándolas mediante un ajuste de curvas con una precisión excepcional. Todo esto tiene como objetivo mejorar la precisión del espacio de parámetros y explorar nuevas configuraciones del potencial. En particular, nos interesan las constantes de acoplamiento del potencial que acompañan a las interacciones $\phi_1^3\phi_2$ y $\phi_1\phi_2^3$, ya que comprenderlas nos permitiría refinar un espacio de parámetros bien definido.

Para estudiar dichas condiciones, inicialmente se utilizó la técnica de copositividad junto con la herramienta de escalamiento diagonal; sin embargo, estos enfoques presentan ciertas limitaciones, dado que las constantes de acoplamiento mencionadas no pueden incluirse en la estructura que surge de la técnica de copositividad. Por esta razón, se procede a parametrizar los campos escalares en coordenadas polares. Esta transformación tiene la ventaja de permitir que el potencial escalar se normalice mediante la componente radial de polares. Como resultado, el comportamiento de los parámetros se estudia dentro de un círculo unitario que surge después de normalizar por r^4. Este procedimiento no solo reduce la cantidad de parámetros libres y facilita la búsqueda de las condiciones de acotado por abajo que estabilizan el vacío, sino que también simplifica la implementación del código para el escaneo del modelo de dos campos escalares reales.

Finalmente, basándonos en los resultados del ajuste de curvas, se observa que este define con gran precisión la interfaz de las regiones acotadas y no acotadas por abajo. Además, el mecanismo desarrollado se utiliza para realizar una comparación con exactamente el mismo potencial escalar, pero reformulado desde la base introducida en "*Vacuum Stability of a General Scalar Potential of a Few Fields*" [1] a la desarrol-

lada en este trabajo. Los resultados son intrigantes, ya que se mostrará que, dadas las mismas configuraciones de parámetros, los resultados pueden ser parcialmente inconmensurables entre sí.

Studying the vacuum stability of a potential with two real scalar fields

Matías Toledo Calderón

Abstract

This thesis is an attempt to study the vacuum stability conditions through the inspection of the boundedness from below constraints of a scalar potential with two real scalar fields (ϕ_1, ϕ_2), then identifying the regions that ensure vacuum stability and characterizing them through a curve-fitting approach with outstanding precision. All of this is aimed at improving the accuracy of the parameter space and exploring new configurations of the potential. In particular, we are interested in the potential's coupling constants accompanying the interactions $\phi_1^3\phi_2$ and $\phi_1\phi_2^3$, as understanding them would allow us to refine a well-defined parameter space.

For studying such conditions. Initially, I use the copositivity technique alongside the diagonal scaling tool; however, these approaches have certain limitations since the mentioned coupling constants cannot be included in the arrangement which emerges from the copositivity. For this reason, we proceed to parametrize the scalar fields into polar coordinates. This transformation has the advantage of allowing the scalar potential to be normalized by the radial component of the polar coordinates. As a result, the behavior of the parameters is studied within a unitary circle which arises after normalizing for r^4. This procedure not only reduces the number of free parameters along with facilitating the search for the Bounded from Below conditions that stabilize the vacuum, but also simplifies the implementation of the code for scanning the model of two real scalar fields.

Finally, based on the curve fitting results, we note that this fit effectively defines the bounded and unbounded from below regions with significant precision. In addition, the developed mechanism is utilized to perform a comparison with exactly the same scalar potential, but reformulated from the basis introduced in "*Vacuum Stability of a General Scalar Potential of a Few Fields*" [1] to the one developed in this work. The results are intriguing, as it will be shown that given the same parameter configurations, the outcomes can be partially incommensurable with one another.

Introduction

A Lagrangian is a quantity that describes the kinematics of a system through energy considerations, and is defined as the kinetic energy minus the potential energy. In particle physics, it is a fundamental pillar since it is an invariant object under the symmetries of the Standard Model of Particle Physics (SM), which are $SU(3)_C \times SU(2)_L \times U(1)_Y$ and Lorentz symmetry [2, 3, 4]. On the other hand, in the Standard Model, vacuum stability is ensured by the presence of a single scalar field, which generates masses at tree level—namely, the Higgs field. A crucial aspect is that the global minimum of the Higgs potential corresponds to approximately 246 GeV, with no additional minima emerging at different energy scales. Moreover, the coupling of this field must remain positive to prevent the formation of metastable vacua [5, 6]. However, when theories beyond the Standard Model (BSM) are developed, it may become necessary to introduce additional fields that can belong to various categories, such as scalar or vector fields, among others. Furthermore, their interactions are described by quartic algebraic structures.

In a renormalizable theory, those quartic order structures are composed of interactions and couplings [7]. The interactions define how particles influence each other, while the couplings determine the strength of these interactions. The sum of all these terms, which have dimension GeV^4, are known as the Scalar Potential, and it must be physically constrained. Sometimes, this algebraic expression can take convoluted forms, making it difficult to find the vacuum stability conditions of a given model in a clear and straightforward manner. This last statement is of relevant importance to keep the physics well-behaved. For instance, let us think in the mechanism of quantum tunneling. The vacuum could transition from a meta-stable minimum to a lower-energy state, which represents the true minimum. Such a transition could result in the annihilation of particles and the collapse of their interactions, destabilizing the system. Similarly, if a particle has a potential energy that is unbounded from below, diverging to negative infinity, the corresponding wave function would

become non-normalizable. This would violate the conservation of the norm in Quantum Mechanics (QM) [8]. Likewise, in the context of Classical Mechanics, small perturbations applied to a potential should not induce destabilization that drives the system to another minimum. This must be avoided as long as the minima (or vacuum states) of the potential are well-defined. A way to get rid of all these issues and ensure vacuum stability is by taking advantage of a mathematical tool: the so-called Copositivity Criteria.

This well-known approach will allow us to write the scalar potential in a more compact form, facilitating the task of imposing strong conditions over the parameters, which can be found directly in the structure named: The Matrix of Couplings. This arrangement represents the scalar potential since it can be rewritten as the multiplication of the transpose vector of the fields, the matrix of the couplings, and again the field vector: $V_4 = \lambda_{ab}\psi_a^2\psi_b^2$. This is called the bi-quadratic form [9], where $\psi_{a,b}$ are the field vectors, and $\lambda_{a,b}$ is the coupling matrix.
The only issue with this tool is that the entire potential cannot always be reduced to a coupling matrix multiplied by the fields, as it is quite common that the interaction terms with the form: $\phi_1^3\phi_2$ and $\phi_1\phi_2^3$ present difficulties in being incorporated into this framework. Precisely for this reason, we decided to explore the alternative of parametrizing the system in polar coordinates, taking advantage of the natural correspondence with the two degrees of freedom represented by the two scalar fields, ϕ_1 and ϕ_2.

The major goal to achieve in this work is to find the necessary and sufficient conditions (NAS) over the couplings, ensuring that the resulting potential is fully constrained. This implies that the two real scalar fields potential model will respect both Quantum Mechanics and Perturbation Theory, guaranteeing that the potential remains stable.
To be clear, in this thesis, I am not focusing on the study of the vacuum expectation value (*vev*) of the theory, but rather on the conditions that safeguard the scalar potential is bounded from below (BFB).

The study of the vacuum stability may be regarded as something trivial, but is more than that. Consider, for instance, the Higgs-like particle, the scalar of 125 GeV [10, 11, 12]. Its discovery was a milestone in theoretical physics, and with it, some relevant questions have arisen. For example, being able to determine where new physics might be found—whether near the TeV scale or below it [13]. If these issues

are taken seriously, the answer could depend on how strongly these fields interact with the Standard Model fields [14]. Understanding these interactions is essential, as it would allow us to establish the magnitude of the couplings and, consequently, study the vacuum and its stability in detail. Therefore, ensuring that a potential is bounded from below (BFB) is also related to the ability of new physics models to preserve the already established vacuum equilibrium.

There are some extensions, such as those that introduce complex or real triplets of $SU(2)$ [15]. In these cases, the emergence of Higgs-like states [16] is unavoidable due to a small mixing between the neutral components of the triplets and doublets.
In scenarios like this, it is crucial to control variables such as the stability of the scalar potential, a well-defined electroweak vacuum, and the experimental exclusions corresponding to each model [17].— There are also generalizations for vacuum stability in theories where the fields are invariant under $SU(n)$, establishing necessary but not sufficient conditions in both fundamental and adjoint representations [18].

However, it is known that the Higgs coupling is positive. Nevertheless, in BSM theories involving multiple scalar fields, analyzing the behavior of the potential in the limit of large field values across all possible directions becomes essential. This is addressed in "*Vacuum Stability of a General Scalar Potential of a Few Fields*" [1], where, through the so-called *orbit space* parametrization [19], the copositivity criterion for homogeneous polynomials can be applied. This allows the characterization of the positiveness for quartic interactions in the scalar potential.

Chapter 1

Importance of the Boundedness from Below

In Quantum Field Theory, the lowest energy state, also called the vacuum, serves as the foundation for the stability of particles and their interactions. If the scalar potential is not bounded from below, then the vacuum may become unstable and eventually collapse, taking with it the particles and interactions defined within that framework [7, 20].

1.1 Scalar Field paradigm

For example. Start considering a free complex scalar field. Which can be expressed in terms of the particle creation and annihilation operators [7]:

$$\phi(x) = \int \frac{d^3p}{(2\pi)^3} \frac{1}{\sqrt{2\omega_p}} \left(a_p e^{-ipx} + b_p^\dagger e^{ipx}\right), \tag{1.1}$$

$$\phi^\star(x) = \int \frac{d^3p}{(2\pi)^3} \frac{1}{\sqrt{2\omega_p}} \left(a_p^\dagger e^{ipx} + b_p e^{-ipx}\right). \tag{1.2}$$

The goal is to encounter an expression positive definite for the total energy of such a field, thus we must spatially integrate over the energy density ε, as follows:

$$E = \int d^3x \varepsilon. \tag{1.3}$$

But the energy density ε is just the component 00 of the energy-momentum tensor. That is because this tensor describes the density and flux of energy along with momentum within the space-time manifold [20]. In its canonical form, it corresponds to:

$$T^{\mu\nu} = \pi_a^\mu \partial^\nu \phi^a - g^{\mu\nu}\mathcal{L}, \tag{1.4}$$

where π_a^μ is the functional derivative, that is just:

$$\pi_a^\mu = \frac{\partial \mathcal{L}}{\partial(\partial_\mu \phi_a)} = \pm \partial^\mu \phi_a, \tag{1.5}$$

and $g^{\mu\nu}$ is the metric tensor [21]:

$$g^{\mu\nu} = \begin{pmatrix} +1 & 0 & 0 & 0 \\ 0 & -1 & 0 & 0 \\ 0 & 0 & -1 & 0 \\ 0 & 0 & 0 & -1 \end{pmatrix}. \tag{1.6}$$

With this in mind, let us proceed to compute the energy-momentum tensor to determine its 00-component. In our case, involving a scalar field, we begin by considering the Lagrangian of the complex scalar field:

$$\mathcal{L} = \partial_\mu \phi^* \partial^\mu \phi - m^2 \phi^* \phi. \tag{1.7}$$

For instance, for this Lagrangian, the energy-momentum object is:

$$T^{\mu\nu} = \frac{\partial \mathcal{L}}{\partial(\partial_\mu \phi)} \partial^\nu \phi + \frac{\partial \mathcal{L}}{\partial(\partial_\mu \phi^*)} \partial^\nu \phi^* - g^{\mu\nu}\mathcal{L}. \tag{1.8}$$

For further details of calculation steps visit the appendix 5. Once we solve the equations, we obtain:

$$T^{\mu\nu} = \partial^\mu \phi^* \partial^\nu \phi + \partial^\mu \phi \partial^\nu \phi^* - g^{\mu\nu}(g^{\alpha\beta}\partial_\alpha \phi^* \partial_\beta \phi - m^2 \phi^* \phi). \tag{1.9}$$

Taking the above reduced product and substituting it back into the expression of the tensor:

$$T^{\mu\nu} = \partial^\mu \phi^* \partial^\nu \phi + \partial^\mu \phi \partial^\nu \phi^* - (\partial_0 \phi^* \partial_0 \phi - \vec{\nabla}\phi^* \cdot \vec{\nabla}\phi) + g^{\mu\nu} m^2 \phi^* \phi. \tag{1.10}$$

As we know, the energy element is analogous to the T^{00} component. Therefore:

$$T^{00} = \partial^0\phi^*\partial^0\phi + \cancel{\partial^0\phi\partial^0\phi^*} - \cancel{\partial^0\phi\partial^0\phi^*} + \vec{\nabla}\phi^* \cdot \vec{\nabla}\phi + m^2\phi^*\phi, \tag{1.11}$$

$$T^{00} = \partial^0\phi^*\partial^0\phi + \vec{\nabla}\phi^* \cdot \vec{\nabla}\phi + m^2\phi^*\phi. \tag{1.12}$$

With this T^{00} component of the energy-momentum tensor, we will decompose it into three parts, each of which will be solved separately. Finally, the three results will be combined to obtain the Hamiltonian or, equivalently, the energy.
Let us start with the expression of the energy related to the kinetic term (for the full derivation, check appendix 2 in 5) $\partial_0\phi^*\partial_0\phi$:

$$E_{\partial_0\phi\partial^0\phi} = \int\int \frac{d^3p}{(2\pi)^3}\frac{d^3q}{(2\pi)^3}\frac{\omega_p\omega_q}{\sqrt{4\omega_p\omega_q}}(a_p^\dagger a_q\delta_{(p-q)}(2\pi)^3 - \cancel{\delta_{(p+q)}}a_p^\dagger b_q^\dagger(2\pi)^3 - b_p a_q\cancel{\delta_{(p+q)}}(2\pi)^3 + b_p b_q^\dagger\delta_{(q-p)}(2\pi)^3), \tag{1.13}$$

$$E_{\partial_0\phi\partial^0\phi} = \int\int \frac{d^3p}{(2\pi)^3}\frac{d^3q}{\cancel{(2\pi)^3}}\frac{\omega_p\omega_q}{\sqrt{4\omega_p\omega_q}}\cancel{(2\pi)^3}(a_p^\dagger a_q\delta_{(p-q)} + b_p b_q^\dagger\delta_{(q-p)}). \tag{1.14}$$

Factoring the expression, we reserve this result for subsequent use:

$$E_{\partial_0\phi\partial^0\phi} = \int\int \frac{d^3pd^3q}{(2\pi)^3}\frac{\omega_p\omega_q}{\sqrt{4\omega_p\omega_q}}(a_p^\dagger a_q + b_p b_q^\dagger)\delta_{(p-q)}. \tag{1.15}$$

On the other side, we have the energy term belonging to the nablas (check the calculations in 5) which is given by:

$$E_{\vec{\nabla}\phi^\star\vec{\nabla}\phi} = \int\int \frac{d^3p}{(2\pi)^3}\frac{d^3q}{\cancel{(2\pi)^3}}\frac{p_\mu q_\nu\cancel{(2\pi)^3}}{\sqrt{4\omega_p\omega_q}}(a_p^\dagger a_q\delta_{(p-q)} - 0 - 0 + b_p b_q^\dagger\delta_{(q-p)}), \tag{1.16}$$

$$E_{\vec{\nabla}\phi^\star\vec{\nabla}\phi} = \int\int \frac{d^3pd^3q}{(2\pi)^3}\frac{p_\mu p_\nu}{\sqrt{4\omega_p\omega_q}}(a_p^\dagger a_q + b_p b_q^\dagger)\delta_{(p-q)}. \tag{1.17}$$

Finally, we find the last energy term:

$$E_{m^2\phi^*\phi} = m^2\int\int \frac{d^3pd^3q}{(2\pi)^3\cancel{(2\pi)^3}\sqrt{4\omega_p\omega_q}}(a_p^\dagger a_q\delta_{(p-q)} + a_p^\dagger b_q\delta_{(p+q)} + b_p a_q\delta_{(p+q)} +$$

$$+ b_p b_q^\dagger \delta_{(p-q)})\cancel{(2\pi)^3},$$
$$E_{m^2\phi^*\phi} = m^2 \int\int \frac{d^3p d^3q}{(2\pi)^3\sqrt{4\omega_p\omega_q}}(a_p^\dagger a_q \delta_{(p-q)} + 0 + 0 + b_p b_q^\dagger \delta_{(p-q)}). \tag{1.18}$$

The final step is simply to gather all the energy contributions:

$$E = \int \varepsilon d^3x,$$
$$E = E_{\partial_0\phi\partial^0\phi} + E_{\vec{\nabla}\phi^\star\vec{\nabla}\phi} + E_{m^2\phi^*\phi}, \tag{1.19}$$

$$E = \int\int \frac{d^3p d^3q}{(2\pi)^3}\frac{\omega_p\omega_q}{\sqrt{4\omega_p\omega_q}}(a_p^\dagger a_q + b_p b_q^\dagger)\delta_{(p-q)} + \int\int \frac{d^3p d^3q}{(2\pi)^3}\frac{p_\mu p_\nu}{\sqrt{4\omega_p\omega_q}}(a_p^\dagger a_q +$$
$$+ b_p b_q^\dagger)\delta_{(p-q)} + +m^2 \int\int \frac{d^3p d^3q}{(2\pi)^3\sqrt{4\omega_p\omega_q}}(a_p^\dagger a_q + b_p b_q^\dagger)\delta_{(p-q)}. \tag{1.20}$$

Now if $p = q$, the integral can be further simplified, as the delta functions, omegas, and momenta can be rearranged into the following expression:

$$E = \int \frac{d^3p}{(2\pi)^3 2\omega_p}(a_p^\dagger a_p + b_p b_p^\dagger)(\omega_p^2 + \vec{p}^2 + m^2) \tag{1.21}$$

We can take advantage of the frequency-energy relation $\omega_p = \sqrt{\vec{p}^2 + m^2}$, then:

$$E = \int \frac{d^3p}{(2\pi)^3 2\omega_p}(a_p^\dagger a_p + b_p b_p^\dagger)(\omega_p^2 + \omega_p^2) \tag{1.22}$$
$$E = \int \frac{d^3p}{(2\pi)^3}(a_p^\dagger a_p + b_p b_p^\dagger)\omega_p \tag{1.23}$$

The ladder operator $a_p^\dagger$ creates particles, while $b_p^\dagger$ operator, creates antiparticles. For a scalar field, whose quanta are bosons with integer spin, we observe that the commutation relation is given by:

$$[b_p, b_q^\dagger] = (2\pi)^3\delta^3(p-q). \tag{1.24}$$

Therefore:

$$b_q b_p^\dagger = b_p^\dagger b_q + (2\pi)^3\delta^3(p-q), \tag{1.25}$$

specifically in this scenario we have $p = q$, so replacing back in the energy expression, we get:

$$E = \int \frac{\omega_p d^3p}{(2\pi)^3}(a_p^\dagger a_p + b_p^\dagger b_p + (2\pi)^3\delta^3(0)), \tag{1.26}$$

$$E = \int \frac{\omega_p d^3p}{(2\pi)^3}(a_p^\dagger a_p + b_p^\dagger b_p) + \int \frac{\omega_p d^3p}{(2\pi)^3}(2\pi)^3\delta^3(0). \tag{1.27}$$

In a volume V, $\delta_{(0)}$ can be adjusted as $\frac{V}{(2\pi)^3}$:

$$E = \int \frac{\omega_p d^3p}{(2\pi)^3}(a_p^\dagger a_p + b_p^\dagger b_p) + \int \frac{\omega_p d^3p}{(2\pi)^3}\cancel{(2\pi)^3}\frac{V}{\cancel{(2\pi)^3}}, \tag{1.28}$$

where the integral $\int \frac{\omega_p d^3p}{(2\pi)^3}$ is defined as ε_0. Thus, the energy takes the following form:

$$E = \int \frac{\omega_p d^3p}{(2\pi)^3}(a_p^\dagger a_p + b_p^\dagger b_p) + V\varepsilon_0. \tag{1.29}$$

The term $V\varepsilon_0$ is known as the zero-point energy [20, 7]. It represents an infinite contribution for a sufficiently large volume, considering the number of particles and antiparticles in Hilbert space. It is worth mentioning that the energy does not acquire negative values, even if there are variations in the number of particles and antiparticles. Specifically:

$$\Delta E = E_j - E_i = \int \frac{\omega_p d^3p}{(2\pi)^3}\left[(a_{p,j}^\dagger a_{p,j} + b_{p,j}^\dagger b_{p,j}) - (a_{p,i}^\dagger a_{p,i} + b_{p,i}^\dagger b_{p,i})\right], \tag{1.30}$$

$$\Delta E = \int \frac{\omega_p d^3p}{(2\pi)^3}\left[\Delta\#\text{particles} + \Delta\#\text{antiparticles}\right], \tag{1.31}$$

indicating that the lowest energy state is non-zero. In addition, the vacuum is stabilized and well-defined as it remains independent of what happens to the particles. If the anticommutation relations had been used instead of the commutation ones, the result would have been entirely non-physical and unstable:

$$\Delta E = \int \frac{\omega_p d^3p}{(2\pi)^3}[\Delta\#\text{particles} - \Delta\#\text{antiparticles}]. \tag{1.32}$$

Look closely at this result; it indicates that the energy can lead to a negative variation; moreover, it implies that the energy can be reduced by increasing the number

of antiparticles. This situation could trigger spontaneous decays of particles into particle-antiparticle pairs, placing the scalar field in a state of unstable equilibrium [7].

A similar development could have been performed for the fermion scenario. Leading to:

$$E = \sum_s \left[\int \frac{d^3q}{(2\pi)^3} \omega_p \left(a_p^{s\dagger} a_p^s + b_p^{s\dagger} b_p^s \right) - V\varepsilon_0 \right], \tag{1.33}$$

here the zero-point energy is negative. Finally, the general lesson in this example is that the energy has to increase independently if we add particles or antiparticles and it is bounded from below, since its minimum belongs to the zero point energy.

1.2 Normalization condition

Here, is presented another case that highlights the importance of why a potential must be bounded from below.
The equation that governs a non-relativistic quantum-mechanical system is known as the Schrödinger equation. For example, considering the case of the following Quantum Hamiltonian:

$$H = -\frac{\hbar^2}{2m}\nabla^2 + V(\mathbf{r}, t). \tag{1.34}$$

Where $\hbar$ is the Planck constant, m the mass of the particle, and $V(\mathbf{r}, t)$ the potential energy. Then plugging it into the time-dependent equation, it becomes:

$$i\hbar\frac{\partial\Psi(\mathbf{r}, t)}{\partial t} = \left[-\frac{\hbar^2}{2m}\nabla^2 + V(\mathbf{r}, t) \right] \Psi(\mathbf{r}, t). \tag{1.35}$$

If $V(\mathbf{r}, t) \to -\infty$, then the time evolution equation is slightly modified to:

$$i\hbar\frac{\partial\Psi(\mathbf{r}, t)}{\partial t} \sim V(\mathbf{r}, t)\Psi(\mathbf{r}, t), \tag{1.36}$$

$$\frac{i\hbar}{\Psi(\mathbf{r}, t)}\frac{\partial\Psi(\mathbf{r}, t)}{\partial t} = V(\mathbf{r}, t), \tag{1.37}$$

$$i\hbar\frac{\partial}{\partial t}\ln(\Psi(\mathbf{r}, t)) = V(\mathbf{r}, t), \tag{1.38}$$

$$i\hbar \int d(\ln(\Psi(\mathbf{r},t))) = \int V(\mathbf{r},t)dt. \tag{1.39}$$

Which leads to:

$$\Psi(\mathbf{r},t) \sim \Psi_{(\mathbf{r},0)} e^{-\frac{i}{\hbar}\int V(\mathbf{r},t)dt}. \tag{1.40}$$

The problem arises when the potential $V(\mathbf{r},t)$ becomes so negative that the wave function becomes highly oscillatory [8, 22]. Therefore, states with arbitrarily negative energy may appear, resulting in a spectrum that is not bounded from below. This becomes highly problematic when evaluating the probability density. Then recall that the wave function must be of squares-integrable as it follows:

$$\int_{-\infty}^{+\infty} |\Psi(r)|^2 \, d^3r = 1, \tag{1.41}$$

which, on the one hand, means that the value of Ψ requires to be bounded and finite. However, this is not the case when $V(\mathbf{r},t)$ diverges negatively, making the wave function not being of square integrable [8], therefore it is non-normalizable. The violation of the norm led to an unphysical problem. This is another reason why the potential energy term has to be bounded from below.

1.3 Higgs Mechanism for a Scalar Field

A more familiar example to our context, is given by a scalar Lagrangian with a ϕ^4 interaction that is considered, associated with a coupling λ, which is also invariant under $\mathbb{Z}_2$, $\phi \to -\phi$, can be written as:

$$\mathcal{L} = \frac{1}{2}\partial_\mu\phi\partial^\mu\phi - \underbrace{\left(\frac{1}{2}\mu^2\phi^2 + \frac{1}{4}\lambda\phi^4\right)}_{\text{Scalar Potential: } V}, \tag{1.42}$$

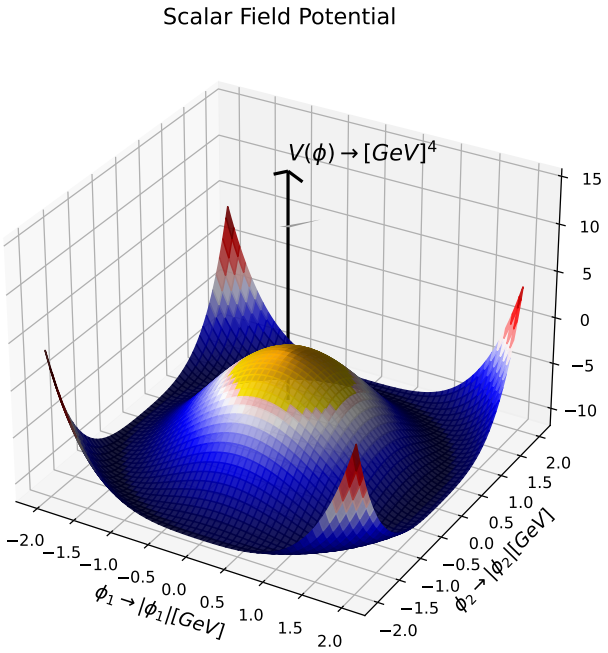

Figure 1.1: Representation of the Scalar Potential $V(\phi)$.

In Figure 1.1 we can observe the plotted Scalar Potential of expression 1.42.
The parameter λ must be greater than zero to safeguard that the potential is bounded from below . The ground state of the system arises from the classical minimum of the potential, but to determine the excitations, it is necessary to expand around this minimum according to perturbation theory [23]. Minimizing the potential as shown:

$$\frac{\partial V}{\partial \phi} = 0, \tag{1.43}$$

$$\frac{1}{\cancel{2}}\cancel{2}\mu^2\phi + \frac{1}{\cancel{4}}\cancel{4}\lambda\phi^3 = 0, \tag{1.44}$$

$$\phi(\mu^2 + \lambda\phi^2) = 0, \tag{1.45}$$

therefore, we have two possible solutions:

$$\phi = 0; \quad \phi = \pm\sqrt{\frac{-\mu^2}{\lambda}}. \tag{1.46}$$

According to the solutions, it seems that there are no real roots in 1.46. Therefore μ^2 requires to be restricted to only two possibilities: $\mu^2 > 0$ or $\mu^2 < 0$.

If $\mu^2 > 0$, then $\phi = 0$. But if $\mu^2 < 0$, then $\phi = \pm\sqrt{\frac{-\mu^2}{\lambda}}$.
Consequently, when $\mu^2 < 0$, we have found a new "vacuum" state, which is known as the vacuum expectation value (vev$\rightarrow v$) [24, 6, 10], $\phi_0 = \langle 0|\phi|0\rangle$, and it corresponds to:

$$\phi_0 = \pm\sqrt{\frac{-\mu^2}{\lambda}} = \pm v. \tag{1.47}$$

In a certain way, $\mu^2 < 0$ implies that the Lagrangian density must be modified, as the only way for spontaneous symmetry breaking to occur is when the potential incorporates this condition. Still, we will proceed with the development while keeping in mind that $\mu^2 < 0$, which means we can redefine it as $\mu^2 = -m^2$.

Now, we can expand the scalar potential around a small perturbation at either of the two previously found minima (ϕ_{0+}, ϕ_{0-}). Let us consider, for instance, a perturbation α around ϕ_{0-}, meaning we take $\phi = \phi_{0-} + \alpha = -v + \alpha$. Substituting this into the potential, we obtain:

$$V = \frac{1}{2}\mu^2(-v+\alpha)^2 + \frac{1}{4}\lambda(-v+\alpha)^4 \tag{1.48}$$

$$= \frac{1}{2}\mu^2(v^2 - 2\alpha v + \alpha^2) + \frac{1}{4}\lambda(v^4 + \alpha^4 - 4\alpha v^3 + 6\alpha^2 v^2 - 4\alpha^3 v) \tag{1.49}$$

$$= \frac{1}{2}\mu^2 v^2 - \mu^2 v\alpha + \frac{1}{2}\mu^2\alpha^2 + \frac{1}{4}\lambda v^4 - \lambda v^3\alpha + \frac{3}{2}\lambda v^2\alpha^2 - \lambda v\alpha^3 + \frac{1}{4}\lambda\alpha^4. \tag{1.50}$$

But we must not forget that the perturbation around the minimum is very small, $\alpha \sim 0$, which allows us to neglect the higher-order terms in α.

$$V \approx \frac{1}{2}\mu^2 v^2 - \mu^2 v\alpha + \frac{1}{2}\mu^2\alpha^2 - \lambda v^3\alpha + \frac{3}{2}\lambda v^2\alpha^2 + \frac{1}{4}\lambda v^4 \tag{1.51}$$

$$= \frac{1}{2}\mu^2 v^2 + \frac{1}{4}\lambda v^4 - \alpha(\mu^2 v + \lambda v^3) + \frac{1}{2}\mu^2\alpha^2 + \frac{3}{2}\lambda v^2\alpha^2 \tag{1.52}$$

The term $\alpha(\mu^2 v + \lambda v^3)$ is neglected mainly because the expansion is around the minimum, while the terms: $\frac{1}{2}\mu^2 v^2 + \frac{1}{4}\lambda v^4$, are part of the vacuum energy, thus can be neglected as well. Resulting in a potential:

$$V \approx \frac{1}{2}\mu^2\alpha^2 + \frac{3}{2}\lambda v^2\alpha^2 \tag{1.53}$$

$$= \frac{1}{2}\underbrace{(\mu^2 + 3\lambda v^2)}_{\text{Higgs mass}}\alpha^2 \tag{1.54}$$

Now, an appropriate mass term arises. Given that we know $2\lambda v^2 = \mu^2 + 3\lambda v^2$, the corresponding term will be $m_\alpha^2 = 2\lambda v$.
Finally, thanks to this perturbation, we were able to determine the Higgs mass. Most importantly, for our purposes, none of this would have been possible if the scalar potential had not been bounded from below in the first place.

Chapter 2

The Copositivity Criteria

In particle physics, some algebraic tools are of great relevance, since they provide us with a feasible mechanism to find the hidden properties of objects such as a scalar potential. It is an attempt to ensure the boundedness from below through a systematical mathematical "recipe".
In linear algebra a real symmetric matrix A:

$$A = \begin{pmatrix} a_{11} & a_{12} & a_{13} & \cdots & a_{1n} \\ a_{21} & a_{22} & a_{23} & \cdots & a_{2n} \\ a_{31} & a_{32} & a_{33} & \cdots & a_{3n} \\ \vdots & \vdots & \vdots & \ddots & \vdots \\ a_{n1} & a_{n2} & a_{n3} & \cdots & a_{nn} \end{pmatrix}. \tag{2.1}$$

The A matrix is copositive if:

$$x^T A x \geq 0, \tag{2.2}$$

where x corresponds to the non-negative vector and x^T to its transpose.
If the x column vector takes any value in $\mathbb{R}^n$ then A in the bi-quadratic form of the equation 2.2 must be redefined as semi-definite positive [25, 9]. Another possibility might be that the column vector satisfies the condition 2.3.

$$x^T A x > 0. \tag{2.3}$$

In the above case, matrix A is said to be positive-definite [17].
The definition of copositivity is important, since the mathematical element in equation 2.2 is analogous to a scalar potential in a particle physics model.

A scalar potential of quartic dimension is written in using the next bi-quadratic form:

$$V_4 = \sum_{a,b} \lambda_{ab} \psi_a^2 \psi_b^2. \tag{2.4}$$

Where λ_{ab} is the coupling matrix and $\psi_{a,b}$ are the field vectors. The domain of the function V_4 are only the positive values of $\psi_{a,b}^2$, while the potential range must be strictly $V_4 \geq 0$. In such a scenario, the only possibility that will allow us to achieve it is making λ_{ab} copositive. Therefore, the potential domain corresponds to the $\mathbb{R}_+^n$ orthant and will behave positively if and only if λ_{ab} is copositive [9].

Obeying this constraint will guarantee a scalar potential which is bounded from below. In such a way that all possible mixed terms in the algebraic form of V_4 always give a positive net result.

Concretely, the matrix of λ_{ab}:

$$\lambda_{ab} = \begin{pmatrix} \lambda_{11} & \lambda_{12} & \lambda_{13} & \cdots & \lambda_{1n} \\ \lambda_{21} & \lambda_{22} & \lambda_{23} & \cdots & \lambda_{2n} \\ \lambda_{31} & \lambda_{32} & \lambda_{33} & \cdots & \lambda_{3n} \\ \vdots & \vdots & \vdots & \ddots & \vdots \\ \lambda_{n1} & \lambda_{n2} & \lambda_{n3} & \cdots & \lambda_{nn} \end{pmatrix}. \tag{2.5}$$

is copositive when Sylvester's criterion is met [26, 9]. Basically, it maintains that the determinants of the sub-matrices are non-negative [27]. Let us start showing the case for a square matrix of dimension 3:

$$\lambda_{ab} = \begin{pmatrix} \lambda_{11} & \lambda_{12} & \lambda_{13} \\ \lambda_{21} & \lambda_{22} & \lambda_{23} \\ \lambda_{31} & \lambda_{32} & \lambda_{33} \end{pmatrix}, \tag{2.6}$$

A strategy described in the literature is taking advantage of a diagonal scaling [28, 9]. For a 3×3 matrix, the belonging scaled element is:

$$\Lambda_{DIAG} = \begin{pmatrix} \frac{1}{\sqrt{\lambda_{11}}} & 0 & 0 \\ 0 & \frac{1}{\sqrt{\lambda_{22}}} & 0 \\ 0 & 0 & \frac{1}{\sqrt{\lambda_{33}}} \end{pmatrix}. \tag{2.7}$$

Consequently, the product with λ_{ab} carries the same information as the original coupling matrix.

$$\Lambda^T_{DIAG}\lambda_{ab}\Lambda_{DIAG} = \begin{pmatrix} \frac{1}{\sqrt{\lambda_{11}}} & 0 & 0 \\ 0 & \frac{1}{\sqrt{\lambda_{22}}} & 0 \\ 0 & 0 & \frac{1}{\sqrt{\lambda_{33}}} \end{pmatrix} \begin{pmatrix} \lambda_{11} & \lambda_{12} & \lambda_{13} \\ \lambda_{21} & \lambda_{22} & \lambda_{23} \\ \lambda_{31} & \lambda_{32} & \lambda_{33} \end{pmatrix} \begin{pmatrix} \frac{1}{\sqrt{\lambda_{11}}} & 0 & 0 \\ 0 & \frac{1}{\sqrt{\lambda_{22}}} & 0 \\ 0 & 0 & \frac{1}{\sqrt{\lambda_{33}}} \end{pmatrix}, \tag{2.8}$$

$$\Lambda_{DIAG} = \begin{pmatrix} 1 & \frac{\lambda_{12}}{\sqrt{\lambda_{11}}\sqrt{\lambda_{22}}} & \frac{\lambda_{13}}{\sqrt{\lambda_{11}}\sqrt{\lambda_{33}}} \\ \frac{\lambda_{21}}{\sqrt{\lambda_{11}}\sqrt{\lambda_{22}}} & 1 & \frac{\lambda_{23}}{\sqrt{\lambda_{22}}\sqrt{\lambda_{33}}} \\ \frac{\lambda_{31}}{\sqrt{\lambda_{11}}\sqrt{\lambda_{33}}} & \frac{\lambda_{32}}{\sqrt{\lambda_{22}}\sqrt{\lambda_{33}}} & 1 \end{pmatrix}. \tag{2.9}$$

Furthermore, we shall introduce another simple constraint which asserts that for "get" a squared and symmetric matrix, the anti-diagonal terms ought to fulfill the following: $\lambda_{12} = \lambda_{21}$ and $\lambda_{23} = \lambda_{32}$ [9].
In the diagonalized coupling matrix, we can find two sub-matrices of the corresponding main object:

$$\begin{pmatrix} 1 & \frac{\lambda_{12}}{\sqrt{\lambda_{11}}\sqrt{\lambda_{22}}} & \frac{\lambda_{13}}{\sqrt{\lambda_{11}}\sqrt{\lambda_{33}}} \\ \frac{\lambda_{12}}{\sqrt{\lambda_{11}}\sqrt{\lambda_{22}}} & 1 & \frac{\lambda_{23}}{\sqrt{\lambda_{22}}\sqrt{\lambda_{33}}} \\ \frac{\lambda_{13}}{\sqrt{\lambda_{11}}\sqrt{\lambda_{33}}} & \frac{\lambda_{23}}{\sqrt{\lambda_{22}}\sqrt{\lambda_{33}}} & 1 \end{pmatrix} \tag{2.10}$$

Let us calculate the determinant of the first red sub-matrix:

$$\Lambda_{2\times 2} = \begin{pmatrix} 1 & \frac{\lambda_{12}}{\sqrt{\lambda_{11}}\sqrt{\lambda_{22}}} \\ \frac{\lambda_{12}}{\sqrt{\lambda_{11}}\sqrt{\lambda_{22}}} & 1 \end{pmatrix}. \tag{2.11}$$

Establishing that it must be greater or equal to zero:

$$det(\Lambda_{2\times 2}) \geq 0, \tag{2.12}$$

$$det(\Lambda_{2\times 2}) = 1 - \frac{\lambda_{12}^2}{\lambda_{11}\lambda_{22}}. \tag{2.13}$$

As a result of that, we can determine the following relation:

$$1 - \frac{\lambda_{12}^2}{\lambda_{11}\lambda_{22}} \geq 0 \rightarrow \lambda_{12} \geq -\sqrt{\lambda_{11}\lambda_{22}} \rightarrow \lambda_{12} + \sqrt{\lambda_{11}\lambda_{22}} \geq 0. \tag{2.14}$$

Finally, this establishes a fundamental condition for BFB, resulting in:

$$\lambda_{12} + \sqrt{\lambda_{11}\lambda_{22}} \geq 0. \tag{2.15}$$

The inequality 2.15 matches up with satisfying partially the vacuum stability conditions. In detail, we shall rename the above quantity as $\overline{\lambda_{12}}$, therefore:

$$\overline{\lambda_{12}} = \lambda_{12} + \sqrt{\lambda_{11}\lambda_{22}} \geq 0. \tag{2.16}$$

Repeating the same logical reasoning but now applied to the blue sub-matrix:

$$\beta_{2\times 2} = \begin{pmatrix} 1 & \frac{\lambda_{23}}{\sqrt{\lambda_{22}}\sqrt{\lambda_{33}}} \\ \frac{\lambda_{23}}{\sqrt{\lambda_{22}}\sqrt{\lambda_{33}}} & 1 \end{pmatrix}. \tag{2.17}$$

It is just needed to take the determinant:

$$det(\beta_{2\times 2}) \geq 0, \tag{2.18}$$

$$det(\beta_{2\times 2}) = 1 - \frac{\lambda_{23}^2}{\lambda_{22}\lambda_{33}}, \tag{2.19}$$

$$1 - \frac{\lambda_{23}^2}{\lambda_{22}\lambda_{33}} \geq 0 \rightarrow \lambda_{23} \geq -\sqrt{\lambda_{22}\lambda_{33}} \rightarrow \lambda_{23} + \sqrt{\lambda_{22}\lambda_{33}} \geq 0. \tag{2.20}$$

Finally it leads to:

$$\lambda_{23} + \sqrt{\lambda_{22}\lambda_{33}} \geq 0. \tag{2.21}$$

Thus, rename it as $\overline{\lambda_{23}}$. Obtaining:

$$\overline{\lambda_{23}} = \lambda_{23} + \sqrt{\lambda_{22}\lambda_{33}} \geq 0. \tag{2.22}$$

Despite the results 2.15 and 2.21, there is still a need to consider that every input in the diagonal ought to achieve the constraint:

$$\begin{aligned} \lambda_{11} &\geq 0, \\ \lambda_{22} &\geq 0, \\ \lambda_{33} &\geq 0. \end{aligned} \tag{2.23}$$

Lema: 'In general, a matrix of order n is copositive if each sub-matrix of order *n-1* is also copositive' [27, 9, 25, 28, 29].
Particularly, that means that each input of the array is $\lambda_{ii} \geq 0$, while the 2×2 sub-matrices, of the principal matrix, accomplish the condition:

$$\lambda_{ij} + \sqrt{\lambda_{ii}\lambda_{jj}} \geq 0. \tag{2.24}$$

In this section of this thesis work, I suggest a way to demonstrate the last Sylvester's condition, mainly due to the different approaches to this property in algebraic literature.

For this task, let us start by taking the determinant of 2.9. Of course, this element shall be greater than zero.

$$det(\Lambda_{DIAG}) \geq 0 \tag{2.25}$$

$$\begin{aligned} det(\Lambda_{DIAG}) &= det\left[\begin{pmatrix} 1 & \frac{\lambda_{12}}{\sqrt{\lambda_{11}}\sqrt{\lambda_{22}}} & \frac{\lambda_{13}}{\sqrt{\lambda_{11}}\sqrt{\lambda_{33}}} \\ \frac{\lambda_{12}}{\sqrt{\lambda_{11}}\sqrt{\lambda_{22}}} & 1 & \frac{\lambda_{23}}{\sqrt{\lambda_{22}}\sqrt{\lambda_{33}}} \\ \frac{\lambda_{13}}{\sqrt{\lambda_{11}}\sqrt{\lambda_{33}}} & \frac{\lambda_{23}}{\sqrt{\lambda_{22}}\sqrt{\lambda_{33}}} & 1 \end{pmatrix}\right] \\ &= 1 - \frac{\lambda_{12}^2}{\lambda_{11}\lambda_{22}} - \frac{\lambda_{13}^2}{\lambda_{11}\lambda_{33}} - \frac{\lambda_{23}^2}{\lambda_{22}\lambda_{33}} + \frac{2\lambda_{12}\lambda_{13}\sqrt{\lambda_{11}\lambda_{22}}\lambda_{23}\sqrt{\lambda_{11}\lambda_{33}}\sqrt{\lambda_{22}\lambda_{33}}}{\lambda_{11}^2\lambda_{22}^2\lambda_{33}^2}, \end{aligned}$$

then factoring:

$$= \frac{1}{\lambda_{11}^2\lambda_{22}^2\lambda_{33}^2}\left[2\lambda_{12}\lambda_{13}\sqrt{\lambda_{11}\lambda_{22}}\lambda_{23}\sqrt{\lambda_{11}\lambda_{33}}\sqrt{\lambda_{22}\lambda_{33}} - \lambda_{11}\lambda_{22}\lambda_{33}\left(\lambda_{13}^2\lambda_{22} + \lambda_{12}^2\lambda_{33}\right)\right.$$

$$+\lambda_{11}^2\lambda_{22}\lambda_{33}\big(-\lambda_{23}^2+\lambda_{22}\lambda_{33}\big)\Big], \tag{2.26}$$

$$=\frac{1}{\lambda_{11}^2\lambda_{22}^2\lambda_{33}^2}\Big[2\lambda_{12}\lambda_{13}\lambda_{23}\lambda_{11}\lambda_{22}\lambda_{33}-\lambda_{11}\lambda_{22}^2\lambda_{33}\lambda_{13}^2-\lambda_{11}\lambda_{22}\lambda_{33}^2\lambda_{12}^2 - \lambda_{11}^2\lambda_{22}\lambda_{33}\lambda_{23}^2+\lambda_{11}^2\lambda_{22}^2\lambda_{33}^2\Big], \tag{2.27}$$

$$=\frac{\lambda_{11}\lambda_{22}\lambda_{33}}{\lambda_{11}^2\lambda_{22}^2\lambda_{33}^2}\left[\lambda_{11}\lambda_{22}\lambda_{33}+2\lambda_{12}\lambda_{13}\lambda_{23}-\lambda_{13}^2\lambda_{22}-\lambda_{12}^2\lambda_{33}-\lambda_{23}^2\lambda_{11}\right], \tag{2.28}$$

$$=\frac{1}{\lambda_{11}\lambda_{22}\lambda_{33}}\left[\lambda_{11}\lambda_{22}\lambda_{33}+2\lambda_{12}\lambda_{13}\lambda_{23}-\lambda_{13}^2\lambda_{22}-\lambda_{12}^2\lambda_{33}-\lambda_{23}^2\lambda_{11}\right] \tag{2.29}$$

The result 2.29 will be significant in a few steps later.
For now, returning to the equation 2.24 we can see that the couplings, λ_{12}, λ_{13} and λ_{23} are already greater than zero, thanks to their expressions given by:

$$\begin{aligned}\lambda_{12}+\sqrt{\lambda_{11}\lambda_{22}}\geq 0 \rightarrow \overline{\lambda_{12}}\geq 0,\\ \lambda_{23}+\sqrt{\lambda_{22}\lambda_{33}}\geq 0 \rightarrow \overline{\lambda_{23}}\geq 0.\end{aligned} \tag{2.30}$$

Although we didn't calculate λ_{13}, it can be easily determined using the generalized relation 2.24 :

$$\lambda_{13}+\sqrt{\lambda_{11}\lambda_{22}}\geq 0 \rightarrow \overline{\lambda_{13}}\geq 0. \tag{2.31}$$

Therefore, coming back to equation 2.29, specially for what is inside the brackets, we have:

$$\underbrace{\left[\lambda_{11}\lambda_{22}\lambda_{33}+2\lambda_{12}\lambda_{13}\lambda_{23}-\lambda_{13}^2\lambda_{22}-\lambda_{12}^2\lambda_{33}-\lambda_{23}^2\lambda_{11}\right]}_{\geq 0} \tag{2.32}$$

It is intuitive that this last statement is likely to be true, since $det(\Lambda_{DIAG})\geq 0$ and certainly it remains valid when a positive amount shifts the asymmetric couplings

(only on those with a plus sign).
If we positively shift the asymmetric couplings, that have a minus sign in front, then showing the positive behavior of inequality 2.33 will not be a straightforward task. Moreover, new constraints are needed in such a case. So, we shall focus on the terms with a positive sign.

$$\begin{aligned}&\left[\lambda_{11}\lambda_{22}\lambda_{33}+2\lambda_{12}\lambda_{13}\lambda_{23}-\lambda_{12}^2\lambda_{33}-\lambda_{13}^2\lambda_{22}-\lambda_{23}^2\lambda_{11}\right]\geq 0\\&\lambda_{11}\lambda_{22}\lambda_{33}+2\lambda_{12}\lambda_{13}\lambda_{23}-(\lambda_{12}^2\lambda_{33}+\lambda_{13}^2\lambda_{22}+\lambda_{23}^2\lambda_{11})\geq 0\end{aligned}\tag{2.33}$$

In the context of the inequalities. We can sum a positive quantity in the left expression. Furthermore, it is in concordance with the order principle [30, 31] along with the monotonicity of the functions. That is to say:

$$\begin{aligned}&c\geq 0,\\&a+b\geq 0\end{aligned}\tag{2.34}$$

For sure, one can agree with the following affirmation:

$$a+b+c\geq c\tag{2.35}$$

However, it is also correct that the expression on the left is greater than zero. Consequently, the order principle in the symbol $\geq$ is respected [31], thus:

$$a+b+c\geq 0.\tag{2.36}$$

Hence, taking the above considerations, we are free to apply it to our case.
Since every coupling is $\lambda_{ij}\geq 0$, therefore it is already guaranteed that the sum of the amount is positive.
For instance, let us propose a novel inequality with a very convenient positive shift. Suppose the next *ansatz*:

$$\begin{aligned}&2\lambda_{13}\sqrt{\lambda_{11}\lambda_{22}}\lambda_{23}+2\lambda_{12}\lambda_{23}\sqrt{\lambda_{11}\lambda_{33}}+2\sqrt{\lambda_{11}\lambda_{22}}\lambda_{23}\sqrt{\lambda_{11}\lambda_{33}}+2\lambda_{12}\lambda_{13}\sqrt{\lambda_{22}\lambda_{33}}+\\&2\lambda_{13}\sqrt{\lambda_{11}\lambda_{22}}\sqrt{\lambda_{22}\lambda_{33}}+2\lambda_{12}\sqrt{\lambda_{11}\lambda_{33}}\sqrt{\lambda_{22}\lambda_{33}}+2\sqrt{\lambda_{11}\lambda_{22}}\sqrt{\lambda_{11}\lambda_{33}}\sqrt{\lambda_{22}\lambda_{33}}\geq 0.\end{aligned}\tag{2.37}$$

Plugging it into the left expression in the inequality 2.33, it follows that:

$$[\lambda_{11}\lambda_{22}\lambda_{33}+2\lambda_{12}\lambda_{13}\lambda_{23}-(\lambda_{12}^2\lambda_{33}+\lambda_{13}^2\lambda_{22}+\lambda_{23}^2\lambda_{11})]+2\lambda_{13}\sqrt{\lambda_{11}\lambda_{22}}\lambda_{23}+$$

$$+ 2\lambda_{12}\lambda_{23}\sqrt{\lambda_{11}\lambda_{33}} + 2\sqrt{\lambda_{11}\lambda_{22}}\lambda_{23}\sqrt{\lambda_{11}\lambda_{33}} + 2\lambda_{12}\lambda_{13}\sqrt{\lambda_{22}\lambda_{33}} +$$
$$+ 2\lambda_{13}\sqrt{\lambda_{11}\lambda_{22}}\sqrt{\lambda_{22}\lambda_{33}} + 2\lambda_{12}\sqrt{\lambda_{11}\lambda_{33}}\sqrt{\lambda_{22}\lambda_{33}} + 2\sqrt{\lambda_{11}\lambda_{22}}\sqrt{\lambda_{11}\lambda_{33}}\sqrt{\lambda_{22}\lambda_{33}} \geq 0. \tag{2.38}$$

Factoring and rearranging the terms:

$$\lambda_{11}\lambda_{22}\lambda_{33} + 2(\lambda_{12} + \sqrt{\lambda_{11}\lambda_{22}})(\lambda_{13} + \sqrt{\lambda_{11}\lambda_{33}})(\lambda_{23} + \sqrt{\lambda_{22}\lambda_{33}}) - \lambda_{12}^2\lambda_{33}$$
$$- \lambda_{13}^2\lambda_{22} - \lambda_{23}^2\lambda_{11} \geq 0 \tag{2.39}$$

The positive magnitude merely affects the asymmetric couplings. But that is a known amount, yielding to:

$$\lambda_{11}\lambda_{22}\lambda_{33} + 2\overline{\lambda_{12}}\,\overline{\lambda_{13}}\,\overline{\lambda_{23}} - \lambda_{12}^2\lambda_{33} - \lambda_{13}^2\lambda_{22} - \lambda_{23}^2\lambda_{11} \geq 0 \tag{2.40}$$

Henceforth, the inequality of Minkowski and the Taxicab norm will be very helpful in a few steps. Thanks to the particular geometry that it offers in which the distance between two points is the sum of the absolute differences of their coordinates [32]. The first step is starting to compute the Minkowski inequality of equation 2.40, as presented below:

$$\|0\|_{p=1/2} \leq \|\lambda_{11}\lambda_{22}\lambda_{33} + 2\overline{\lambda_{12}}\,\overline{\lambda_{13}}\,\overline{\lambda_{23}} - \lambda_{12}^2\lambda_{33} - \lambda_{13}^2\lambda_{22} - \lambda_{23}^2\lambda_{11}\|_{p=1/2} \tag{2.41}$$

Using the property in the expression at the right part of the inequality:

$$\|\lambda_{11}\lambda_{22}\lambda_{33} + 2\overline{\lambda_{12}}\,\overline{\lambda_{13}}\,\overline{\lambda_{23}} - \lambda_{12}^2\lambda_{33} - \lambda_{13}^2\lambda_{22} - \lambda_{23}^2\lambda_{11}\|_{p=1/2} \leq \|\lambda_{11}\lambda_{22}\lambda_{33}\|_{p=1/2} +$$
$$+ 2\|\overline{\lambda_{12}\lambda_{13}\lambda_{23}}\|_{p=1/2} + \|-\lambda_{12}^2\lambda_{33}\|_{p=1/2} + \|-\lambda_{13}^2\lambda_{22}\|_{p=1/2} + \|-\lambda_{23}^2\lambda_{11}\|_{p=1/2} \tag{2.42}$$

The right part is just:

$$= [\sqrt{(\lambda_{11}\lambda_{22}\lambda_{33})^2}^{1/2}]^2 + [\sqrt{(2\overline{\lambda_{12}}\,\overline{\lambda_{13}}\,\overline{\lambda_{23}})^2}^{1/2}]^2 + [\sqrt{(-\lambda_{12}^2\lambda_{33})^2}^{1/2}]^2 +$$
$$+ [\sqrt{(-\lambda_{13}^2\lambda_{22})^2}^{1/2}]^2 + [\sqrt{(-\lambda_{23}^2\lambda_{11})^2}^{1/2}]^2. \tag{2.43}$$

Yielding to:

$$= \lambda_{11}\lambda_{22}\lambda_{33} + 2\overline{\lambda_{12}}\,\overline{\lambda_{13}}\,\overline{\lambda_{23}} + \lambda_{12}^2\lambda_{33} + \lambda_{13}^2\lambda_{22} + \lambda_{23}^2\lambda_{11}, \tag{2.44}$$

by transitivity, the result of this norm will also be greater than zero :

$$\lambda_{11}\lambda_{22}\lambda_{33} + 2\overline{\lambda_{12}}\,\overline{\lambda_{13}}\,\overline{\lambda_{23}} + \lambda_{12}^2\lambda_{33} + \lambda_{13}^2\lambda_{22} + \lambda_{23}^2\lambda_{11} \geq 0 \tag{2.45}$$

At this stage, transitioning to a vectorial paradigm becomes necessary, allowing the use of the taxicab norm. Hence, arranging the aforementioned terms into a vector within a five-dimensional basis results in:

$$\begin{aligned}\vec{\Lambda} =& \lambda_{11}\lambda_{22}\lambda_{33}\begin{pmatrix}1\\0\\0\\0\\0\end{pmatrix} + 2\overline{\lambda_{12}}\,\overline{\lambda_{13}}\,\overline{\lambda_{23}}\begin{pmatrix}0\\1\\0\\0\\0\end{pmatrix} + \lambda_{12}^2\lambda_{33}\begin{pmatrix}0\\0\\1\\0\\0\end{pmatrix} + \lambda_{13}^2\lambda_{22}\begin{pmatrix}0\\0\\0\\1\\0\end{pmatrix} + \\ &+ \lambda_{23}^2\lambda_{11}\begin{pmatrix}0\\0\\0\\1\\0\end{pmatrix},\end{aligned} \tag{2.46}$$

the corresponding taxicab norm of $\vec{\Lambda}$ with $p = 1/2$ is:

$$\begin{aligned}|\vec{\Lambda}|_{p=1/2} =& \left[\sqrt{(\lambda_{11}\lambda_{22}\lambda_{33})^2}^{1/2} + \sqrt{(2\overline{\lambda_{12}}\,\overline{\lambda_{13}}\,\overline{\lambda_{23}})^2}^{1/2} + \sqrt{(-\lambda_{12}^2\lambda_{33})^2}^{1/2}\right. \\ &\left. + \sqrt{(-\lambda_{13}^2\lambda_{22})^2}^{1/2} + \sqrt{(-\lambda_{23}^2\lambda_{11})^2}^{1/2}\right]^2 \qquad (2.47)\\ =& \left[\sqrt{\lambda_{11}\lambda_{22}\lambda_{33}} + \sqrt{2\overline{\lambda_{12}}\,\overline{\lambda_{13}}\,\overline{\lambda_{23}}} + \sqrt{\lambda_{12}^2\lambda_{33}} + \sqrt{\lambda_{13}^2\lambda_{22}} + \sqrt{\lambda_{23}^2\lambda_{11}}\right]^2. \qquad (2.48)\end{aligned}$$

Since there are no negative signs and it is squared, the expression should also be greater than zero:

$$\left[\sqrt{\lambda_{11}\lambda_{22}\lambda_{33}} + \sqrt{2\overline{\lambda_{12}}\,\overline{\lambda_{13}}\,\overline{\lambda_{23}}} + \sqrt{\lambda_{12}^2\lambda_{33}} + \sqrt{\lambda_{13}^2\lambda_{22}} + \sqrt{\lambda_{23}^2\lambda_{11}}\right]^2 \geq 0. \tag{2.49}$$

Finally, taking the square root, the last Sylvester's inequality is obtained:

$$\sqrt{\lambda_{11}\lambda_{22}\lambda_{33}} + \sqrt{2\overline{\lambda_{12}}\,\overline{\lambda_{13}}\,\overline{\lambda_{23}}} + \lambda_{12}\sqrt{\lambda_{33}} + \lambda_{13}\sqrt{\lambda_{22}} + \lambda_{23}\sqrt{\lambda_{11}} \geq 0. \tag{2.50}$$

In summary, the necessary and sufficient (**NAS**) conditions that establish the copositivity criteria are:

$$\lambda_{11} \geq 0, \lambda_{22} \geq 0, \lambda_{33} \geq 0, \tag{2.51}$$

$$\overline{\lambda}_{12} = \lambda_{12} + \sqrt{\lambda_{11}\lambda_{22}}, \tag{2.52}$$

$$\overline{\lambda}_{13} = \lambda_{13} + \sqrt{\lambda_{11}\lambda_{33}}, \tag{2.53}$$

$$\overline{\lambda}_{23} = \lambda_{23} + \sqrt{\lambda_{22}\lambda_{33}}, \tag{2.54}$$

$$\sqrt{\lambda_{11}\lambda_{22}\lambda_{33}} + \lambda_{12}\sqrt{\lambda_{33}} + \lambda_{13}\sqrt{\lambda_{22}} + \lambda_{23}\sqrt{\lambda_{11}} + \sqrt{2\overline{\lambda_{12}}\,\overline{\lambda_{13}}\,\overline{\lambda_{23}}} \geq 0. \tag{2.55}$$

The above inequalities ensure the vacuum stability of a particle physics model through imposing those conditions on the scalar potential's couplings, as they guarantee that it is bounded from below (BFB). In other words, if the parameters in a potential satisfy these conditions, the potential will always increase, regardless of the direction of the fields and their interactions [1].

2.1 The inert Higgs Model

An instance where the boundedness from below can be completely characterized by the copositivity criteria is closely associated with the Two Higgs Doublet Model (2HDM). Where a new Higgs state is considered, but only one acquires a vacuum expectation value [33, 34, 35].
The Inert Higgs Model serves as a paradigmatic example of how algebraic tools can be effectively applied to develop the NAS conditions that accomplish getting a BFB potential.

2.1.1 Two Higgs Doublet model

The 2HDM framework is one of the most minimal extensions to the Standard Model [33]; basically, an extra $SU(2)$ scalar doublet is added. The model, with no explicit CP violation, is given by the Scalar Potential:

$$\begin{aligned} V =& \lambda_1|H_1|^4 + \lambda_2|H_2|^4 + \lambda_3|H_1|^2|H_2|^2 + \\ &+ \lambda_4(H_1^\dagger H_2)(H_2^\dagger H_1) + \frac{1}{2}[\lambda_5(H_1^\dagger H_2)^2 + \lambda_5^*(H_2^\dagger H_1)^2] \\ &+ |H_1|^2(\lambda_6 H_1^\dagger H_2 + \lambda_6^* H_2^\dagger H_1) + |H_2|^2(\lambda_7 H_1^\dagger H_2 + \lambda_7^* H_2^\dagger H_1). \end{aligned} \tag{2.56}$$

Moving the fields to a polar coordinate basis will enable us to work with a compact form of potential 2.56. The change of coordinates is given by:

$$|H_1|^2 = h_1^2, \quad |H_2| = h_2^2, \quad H_1^\dagger H_2 = h_1 h_2 \rho e^{i\phi} \ .$$

Here, h_1 corresponds to the X-coordinate, while h_2 represents the Y-coordinate, with ϕ denoting the angle between the radial component $r = \sqrt{h_1^2 + h_2^2}$ and the X-axis. On the other hand, the factor ρ describes how both Higgs-like states mix, indicating how the scalar field space is traversed.
Therefore, the potential is rewritten as follows:

$$\begin{aligned} V =& h_1^4\lambda_1 + h_2^4\lambda_2 + h_1^2h_2^2\lambda_3 + e^{-i\phi}h_1^3h_2\lambda_6\rho + e^{i\phi}h_1^3h_2\lambda_6\rho + e^{-i\phi}h_1h_2^3\lambda_7\rho + \\ &+ e^{i\phi}h_1h_2^3\lambda_7\rho + h_1^2h_2^2\lambda_4\rho^2 + \frac{1}{2}e^{-2i\phi}h_1^2h_2^2\lambda_5\rho^2 + \frac{1}{2}e^{2i\phi}h_1^2h_2^2\lambda_5\rho^2, \end{aligned} \tag{2.57}$$

collecting some terms, it reduces to the equivalent expression:

$$\begin{aligned} V =& h_1^4\lambda_1 + h_2^4\lambda_2 + h_1^2\left(h_2^2\left(\lambda_3 + \lambda_4\rho^2\right)\right) + \\ &+ h_1h_2\rho\Big(2\big(h_1^2\lambda_6 + h_2^2\lambda_7\big)\cos(\phi) + h_1h_2\lambda_5\rho\cos(2\phi)\Big) \end{aligned} \tag{2.58}$$

When $\lambda_6 = \lambda_7 = 0$ and H_2 transform under $\mathbb{Z}_2$, the model drifts to the **inert Higgs model**. And the Scalar Potential takes the form:

$$V = h_1^4\lambda_1 + h_2^4\lambda_2 + h_2^2\mu_{22} + h_1^2\left(\mu_{12} + h_2^2\left(\lambda_3 + \lambda_4\rho^2\right)\right) + h_1^2h_2^2\lambda_5\rho^2\cos(2\phi), \tag{2.59}$$

but the trigonometric function $\cos(2\phi)$ takes values in the range $[-1, 1]$. Consequently, when it is extremized, the only plausible values of the cosine are -1 and $+1$. Writing the expression at the extreme value of -1, it results in:

$$V = \mu_1h_1^2 + \mu_2h_2^2 + \lambda_1h_1^4 + \lambda_2h_2^4 + \lambda_3h_1^2h_2^2 + \lambda_4\rho^2h_1^2h_2^2 - |\lambda_5|\rho^2h_1^2h_2^2. \tag{2.60}$$

Subsequently, let us find the coupling matrix. Start getting the second derivatives of the potential with respect to the fields:

$$\frac{\partial^2 V}{\partial h_1^2 \partial h_1^2} = 2\lambda_1, \tag{2.61}$$

$$\frac{\partial^2 V}{\partial h_1^2 \partial h_2^2} = \lambda_3 + \lambda_4\rho^2 - |\lambda_5|\rho^2, \tag{2.62}$$

$$\frac{\partial^2 V}{\partial h_2^2 \partial h_1^2} = \lambda_3 + \lambda_4 \rho^2 - |\lambda_5| \rho^2, \tag{2.63}$$

$$\frac{\partial^2 V}{\partial h_2^2 \partial h_2^2} = 2\lambda_2. \tag{2.64}$$

Actually, with this, we can arm the Hessian matrix, which could give us the mass eigenstates:

$$\mathcal{M}^2 = \begin{pmatrix} 2\lambda_1 & \lambda_3 + \rho^2(\lambda_4 - |\lambda_5|) \\ \lambda_3 + \rho^2(\lambda_4 - |\lambda_5|) & 2\lambda_2 \end{pmatrix}. \tag{2.65}$$

Factoring:

$$\mathcal{M}^2 = 2 \underbrace{\begin{pmatrix} \lambda_1 & \frac{1}{2}[\lambda_3 + \rho^2(\lambda_4 - |\lambda_5|)] \\ \frac{1}{2}[\lambda_3 + \rho^2(\lambda_4 - |\lambda_5|)] & \lambda_2 \end{pmatrix}}_{\Lambda \text{ : Coupling Matrix}}. \tag{2.66}$$

The matrix in the expression 2.66 has the role of a coupling matrix. It means that the potential can be scaled as:

$$V = (h_1^2, h_2^2)\Lambda(h_1^2, h_2^2)^T \tag{2.67}$$

$$V = \begin{pmatrix} h_1^2 & h_2^2 \end{pmatrix} \begin{pmatrix} \lambda_1 & \frac{1}{2}[\lambda_3 + \rho^2(\lambda_4 - |\lambda_5|)] \\ \frac{1}{2}[\lambda_3 + \rho^2(\lambda_4 - |\lambda_5|)] & \lambda_2 \end{pmatrix} \begin{pmatrix} h_1^2 \\ h_2^2 \end{pmatrix} \tag{2.68}$$

Therefore, one of the necessary and sufficient conditions can be encountered directly in the diagonal, claiming that:

$$\lambda_1 \geq 0, \tag{2.69}$$

$$\lambda_2 \geq 0. \tag{2.70}$$

Additionally, the others can be found simply by replacing the positional term Λ_{12} in equation 2.52. That term corresponds to:

$$\lambda_{12} = \frac{1}{2}[\lambda_3 + \rho^2(\lambda_4 - |\lambda_5|)], \tag{2.71}$$

then plugging it into the Sylvester condition 2.52:

$$\frac{1}{2}[\lambda_3 + \rho^2(\lambda_4 - |\lambda_5|)] + \sqrt{\lambda_1 \lambda_2} \geq 0,$$

$$\lambda_3 + \rho^2(\lambda_4 - |\lambda_5|) \geq -2\sqrt{\lambda_{11}\lambda_{22}},$$

resulting:

$$\rho^2(\lambda_4 - |\lambda_5|) \geq -(2\sqrt{\lambda_1\lambda_2} + \lambda_3). \tag{2.72}$$

But ρ is a free parameter that goes between $[0, 1]$. Evaluating in the extreme cases. When $\underline{\rho = 0:}$

$$0 \geq -(2\sqrt{\lambda_1\lambda_2} + \lambda_3), \tag{2.73}$$
$$\lambda_3 \geq -\sqrt{\lambda_1\lambda_2}. \tag{2.74}$$

When $\underline{\rho = 1:}$

$$\lambda_4 - |\lambda_5| \geq -(2\sqrt{\lambda_1\lambda_2} + \lambda_3), \tag{2.75}$$
$$\lambda_4 - |\lambda_5| + 2\sqrt{\lambda_1\lambda_2} + \lambda_3 \geq 0. \tag{2.76}$$

Finally, combining all the inequalities we found, we obtain the following collection of constraints:

$$\lambda_1 \geq 0, \tag{2.77}$$
$$\lambda_2 \geq 0, \tag{2.78}$$
$$\lambda_4 - |\lambda_5| + 2\sqrt{\lambda_1\lambda_2} + \lambda_3 \geq 0, \tag{2.79}$$
$$\lambda_3 \geq -\sqrt{\lambda_1\lambda_2}. \tag{2.80}$$

These are the well-known inequalities that secure vacuum stability for the Inert Higgs Model, as they satisfy the copositivity criteria. This indicates that these necessary and sufficient conditions are adequate to guarantee the vacuum stability of such a potential.
As $\lambda_6 \neq 0$ and $\lambda_7 \neq 0$, then condition 2.79 is necessary. Finding the minima of a potential in its general form, such as the Inert Higgs potential, is not a straightforward task due to the nonlinear dependence on the orbital parameters ρ and ϕ. Moreover, if one considers constraints derived from polynomial approximations [4.11], then a general minimization is not feasible [1]. Instead, it becomes necessary to use a Lagrange multiplier that encompasses the parameters h_1, h_2, ρ, and ϕ, along with the constraint that h_1 and h_2 lie within a unit circle ($r = 1$), $h_1^2 + h_2^2 = r^2$. These minimizations are non-trivial, just as it is challenging to determine an allowed region for

all couplings simultaneously, including cases where $\lambda_6 \neq 0$ and $\lambda_7 \neq 0$.

In the following chapter, we will illustrate a much simpler case: the Two Real Scalar Fields model. However, our approach allows us to handle all couplings being "switched on" simultaneously without the need to impose polynomial constraints, which can often be awkward.

Chapter 3

Exploring the copositivity paradigm: Implementation and Limitation

This chapter focuses on the implementation of the copositivity criterion. Nonetheless, it is observed that this approach is not sufficient for the studied scalar potential. As a consequence, certain variable transformations are introduced, along with a rewriting in polar coordinates. These modifications enable the proposal of a curve-fitting approach for cases where the scalar potential satisfies the BFB condition. The accuracy of this fit is assessed through a mini statistical analysis.

We now proceed to analyze a scalar potential that presents challenges for the copositivity technique: the scalar potential of two real scalar fields, that fields are given by:

$$\Phi' = \begin{pmatrix} \phi_1' \\ \phi_2' \end{pmatrix}, \tag{3.1}$$

while the couplings governing their interactions can be expressed in the arrangement:

$$\lambda_{2\times 2} = \begin{pmatrix} \lambda_{11} & \lambda_{12} \\ \lambda_{21} & \lambda_{22} \end{pmatrix}. \tag{3.2}$$

In later steps, we will see that, in the scalar potential, the couplings λ_{12} and λ_{21} must be equal. For now, let us construct a potential that is of quartic order and includes cubic interactions, written as:

$$V = \lambda_{11}\phi\prime_1^4 + \lambda_{12}\phi\prime_1^2\phi\prime_2^2 + \lambda_{21}\phi\prime_1^2\phi\prime_2^2 + \lambda_{22}\phi\prime_2^4 + \kappa_{12}\phi\prime_1^3\phi\prime_2 + \kappa_{21}\phi\prime_1\phi\prime_2^3, \tag{3.3}$$

where λ_{ij} are the different couplings accompanying the quartic terms, and κ_{mn} are the coupling constants associated with the cubic terms.
Here the most irreducible matrix form that we can obtain is:

$$\begin{aligned} V =& \begin{pmatrix} \phi\prime_1^2 & \phi\prime_2^2 \end{pmatrix} \begin{pmatrix} \lambda_{11} & \lambda_{12} \\ \lambda_{21} & \lambda_{22} \end{pmatrix} \begin{pmatrix} \phi\prime_1^2 \\ \phi\prime_2^2 \end{pmatrix} + \kappa_{12}\phi\prime_1^3\phi\prime_2 + \kappa_{21}\phi\prime_1\phi\prime_2^3 \\ V =& \Phi\prime^{2T}\lambda_{2\times2}\Phi\prime^2 + \kappa_{12}\phi\prime_1^3\phi\prime_2 + \kappa_{21}\phi\prime_1\phi\prime_2^3. \end{aligned} \tag{3.4}$$

Although it can be rearranged into a matrix, the asymmetric terms that remain outside cannot be structured in this form. Then set them aside for later analysis. For now, we shall proceed with the diagonal scaling.
Invoking the equation 2.10, which states that an arrangement can be scaled so that its diagonal consists exclusively of ones. On the other hand, since the matrix $\lambda_{2\times2}$ is positive definite, it can be scaled by a certain factor while remaining positive definite as well [28].
Applying this procedure to our case, results in a scalar potential that is easier to characterize and offers insights into its growth behavior across all directions of the scalar fields.

Beginning by applying the diagonal scaling to the coupling matrix, using the square root of its diagonal entries. This is done by multiplying the matrix from the left and right with the following scaling factor:

$$\Theta_{diag} = \begin{pmatrix} \frac{1}{\sqrt{\lambda_{11}}} & 0 \\ 0 & \frac{1}{\sqrt{\lambda_{22}}} \end{pmatrix}. \tag{3.5}$$

In later steps, we will see that this scaling can be conveniently incorporated directly into the fields. For now, let us compute the matrix product:

$$\Theta_{diag}^T\lambda_{2\times2}\Theta_{diag} = \begin{pmatrix} \frac{1}{\sqrt{\lambda_{11}}} & 0 \\ 0 & \frac{1}{\sqrt{\lambda_{22}}} \end{pmatrix} \begin{pmatrix} \lambda_{11} & \lambda_{12} \\ \lambda_{21} & \lambda_{22} \end{pmatrix} \begin{pmatrix} \frac{1}{\sqrt{\lambda_{11}}} & 0 \\ 0 & \frac{1}{\sqrt{\lambda_{22}}} \end{pmatrix}, \tag{3.6}$$

$$= \begin{pmatrix} 1 & \frac{\lambda_{12}}{\sqrt{\lambda_{11}}\sqrt{\lambda_{22}}} \\ \frac{\lambda_{21}}{\sqrt{\lambda_{11}}\sqrt{\lambda_{22}}} & 1 \end{pmatrix}. \tag{3.7}$$

Yet, we must keep in mind that this method applies to matrices where the anti-diagonal couplings are equal. As we mentioned earlier, this assumption will slightly

modify the scalar potential, reducing it to one with only a single asymmetric coupling. This is achieved simply by setting $\lambda_{21} = \lambda_{12}$ [9].

Now, if we include the field vectors, the result will be a partially scaled scalar potential. It is considered partially scaled because the interactions $\kappa_{21}\phi\prime_1\phi\prime_2^3$, $\kappa_{12}\phi\prime_1^3\phi\prime_2$ terms have not yet been included. The expression takes the form:

$$\Phi\prime^{2T}\Theta_{diag}^{T}\lambda_{2\times2}\Theta_{diag}\Phi\prime^2 = \begin{pmatrix}\phi\prime_1^2 & \phi\prime_2^2\end{pmatrix}\begin{pmatrix}1 & \frac{\lambda_{12}}{\sqrt{\lambda_{11}}\sqrt{\lambda_{22}}} \\ \frac{\lambda_{12}}{\sqrt{\lambda_{11}}\sqrt{\lambda_{22}}} & 1\end{pmatrix}\begin{pmatrix}\phi\prime_1^2 \\ \phi\prime_2^2\end{pmatrix} \tag{3.8}$$

$$= \underbrace{\phi\prime_1^4 + \frac{2\lambda_{12}\phi\prime_1^2\phi\prime_2^2}{\sqrt{\lambda_{11}\lambda_{22}}} + \phi\prime_2^4}_{\text{Partially scaled potential}} \tag{3.9}$$

Renaming the factor of coupling normalization, $\frac{\lambda_{12}}{\sqrt{\lambda_{11}}\sqrt{\lambda_{22}}}$ as δ_{12}:

$$\Phi\prime^{2T}\Theta_{diag}^{T}\lambda_{2\times2}\Theta_{diag}\Phi\prime^2 = \phi\prime_1^4 + 2\delta_{12}\phi\prime_1^2\phi\prime_2^2 + \phi\prime_2^4. \tag{3.10}$$

However, if one shifts the diagonal scaling to the fields, the structure remains unchanged [36]. Therefore, we state that, physically, the diagonal scaling is applied to the fields ϕ'_1 and ϕ'_2. This is very meaningful, because we are working with the same potential, but scaled in the fields.

$$\Phi\prime^{2T}\Theta_{diag}^{T}\lambda_{2\times2}\Theta_{diag}\Phi\prime^2 = \begin{pmatrix}\frac{\phi\prime_1^2}{\sqrt{\lambda_{11}}} & \frac{\phi\prime_2^2}{\sqrt{\lambda_{22}}}\end{pmatrix}\begin{pmatrix}1 & 0 \\ 0 & 1\end{pmatrix}\begin{pmatrix}\lambda_{11} & \lambda_{12} \\ \lambda_{12} & \lambda_{22}\end{pmatrix}\begin{pmatrix}1 & 0 \\ 0 & 1\end{pmatrix}\begin{pmatrix}\frac{\phi\prime_1^2}{\sqrt{\lambda_{11}}} \\ \frac{\phi\prime_2^2}{\sqrt{\lambda_{22}}}\end{pmatrix} \tag{3.11}$$

$$= \phi\prime_1^4 + \frac{2\lambda_{12}\phi\prime_1^2\phi\prime_2^2}{\sqrt{\lambda_{11}\lambda_{22}}} + \phi\prime_2^4, \tag{3.12}$$

which is equivalent to :

$$\Phi\prime^{2T}\Theta_{diag}^{T}\lambda_{2\times2}\Theta_{diag}\Phi\prime^2 = \phi\prime_1^4 + 2\delta_{12}\phi\prime_1^2\phi\prime_2^2 + \phi\prime_2^4. \tag{3.13}$$

The result above is identical to that in equation 3.9. Thus, we can proceed to apply the scaling directly to the fields in order to extend it to the entire potential. Summaryzing:

$$\phi\prime_1^2 \to \frac{\phi_1^2}{\sqrt{\lambda_{11}}},$$

$$\phi\prime_2^2 \to \frac{\phi_2^2}{\sqrt{\lambda_{22}}},$$
$$\lambda_{12} \to \delta_{12}\sqrt{\lambda_{11}\lambda_{22}}.$$

Replacing into the scalar potential 3.3:

$$V = \cancel{\lambda_{11}}\frac{\phi_1^4}{\cancel{\lambda_{11}}} + 2\delta_{12}\sqrt{\cancel{\lambda_{11}\lambda_{22}}}\frac{\phi_1^2\phi_2^2}{\sqrt{\cancel{\lambda_{11}\lambda_{22}}}} + \cancel{\lambda_{22}}\frac{\phi_2^4}{\cancel{\lambda_{22}}} + \kappa_{12}\frac{\phi_1^3}{\lambda_{11}^{3/4}}\frac{\phi_2}{\lambda_{22}^{1/4}} + \kappa_{21}\frac{\phi_1}{\lambda_{11}^{1/4}}\frac{\phi_2^3}{\lambda_{22}^{3/4}}, \quad (3.14)$$

$$V = \phi_1^4 + 2\delta_{12}\phi_1^2\phi_2^2 + \phi_2^4 + \kappa_{12}\frac{\phi_1^3}{\lambda_{11}^{3/4}}\frac{\phi_2}{\lambda_{22}^{1/4}} + \kappa_{21}\frac{\phi_1}{\lambda_{11}^{1/4}}\frac{\phi_2^3}{\lambda_{22}^{3/4}}. \quad (3.15)$$

From now on it is time to analyze κ_{12} and κ_{21}. Note that the first three terms in 3.15 are of dimension GeV^4 and are free from direct coupling dependence. Consequently, each κ_{12} and κ_{21} ought to include an appropriate normalization factor. For instance, κ_{12} explicitly has to incorporate the terms $\lambda_{11}^{3/4}$ and $\lambda_{22}^{1/4}$, while for κ_{21} the corresponding factors are $\lambda_{11}^{1/4}$ and $\lambda_{22}^{3/4}$.

If these factors are simply placed manually, then the denominator terms will cancel out, implying that the κ_{ij} were never truly significant. For that reason, we are going to include the factors ξ_{12} and ξ_{21} that play the roles of a novel-like κ_{ij}.

$$\kappa_{12} \to \xi_{12}\lambda_{11}^{3/4}\lambda_{22}^{3/4}$$
$$\kappa_{21} \to \xi_{21}\lambda_{11}^{1/4}\lambda_{22}^{3/4}.$$

Hence, the diagonally scaled scalar potential takes the form:

$$V = \phi_1^4 + 2\delta_{12}\phi_1^2\phi_2^2 + \phi_2^4 + \xi_{12}\cancel{\lambda_{11}^{3/4}}\cancel{\lambda_{22}^{3/4}}\frac{\phi_1^3}{\cancel{\lambda_{11}^{3/4}}}\frac{\phi_2}{\cancel{\lambda_{22}^{1/4}}} + \xi_{21}\cancel{\lambda_{11}^{1/4}}\cancel{\lambda_{22}^{3/4}}\frac{\phi_1}{\cancel{\lambda_{11}^{1/4}}}\frac{\phi_2^3}{\cancel{\lambda_{22}^{3/4}}},$$
$$V = \phi_1^4 + 2\delta_{12}\phi_1^2\phi_2^2 + \phi_2^4 + \xi_{12}\phi_1^3\phi_2 + \xi_{21}\phi_1\phi_2^3. \quad (3.16)$$

This potential provides a very compact form, where all the interaction information is encapsulated within the factors δ_{12}, ξ_{12} and ξ_{21}. On purpose, the term δ_{12} partially satisfies one of the copositivity conditions, since the determinant of matrix 3.7 must be greater than zero.

$$det[\Theta_{diag}^T\lambda_{ab}\Theta_{diag}] = 1 - \frac{\lambda_{12}\lambda_{21}}{\sqrt{\lambda_{11}^2\lambda_{22}^2}} \geq 0 \quad (3.17)$$

Do not forget that we have only one λ_{12}, in consequence:

$$1 - \frac{\lambda_{12}^2}{\lambda_{11}\lambda_{22}} \geq 0, \tag{3.18}$$

remember as well that, $\delta_{12} = \frac{\lambda_{12}}{\sqrt{\lambda_{11}\lambda_{22}}}$, henceforth:

$$\begin{aligned} 1 - \delta_{12}^2 &\geq 0, \\ (1 - \delta_{12})(1 + \delta_{12}) &\geq 0, \end{aligned} \tag{3.19}$$

limiting the range of δ_{12} to:

$$-1 \leq \delta_{12} \leq 1. \tag{3.20}$$

Taking the lower limit of δ_{12}, in the vicinity of $\delta_{12} \approx -1$, where the determinant barely achieves copositivity. It is possible to shift it a positive amount χ_{12}. Then:

$$\delta_{12} \to -1 + \chi_{12}. \tag{3.21}$$

This leads the potential to a form that allows for study in the limitating regimes, where it may or may not take negative values.
Then the expression is modified to:

$$V = \phi_1^4 + 2(-1 + \chi_{12})\phi_1^2\phi_2^2 + \phi_2^4 + \xi_{12}\phi_1^3\phi_2 + \xi_{21}\phi_1\phi_2^3. \tag{3.22}$$

Whereas ξ_{12} and ξ_{21} can be splitted into two new variables, in principle this change allows enhancing the algebraic steps. When we are referring to ξ_{12} the next change of variables ought to be used:

$$\xi_{12} \to \xi_1 + \xi_2, \tag{3.23}$$

otherwise, for ξ_{21} the next change must be performed:

$$\xi_{21} \to \xi_1 - \xi_2. \tag{3.24}$$

Now, replacing into potential 3.22:

$$V = \phi_1^4 + 2(-1 + \chi_{12})\phi_1^2\phi_2^2 + \phi_2^4 + (\xi_1 + \xi_2)\phi_1^3\phi_2 + (\xi_1 - \xi_2)\phi_1\phi_2^3. \tag{3.25}$$

We are nearing the conclusion of the modifications to the scalar potential. One of the last steps consists of exploring all possible configurations of the scalar fields to

ensure that the potential does not acquire negative values at infinity. A feasible way to study it is by converting the fields to a polar coordinate system. The polar angle has the advantage that it naturally explores the sign of a sinusoidal function. Therefore, rewriting the scalar fields:

$$\Phi = \begin{pmatrix} \phi_1 \\ \phi_2 \end{pmatrix} \rightarrow \begin{pmatrix} r\cos\theta \\ r\sin\theta \end{pmatrix}, \tag{3.26}$$

here, the degrees of freedom are given by the radial coordinate r and the polar angle θ. Substituting this parametrization into Eq. (3.25), we obtain:

$$\begin{aligned} V =& r^4\cos^4\theta + 2(-1+\chi_{12})r^4\cos^2\theta\sin^2\theta + r^4\sin^4\theta + (\xi_1+\xi_2)r^4\cos^3\theta\sin\theta + \\ &+ (\xi_1-\xi_2)r^4\cos\theta\sin^3\theta. \end{aligned} \tag{3.27}$$

Note that r^4 increases for any value of θ. Then we must restrict the analysis to one centered in the parameters, ξ_1, ξ_2, χ_{12} and θ. Therefore, it is more convenient to use the normalized form of the scalar potential:

$$\begin{aligned} V_{NORM} = \frac{V}{r^4} =& \cos^4\theta + 2(-1+\chi_{12})\cos^2\theta\sin^2\theta + \sin^4\theta + (\xi_1+\xi_2)\cos^3\theta\sin\theta + \\ &+ (\xi_1-\xi_2)\cos\theta\sin^3\theta, \end{aligned} \tag{3.28}$$

furthermore, it can be rewritten in terms of only one sinusoidal function. Using the property:

$$\sin^2\theta + \cos^2\theta = 1 \tag{3.29}$$

$$\sin\theta = \pm\sqrt{1-\cos^2\theta}, \tag{3.30}$$

redefining $\pm$ as a sign, sgn:

$$\begin{aligned} V_{NORM} =& \cos^4\theta + 2(-1+\chi_{12})\cos^2\theta(1-\cos^2\theta) + (1-\cos^2\theta)^2 + \\ &+ sgn(\xi_1+\xi_2)\sqrt{(1-\cos^2\theta)}\cos^3\theta + (\xi_1-\xi_2)\cos\theta(1-\cos^2\theta)^{3/2}sgn^3. \end{aligned} \tag{3.31}$$

In the next step, a rotation by the angle θ will be introduced. Particularly between the fields. By doing so, we can study privileged field directions where the influence of the parameters ξ_1 and ξ_2 becomes more significant.
Taking that into consideration, we are free to apply it to the normalized diagonally scaled scalar potential. For instance, we can leverage a field rotation in $\theta_0 = 3\pi/4$,

since the potential is exactly the same, it doesn't really affect its behavior. Specifically, with this we can explore in a clear way the influence of the asymmetric couplings.
Likewise, it is equivalent to a direct shift in the azimuthal angle just placing it in the cosine function:

$$\begin{aligned} V_{NORM} =& \cos^4(\theta-\theta_0) + 2(-1+\chi_{12})\cos^2(\theta-\theta_0)(1-\cos^2(\theta-\theta_0)) + \\ &+ (1-\cos^2(\theta-\theta_0))^2 + sgn(\xi_1+\xi_2)\sqrt{1-\cos^2(\theta-\theta_0)}\cos^3(\theta-\theta_0) + \\ &+ (\xi_1-\xi_2)\cos(\theta-\theta_0)(1-\cos^2(\theta-\theta_0))^{3/2}sgn^3. \end{aligned} \tag{3.32}$$

With that, the preliminary normalized potential turns into:

$$\begin{aligned} V_{NORM} =& \, 4\cos^2\theta - 4\cos^4\theta - \frac{\xi_1}{2} + \xi_1\cos^2\theta + sgn\cos\theta\sqrt{1-\cos^2\theta}\,\xi_2 \\ &-2sgn\cos^3\theta\sqrt{1-\cos^2\theta}\,\xi_2 + \frac{\chi_{12}}{2} - 2\chi_{12}\cos^2\theta + 2\chi_{12}\cos^4\theta. \end{aligned} \tag{3.33}$$

For instance, let us examine how V_{NORM} behaves for specific values. In Figure 3.1, we observe an unbounded-from-below case, where the black circle represents the plane $Z = 0$. Clearly, there are regions of the potential that take negative values. On the other hand, in Figure 3.2, the potential is bounded from below, as there are no intersections with the black plane, and the curve consistently takes positive values for the tested parameter configurations.

Notice that now V_{NORM} is solely a function of $(\xi_1, \xi_2, \chi_{12}, \theta)$. With the result in 3.33, we proceed to explore and constrain the parameter space in terms of $\xi_{1,2}$ and χ_{12}, analyzing how they regulate the positivity of the diagonally scaled scalar potential.

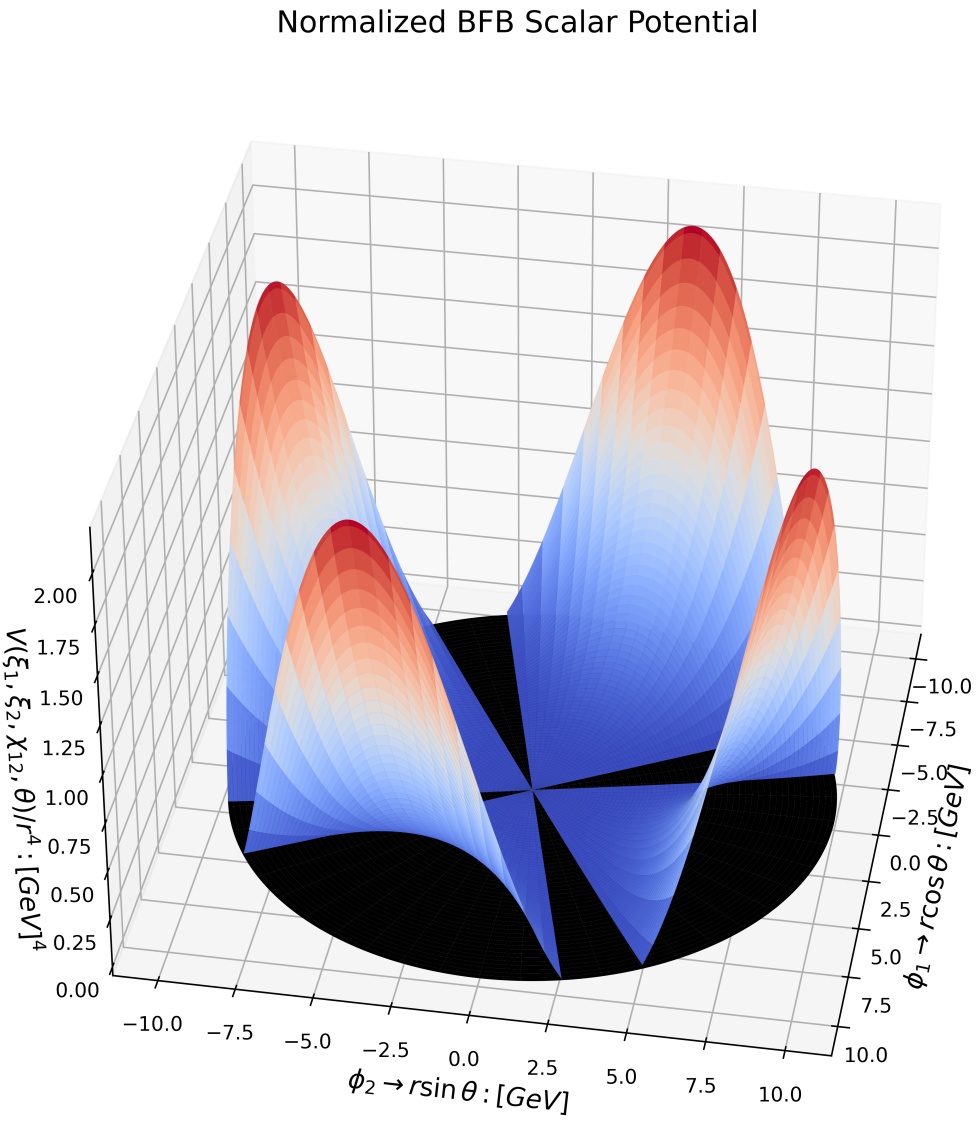

Figure 3.1: Normalized Scalar Potential versus ϕ_1, ϕ_2, the election of parameters: $\xi_1 = 0.05$, $\xi_2 = 4.64$, $\chi_{12} = 2.0$ and $sgn = +1$. gives place to an unbounded from below potential.

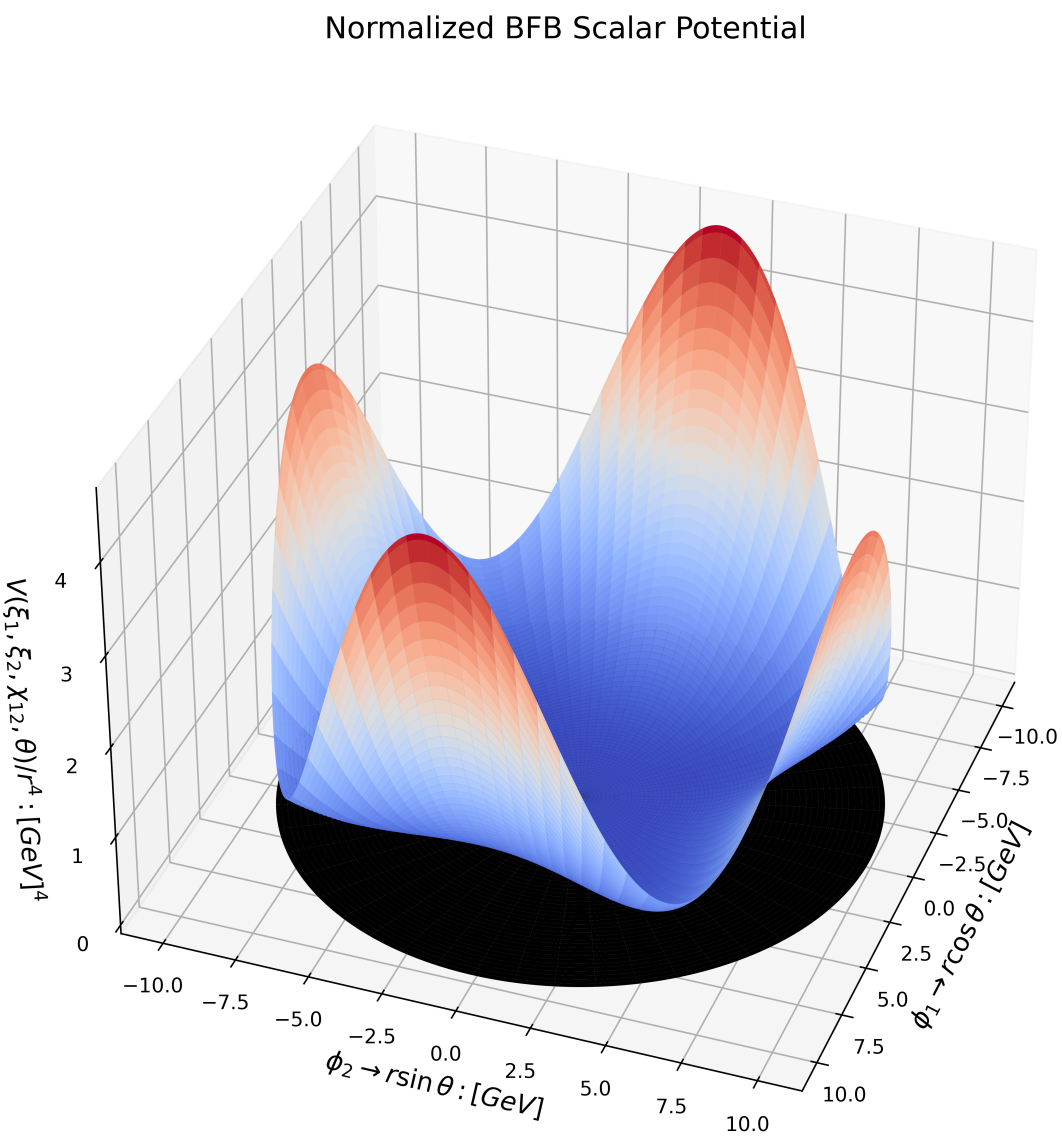

Figure 3.2: Normalized Scalar Potential versus ϕ_1, ϕ_2, with the parameters: $\xi_1 = 0.84$, $\xi_2 = 3.79$, $\chi_{12} = 8.0$ and $sgn = +1$. For this arrangement bounded from below potential takes place.

At this stage in the development of a compact generalization of the potential, it is worth highlighting that the free parameters have been reduced from four λ_{ij} and two κ_{mn} to just ξ_1, ξ_2, χ_{12} and a ± 1 corresponding to sgn. This simplification also

provides a more efficient parameter scan, requiring fewer variables compared to the initial framework.

3.1 Cases at the copositivity threshold $\xi_{i,j} = 0$

The developed algebraic reduction is highly useful for both theoretical and implementation purposes. In the latter case, reducing the number of parameters has a direct impact on the computational efficiency, as it minimizes the complexity of the code and decreases the number of `for` loops required when searching for parameter configurations that satisfy the boundedness-from-below (BFB) conditions of the scalar potential.

In this analysis, we can distinguish three main cases: when κ_{12} and κ_{21} are "fully switched on", when they are "partially switched on" and when they are "turned off". The last case corresponds to the well-defined copositivity, allowing us to neglect it, focusing only on the fully and partially "turned on" scenarios. These cases are managed through the manipulation of the ξ_1 and ξ_2.

3.1.1 Case 1: $\xi_1 = 0$

When $\xi_1 = 0$ the resulting normalized potential acquires the next reduced form:

$$\begin{aligned} V_{NORM,\xi_1=0} =& 4\cos^2\theta - 4\cos^4\theta + sgn\xi_2 \cos\theta\sqrt{1-\cos^2\theta} - 2sgn\xi_2\cos^3\theta\sqrt{1-\cos^2\theta} + \\ &+ \frac{\chi_{12}}{2} - 2\chi_{12}\cos^2\theta - 2\chi_{12}\cos^4\theta. \end{aligned} \tag{3.34}$$

Here, $\cos\theta$ is within the range $[-1,+1]$, sgn corresponds just to ± 1, while χ_{12} could be any given value $\chi_{12} > 0$.
The extrema of this potential can be calculated by setting the first derivatives with respect to $\cos\theta$ to zero, treating it as a variable, as detailed below:

$$\begin{aligned} \frac{\partial V_{NORM,\xi_1=0}}{\partial\cos\theta} =& 8\cos(\theta) - 16\cos^3(\theta) + \frac{sz(1-8\cos^2(\theta)+8\cos^4(\theta))\xi_2}{\sqrt{1-\cos^2(\theta)}} \\ &- 4\cos(\theta)\chi_{12} + 8\cos^3(\theta)\chi_{12} = 0 \end{aligned} \tag{3.35}$$

Finding the extrema values of $\cos\theta$ leads to the set of critical points 3.37, whose cosine values satisfy the above equality. Moreover, when these values are substituted into the scalar potential to evaluate its corresponding potential values, we find at least 18 solutions. Some of them take the following form:

$$V_{\text{NORM},\xi_1=0}\left(-\frac{1}{2}\sqrt{2-\sqrt{2-\frac{2|-2+\chi_{12}|}{\sqrt{\xi_2^2+(-2+\chi_{12})^2}}}},1\right)$$
$$\text{if } -1\leq -\frac{1}{2}\Re\left[\sqrt{2-\sqrt{2-\frac{2|-2+\chi_{12}|}{\sqrt{\xi_2^2+(-2+\chi_{12})^2}}}}\right]\leq 1,$$
$$\text{and } \frac{1}{4}\left(2-\Re\left[\sqrt{2-\frac{2|-2+\chi_{12}|}{\sqrt{\xi_2^2+(-2+\chi_{12})^2}}}\right]\right)\geq 0, \tag{3.36}$$
$$\infty \quad \text{otherwise}$$

We observe that an important restriction arises: the solutions require to be real due to the presence of square roots and absolute values in the arguments. To check all the solutions, refer to Appendix 5.

$$\left\{\begin{array}{l}
\cos(\theta) \to -\frac{1}{2}\sqrt{2-\sqrt{2-\frac{2|-2+\chi_{12}|}{\sqrt{\xi_2^2+(-2+\chi_{12})^2}}}}, \\
\cos(\theta) \to \frac{1}{2}\sqrt{2-\sqrt{2-\frac{2|-2+\chi_{12}|}{\sqrt{\xi_2^2+(-2+\chi_{12})^2}}}}, \\
\cos(\theta) \to -\frac{1}{2}\sqrt{2+\sqrt{2-\frac{2|-2+\chi_{12}|}{\sqrt{\xi_2^2+(-2+\chi_{12})^2}}}}, \\
\cos(\theta) \to \frac{1}{2}\sqrt{2+\sqrt{2-\frac{2|-2+\chi_{12}|}{\sqrt{\xi_2^2+(-2+\chi_{12})^2}}}}, \\
\cos(\theta) \to -\frac{1}{2}\sqrt{2-\sqrt{2+\frac{2|-2+\chi_{12}|}{\sqrt{\xi_2^2+(-2+\chi_{12})^2}}}}, \\
\cos(\theta) \to \frac{1}{2}\sqrt{2-\sqrt{2+\frac{2|-2+\chi_{12}|}{\sqrt{\xi_2^2+(-2+\chi_{12})^2}}}}, \\
\cos(\theta) \to -\frac{1}{2}\sqrt{2+\sqrt{2+\frac{2|-2+\chi_{12}|}{\sqrt{\xi_2^2+(-2+\chi_{12})^2}}}}, \\
\cos(\theta) \to \frac{1}{2}\sqrt{2+\sqrt{2+\frac{2|-2+\chi_{12}|}{\sqrt{\xi_2^2+(-2+\chi_{12})^2}}}}, \\
\cos(\theta) \to 0, \quad \cos(\theta) \to 1, \quad \cos(\theta) \to -1, \quad \cos(\theta) \to \frac{1}{\sqrt{2}}, \quad \cos(\theta) \to -\frac{1}{\sqrt{2}}
\end{array}\right\} \tag{3.37}$$

When evaluating some of the resulting scalar potentials that satisfy the minimization constraints and are also positive definite, meaning they fulfill the BFB condition, we obtain a prototype graph like the one described in Figure 3.3. Here, the light blue region represents the set of positive-definite values of the potential in terms of ξ_2 and χ_{12}. The red dashed line, which encloses the light blue region, corresponds to the curve $2\sqrt{2}\sqrt{\chi_{12}}$.

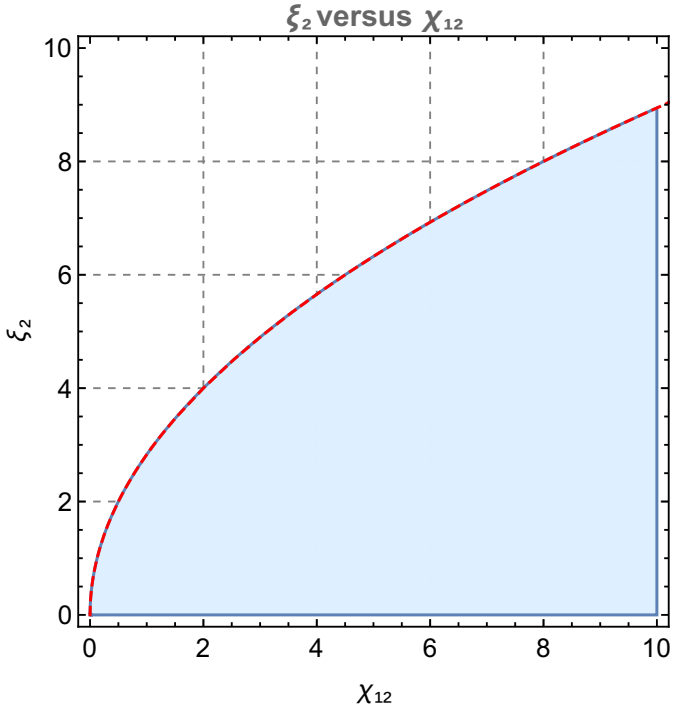

Figure 3.3: Representation of the region that satisfies BFB conditions in $V_{NORM,\xi_1=0}$.

Given the technical difficulty of scanning each individual restriction of the potential $V_{NORM,\xi_1=0}$, it is more convenient to perform a scan over the parameter space and simply verify whether the potential itself is BFB or not. The statistical output of such a procedure is equivalent to analyzing each of the constraints derived in Appendix 5.

After conducting the scan for some values of χ_{12}, it is insightful to plot ξ_2 against χ_{12}, as shown in Figure 3.4, where the red curve with scatter points represents the data. An intriguing pattern emerges for small values of ξ_2, suggesting a square root relationship between χ_{12} and ξ_2, similar to what is observed in Figure 3.3.

Consequently, in Figure 3.4, a "provisional" fit is proposed, expressed as $f(x) = \sqrt{x - 0.44} + 1.21$, shown by the blue curve, where the numerical factors are fitting parameters and x corresponds to χ_{12}. In this particular case, the key takeaway is the existence of a square root-like relationship, independent of any additional refinements.

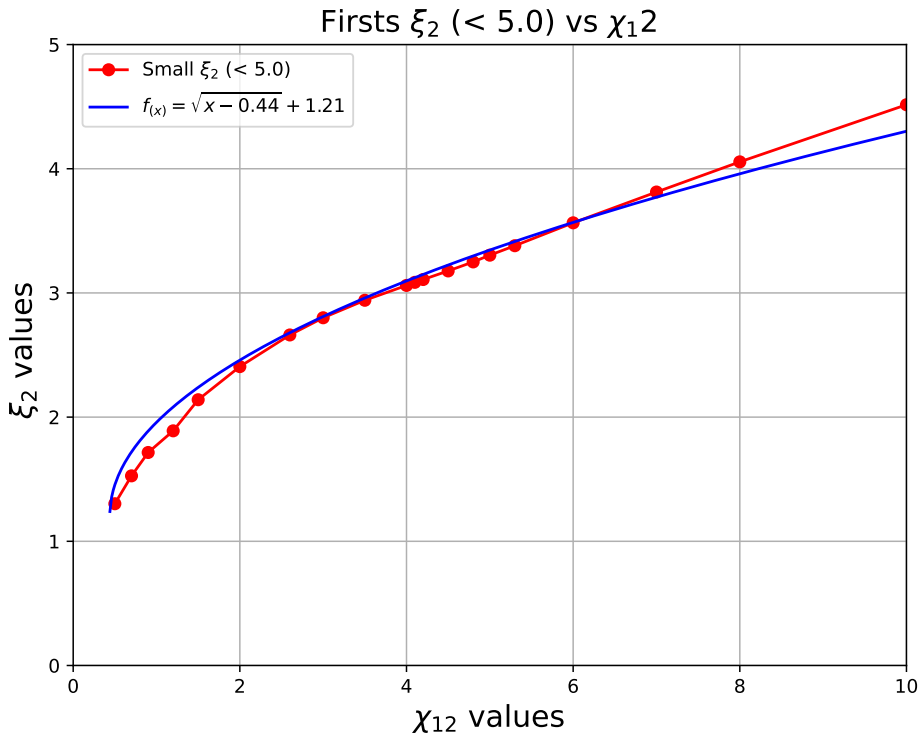

Figure 3.4: The red scatter points represent an average, based on a low sample size, of the ξ_2 values associated with a given χ_{12}. For now, the mismatches in the initial values where $\chi_{12} \leq 2$ can be disregarded, as the information from this plot will not be used in further developments.

At great values of χ_{12}, the parameter ξ_2 increases monotonically, but as it is shown, the important study is located at the first values, where the square root behavior can be observed.
Nevertheless, that assumption needs to be tested in a proper curve fitting analysis.

3.1.2 Case 2: $\xi_2 = 0$

When $\xi_2 = 0$, the scalar potential takes the reduced form:

$$V_{NORM,\xi_2=0} = 4\cos^2\theta - 4\cos^4\theta - \frac{\xi_1}{2} + \xi_1\cos^2\theta + \frac{\chi_{12}}{2} - 2\chi_{12}\cos^2\theta + \\ + 2\chi_{12}\cos^4\theta, \tag{3.38}$$

here, we observe independence from the sign ± 1 , which is evident since the exponent of each sinusoidal function is raised to an even power. Notwithstanding this, there

are two terms involving ξ_1 while the parameter χ_{12} has a strong dependence on the cosines; it represents the interaction with the scalar fields.

Now, it is necessary to find the extreme points of the function V_{NORM,ξ_2}. Therefore, we must differentiate it with respect to the cosine of θ, aiming to determine the field directions that provide meaningful insights for this case. Taking the derivative, we obtain:

$$\frac{\partial V_{NORM,\xi_2=0}}{\partial \cos(\theta)} = 2\cos(\theta)\left(4+\xi_1+4\cos^2(\theta)(-2+\chi_{12})-2\chi_{12}\right). \tag{3.39}$$

Now, setting it to zero to find the extreme points:

$$2\cos(\theta)\left(4+\xi_1+4\cos^2(\theta)(-2+\chi_{12})-2\chi_{12}\right)=0. \tag{3.40}$$

This leads to the following set of solutions:

$$\begin{cases} \cos(\theta)\to 0, & \cos(\theta)\to -\dfrac{\sqrt{-4-\xi_1+2\chi_{12}}}{2\sqrt{-2+\chi_{12}}}, & \cos(\theta)\to \dfrac{\sqrt{-4-\xi_1+2\chi_{12}}}{2\sqrt{-2+\chi_{12}}}, \\ \cos(\theta)\to 1, & \cos(\theta)\to -1, & \cos(\theta)\to \dfrac{1}{\sqrt{2}}, \quad \cos(\theta)\to -\dfrac{1}{\sqrt{2}}. \end{cases} \tag{3.41}$$

Substituting these solutions back into the potential $V_{NORM,\xi_2=0}$, we obtain:

$$V_{NORM,\xi_2=0} = \begin{cases} \frac{1}{2}(-\xi_1+\chi_{12}), \\ \begin{cases} 1+\frac{\xi_1^2}{16-8\chi_{12}}, & -2\le \Re\left(\frac{\sqrt{-4-\xi_1+2\chi_{12}}}{\sqrt{-2+\chi_{12}}}\right)\le 2, \\ & (4+\xi_1-2\chi_{12})\Re\left(\frac{1}{-2+\chi_{12}}\right)\le 0, \\ \infty, & \text{otherwise} \end{cases} \\ \frac{\xi_1+\chi_{12}}{2}, \quad \frac{\xi_1+\chi_{12}}{2}, \quad 1, \quad 1 \end{cases} \tag{3.42}$$

The solutions that extremize the potential exhibit high complexity, which, on the one hand, can cause immediate divergence, or, on the other, require taking the real part of complex terms, as shown in expression 3.42.
Taking these solutions into account, we can construct a "mini" region-plot, displayed in Figure 3.5. In this case, we evaluate 200 potentials that satisfy the conditions in equation 3.42 and are also BFB.

We observe that for small values of χ_{12}, there is an approximately linear behavior. However, for slightly larger values, such as in the case of the red dashed line, the BFB region in the region-plot follows the function $2\sqrt{2}\sqrt{x-2}$.
To carry out a more thorough study, it is necessary to obtain results from thousands of BFB and non-BFB scalar potentials. With these, we can provide a more definitive answer. For this reason, among others, the highly discussed scan has to be performed.

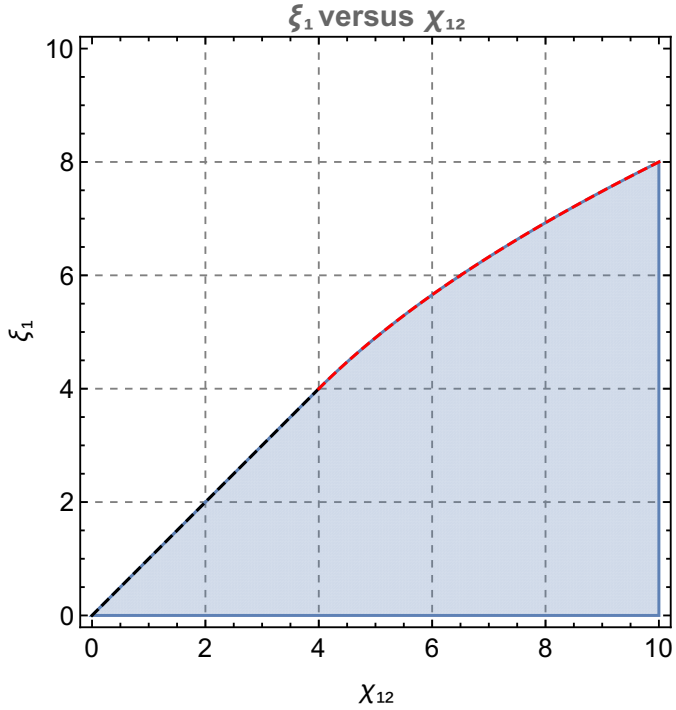

Figure 3.5: The dashed black line corresponds to a linear behavior, while the red dashed line follows a square root trend.

Once the scan is completed, our focus shifts to plotting the parameters ξ_1 versus χ_{12}, in a similar manner, and specially focused on relatively "short" values of $\chi_{12} \leq 4$.
In Figure 3.6, the data is represented by the blue dashed line. If we disregard the "anomalies" within the range $\chi_{12} = [0.9, 1.5]$, the data suggests a linear trend. Consequently, a linear curve fitting is reasonable, depicted by the red curve; for instance, we may express it as $y = \frac{1}{2}x$, where the slope is $1/2$ and the y-intercept is $y = 0$.

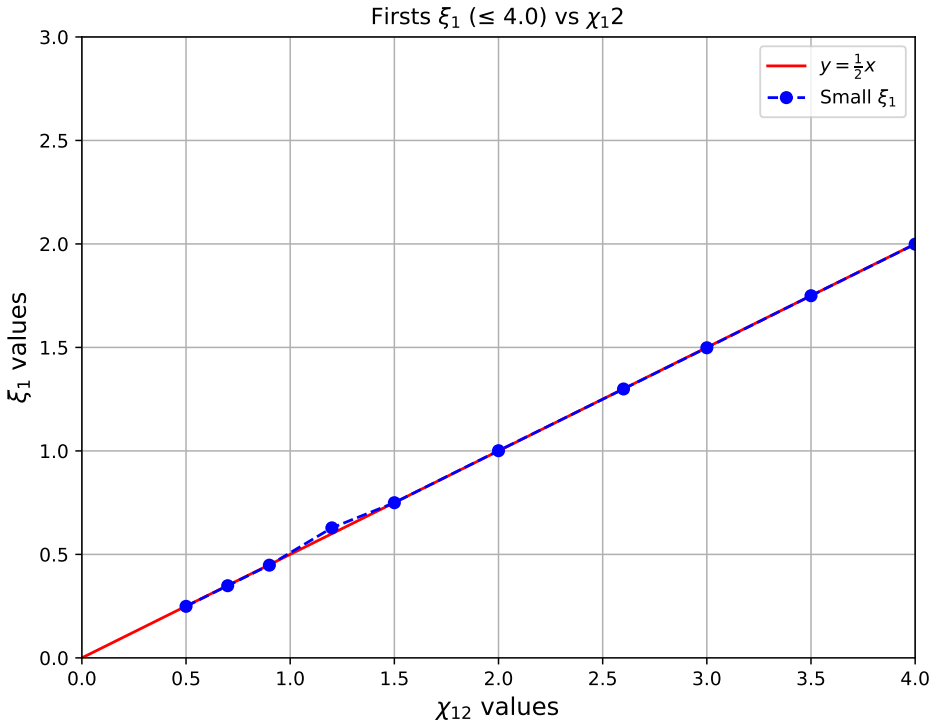

Figure 3.6: Relation between "small" values of ξ_1 and χ_{12}, represented by the dashed blue line. Additionally, the data follows a linear equation, depicted in red.

3.2 BFB in the Scalar Potential (Case 3 $\xi_1, \xi_2 \neq 0$)

For the results presented in this section, an exhaustive search was conducted over thousands of possible configurations for scalar potentials associated with a given χ_{12}, including both BFB and non-BFB cases. Once finishing the scan, the analysis will be centered on the behavior of the κ_{ij} terms and their influence on the copositivity matrix, given that they cannot be incorporated into it. More specifically, the study will examine ξ_1 and ξ_2.

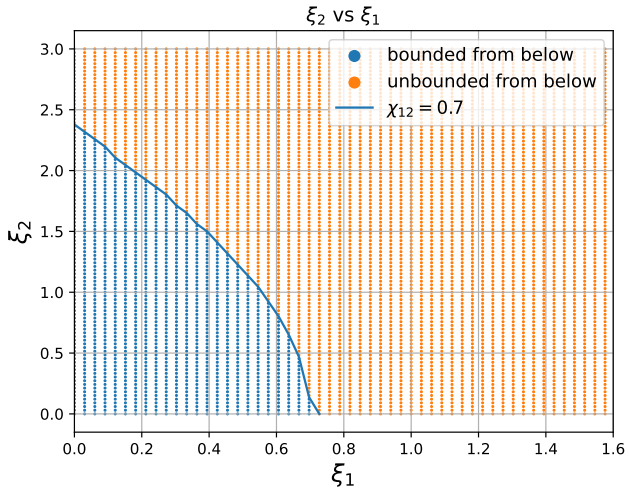

Figure 3.7: Scatter plot with $\chi_{12} = 0.7$.

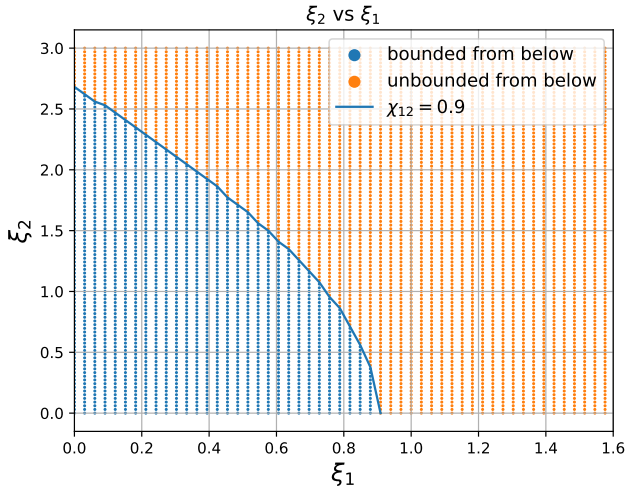

Figure 3.8: Scatter plot with $\chi_{12} = 0.9$.

In Figures 3.7 and 3.8, we observe the behavior of ξ_2 versus ξ_1 for two small values of χ_{12}. Each point in the scatter plots corresponds to a scalar potential. In both cases, we see that there are configurations of ξ_1 and ξ_2 that result in a bounded-from-below scalar potential, while others lead to an unbounded-from-below potential. In these plots, the blue scatter points represent bounded-from-below combinations, whereas the orange points correspond to unbounded combinations. While the solid blue line represents the interface separating both stability scenarios, whose behavior and po-

sition change as χ_{12} increases.

On the other hand, in large values of χ_{12}, the ξ_2 versus ξ_1 scatter plot behaves differently. Now we observe that the relation is more linear rather than quadratic or square root, as in the previous case, suggesting that the behavior at both short and large ranges of ξ_i values can be validated through a simulation. Again, the points below the interface blue line are bounded from below, while the points that are located above the line correspond to potentials that are unbounded from below. For instance, in Figures 3.9 and 3.10, the value of χ_{12} is $\chi_{12} = 7$ and $\chi_{12} = 15$ respectively. It is key to remark that the blue χ_{12} line just indicates the upper and lower limits of the boundedness.

Reconsidering the paradigm, if we find the interface curve for a given χ_{12}, then we can automatically determine the bounded and unbounded sector, thereby considerably reducing the computational effort and time. Of course, proposing this will allow us to gain independence from the two regimes of χ_{12}, drifting our work to a generalization.

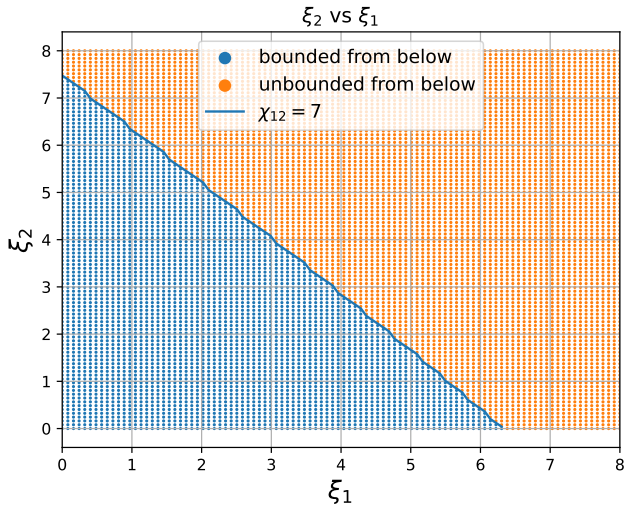

Figure 3.9: Scatter plot with $\chi_{12} = 7$.

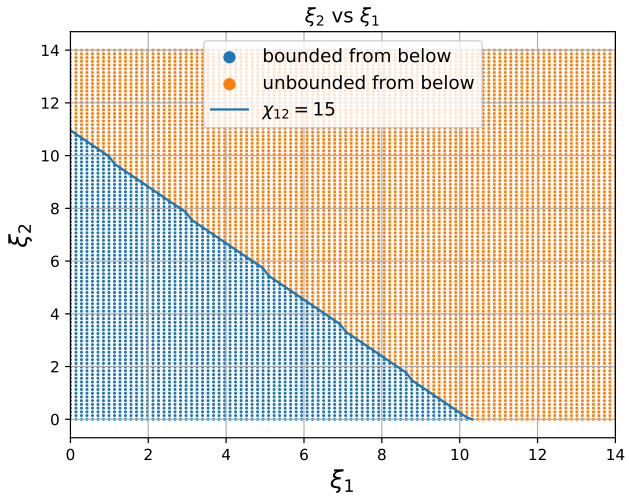

Figure 3.10: Scatter plot with $\chi_{12} = 15$.

Improving the searching technique

As the last paragraph states, here is presented an attempt to optimize searching for where the limit between physical and unphysical scenarios is.
In this way, we hope to find the interface between bounded and unbounded scenarios with an easier method which saves time in the optimization process, instead of

exploring the entire ξ_1-ξ_2 parameter space.
Basically, it consists of replacing the brute scan with a bounded area search, which forms a parallelogram; therefore, the code responsible for finding such bounded and unbounded potentials is limited to a specified area. For instance, we shall assume that the curve for small χ_{12} values can be indeed modeled as a function of the type $y = \sqrt{1-x}$, while the curve for large χ_{12} values can be represented by a linear equation $y = 1 - x$. More specifically, $\xi_2 = \sqrt{1-\xi_1}$ and $\xi_2 = 1 - \xi_1$, respectively for $\chi_{12small}$ and $\chi_{12large}$.

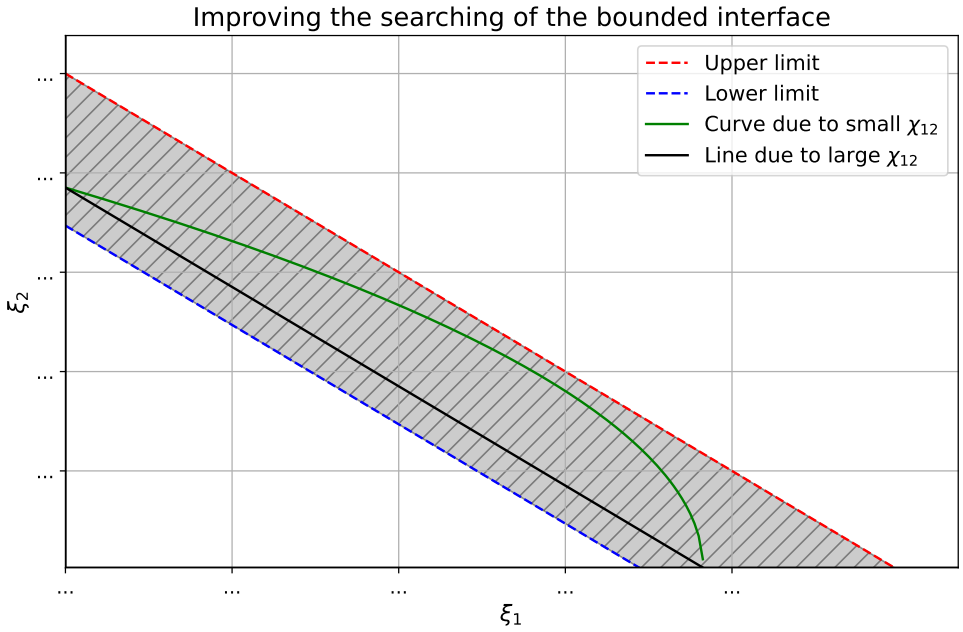

Figure 3.11: Illustration of both curves, for large and small χ_{12} overlapping in the same position although they behave different for such scale.

In Figure 3.11, just for illustrative purposes, it is shown that the curves are overlapped into the same extrema of ξ_1 and ξ_2 positions, although their shapes belong to a different ξ_i configuration . Here the green plot corresponds to short χ_{12} values, the black line is related to the curve of great values of χ_{12}, while the dashed lower blue line is a shift indicating a part of the bfb sector; on the other side, we have the dashed red line in the upper side which indicates part of the unbounded sector. The gray dashed area, which forms a parallelogram, allows us to reduce considerably the scanning space, ξ_1-ξ_2 in where to look for.

Implementing such a technique helped us to perform a scan in a huge parameter space of $\xi_1 - \xi_2$ for different values of χ_{12}.

3.3 Main results

This section presents the most relevant developments regarding to the ξ_1-ξ_2 space. Specifically, it shows the behavior of several χ_{12} curves and proposes a possible curve fitting.

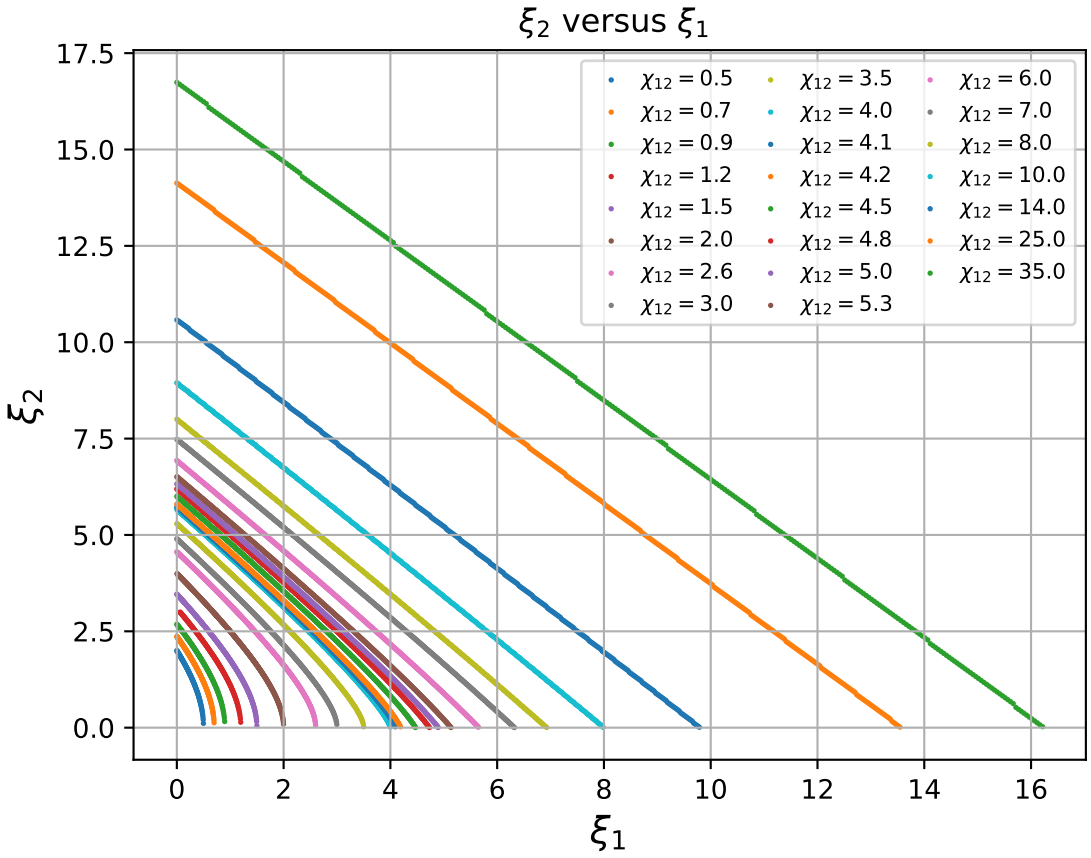

Figure 3.12: Twenty-three curves of ξ_2 vs. ξ_1, each one associated with a specific χ_{12}.

In the Figure 3.12 is shown the scatter plot which illustrates the interface section for 23 different cases. It is possible to observe a zone of higher density around $\xi_1 \to [4, 6]$ and $\xi_2 \to [5, 7.5]$. This is not a coincidence, as it is precisely at that sector where the curves seem to start behaving from a squared root to a linear function. In consequence, that well-populated zone is fundamental to infer a nice adjust.

To derive a function that encompasses both small and large values of χ_{12}, a normalization to one will be applied to the previous scatter plot.

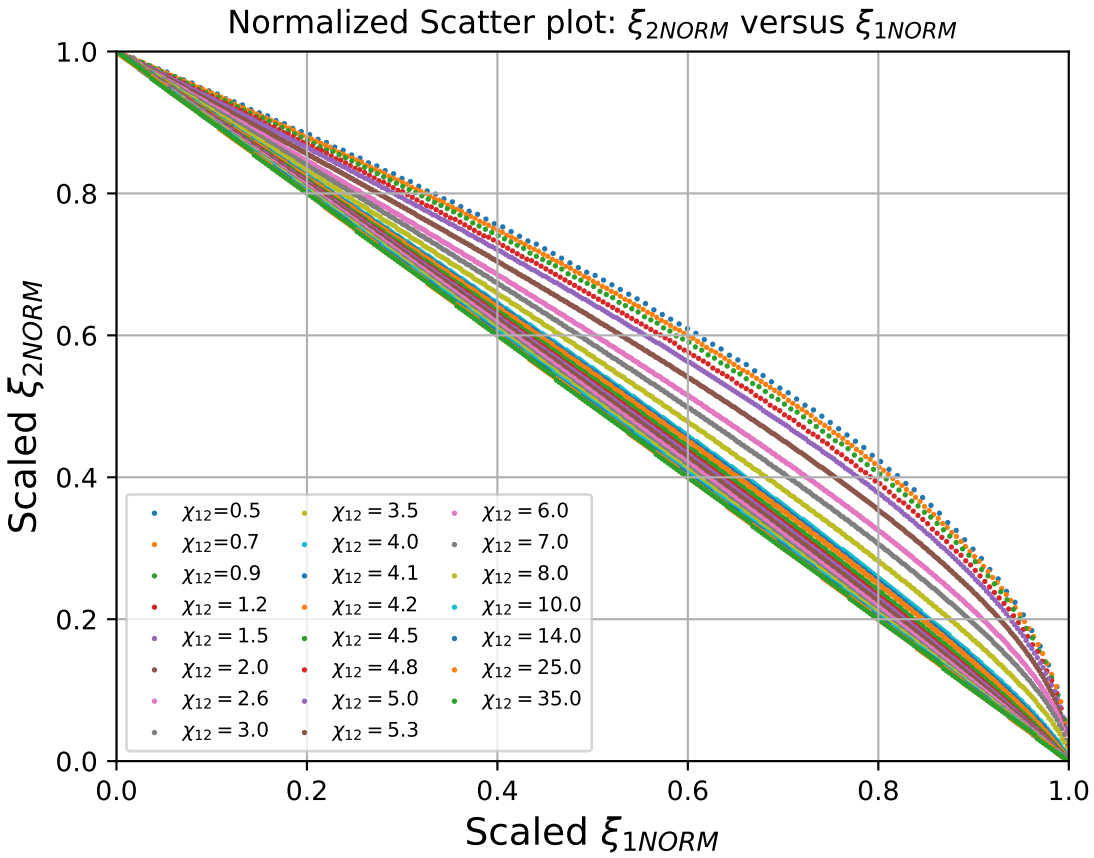

Figure 3.13: Normalized scatter plot of 23 different χ_{12} curves.

Figure 3.13 confirms what was already anticipated in plot 3.12: each scatter plot for a given χ_{12} appears to follow a combination of a linear function and a square root function. For large χ_{12} values, the behavior is predominantly linear, whereas

for small χ_{12} values, it aligns exclusively with a square root curve. This outcome is quite intuitive, given the assumption of the superposition principle.
In table 3.1 is presented the data for every ξ_1 and ξ_2 according to each χ_{12} as well as their normalized values. Among other things, this data was used to construct scatter plot 3.13.

ξ_1	ξ_2	χ_{12}	ξ_{1NORM}	ξ_{2NORM}
0.000000	1.999399	0.5	0.000000	0.999699
0.004409	1.990581	0.5	0.008818	0.995291
0.008818	1.981764	0.5	0.017635	0.990882
0.013226	1.968537	0.5	0.026453	0.984269
0.017635	1.959719	0.5	0.035271	0.979860
⋮	⋮	⋮	⋮	⋮
16.016016	0.225225	35.0	0.985718	0.013460
16.066066	0.175175	35.0	0.988798	0.010469
16.116116	0.125125	35.0	0.991878	0.007478
16.166166	0.075075	35.0	0.994959	0.004487
16.216216	0.025025	35.0	0.998039	0.001496

Table 3.1: Sample data of ξ_1, ξ_2, χ_{12}, ξ_{1NORM}, and ξ_{2NORM}.

Certainly, it is possible to identify a curve fit directly in Figure 3.13, but it somehow becomes more straightforward when the data aligns with one of the axes. A more practical way to interpret it is by rotating the upper corner points to coincide with the origin of coordinates in the X axis; in other words, it is equivalent to applying a simple rotation to every point in scatter-plot.

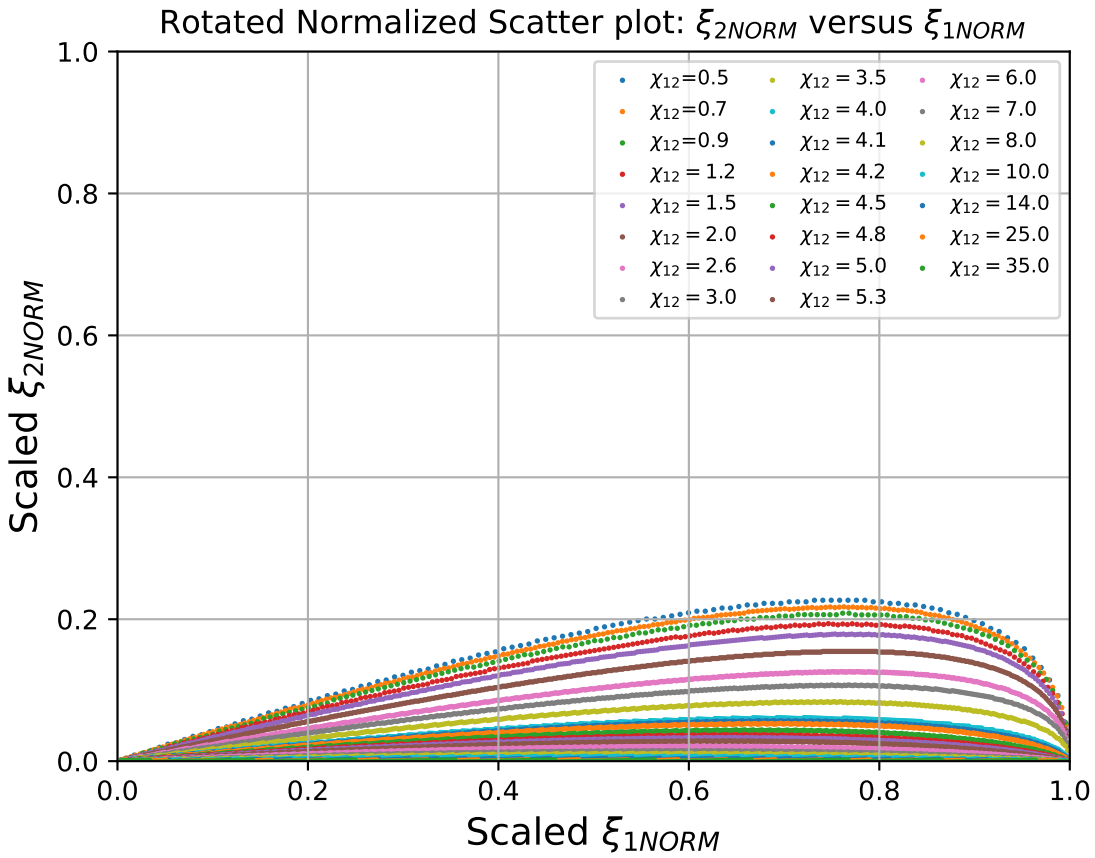

Figure 3.14: Rotated interfaces curves of χ_{12} which defines the limit of BFB.

Here, in Figure 3.14, $\chi_{12} = 35.0$ corresponds to the horizontal line at $\xi_2 = 0$, while $\chi_{12} = 0.5$ matches with a totally curved shape.

3.3.1 First attempt

An interesting case arises when the underlying curve fit adheres to the relation introduced much earlier, naturally considering the superposition principle:

$$y = \alpha(1 - x) + (1 - \alpha)\sqrt{1 - x}, \tag{3.43}$$

where y coincides with scaled ξ_2, x with scaled ξ_1, and α is a weighting parameter that ranges from 0 to 1. Thus, when α is equal to 0, the ξ_2 vs. ξ_1 plot corresponds

to a 100% curve-shaped scenario, and when it is equal to 1, it represents a purely linear case.
For instance, we can study its accuracy for a random χ_{12}, let us say $\chi_{12} = 0.9$. Consequently, in Table 3.2, the corresponding values of $\xi_{1,2}$ and $\xi_{1,2\mathrm{NORM}}$ are shown for this arrangement of data with respect to $\chi_{12} = 0.9$.

ξ_1	ξ_2	χ_{12}	ξ_{1NORM}	ξ_{2NORM}
0.006012	2.672345	0.9	0.006680	0.995924
0.012024	2.660321	0.9	0.013360	0.991443
0.018036	2.648297	0.9	0.020040	0.986962
0.024048	2.642285	0.9	0.026720	0.984721
0.030060	2.630261	0.9	0.033400	0.980240
⋮	⋮	⋮	⋮	⋮
0.871743	0.417836	0.9	0.968604	0.155718
0.877756	0.375752	0.9	0.975284	0.140034
0.883768	0.315631	0.9	0.981964	0.117629
0.889780	0.249499	0.9	0.988644	0.092983
0.895792	0.159319	0.9	0.995324	0.059375

Table 3.2: Sample data of ξ_1, ξ_2, χ_{12}, ξ_{1NORM}, and ξ_{2NORM}.

The idea now is to test whether the proposed fit is capable of achieving a root mean square error (RMSE) value that is not excessively large. The RMSE is given by:

$$\mathrm{RMSE} = \sqrt{\frac{1}{n}\sum_{i=1}^{n}(X_i - x_0)^2}. \tag{3.44}$$

Here, x_0 corresponds to the true mean value, n to the available data, and X_i represents a sample population. In our case, X_i is $\xi_{2\mathrm{NORM}}$, and x_0 is the fit applied to each point on the X-axis, which is equivalent to $\xi_{1\mathrm{NORM}}$ values, and remaining α constant.
In Figure 3.17b, can be observed the resulting curve fitting and, at first glance, the fit aligns quite well with the data. Nonetheless, in the logarithmic error, some inhomogeneities appear. Ideally, the RMSE should remain below -3.0, which would indicate a very low uncertainty. Despite that, there are parts where it exceeds $\log_{10}\mathrm{RMSE} \sim -2.3$, suggesting an accuracy of only two decimal places between the sampled and actual data.

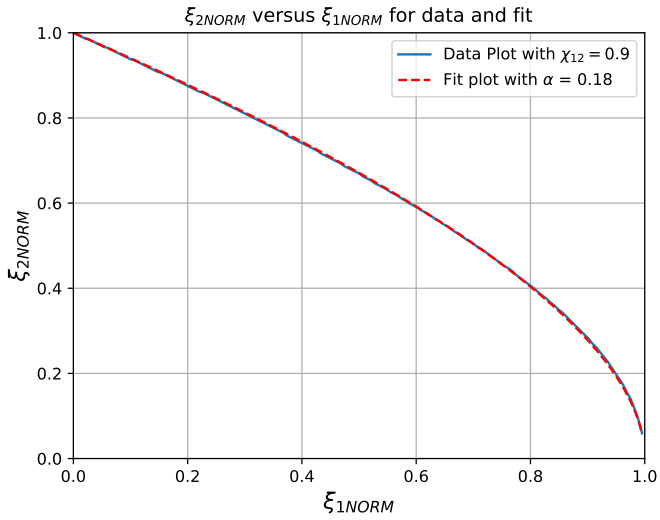

(a) $\xi_{2\text{NORM}}$ vs $\xi_{1\text{NORM}}$ for a fixed $\chi_{12} = 0.9$, alongside the corresponding fit for this χ_{12}.

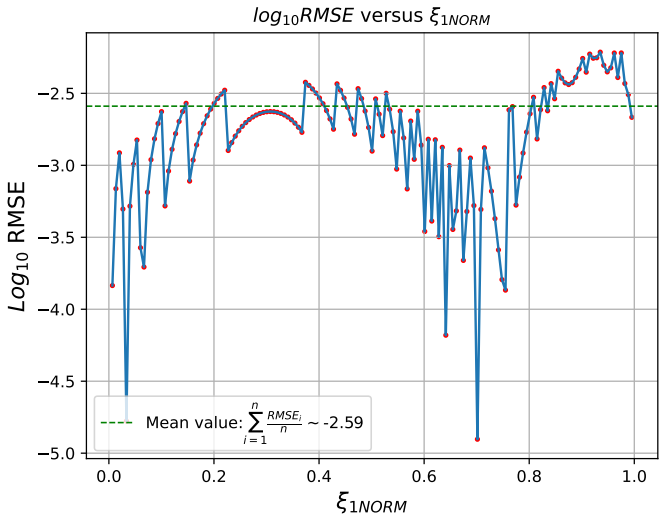

(b) Logarithmic root mean squared error with respect to $\xi_{1\text{NORM}}$.

Figure 3.15: Combined visualizations of data fitting and error analysis.

On the other hand, the same model can be used, but this time with a slightly larger value of χ_{12}, where the linear-like behavior is already noticeable. For this case, use $\chi_{12} = 5.0$ as it is shown in Figure 3.16.

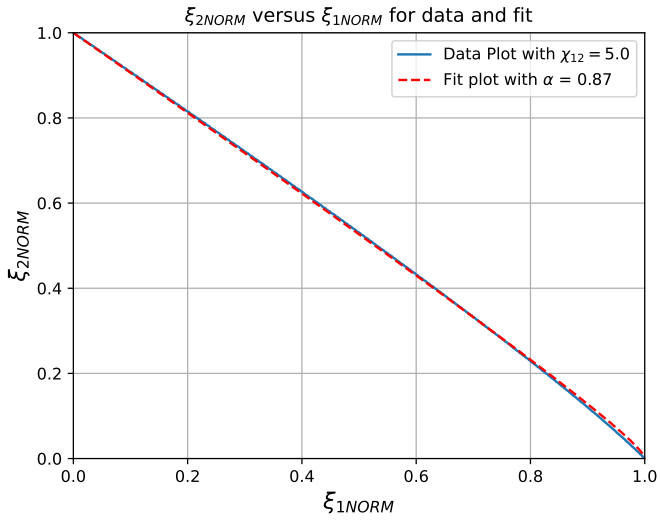

(a) $\xi_{2\text{NORM}}$ vs $\xi_{1\text{NORM}}$ for $\chi_{12} = 5.0$, where the blue curve represents the data and the red curve corresponds to the fit.

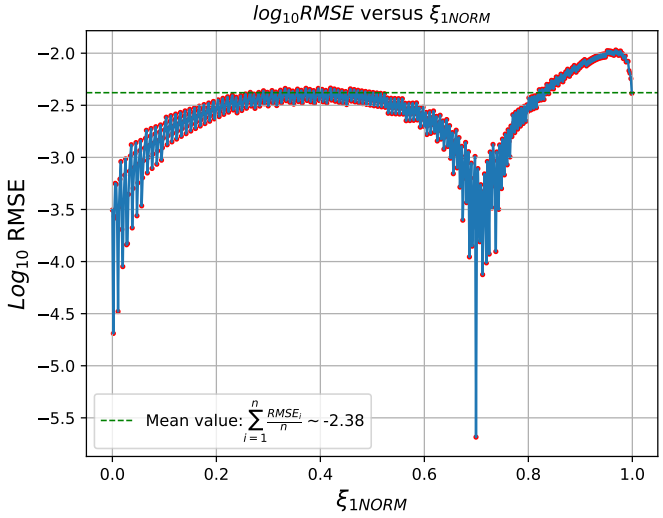

(b) Logarithmic root mean squared error with respect to $\xi_{1\text{NORM}}$.

Figure 3.16: Combined visualizations of data fitting and error analysis when $\chi_{12} = 5.0$.

Let us analyze the case where $\chi_{12} = 5.0$. Once again, it is observed that the fit performs reasonably well; however, the RMSE increases significantly near the value of $\xi_{1\text{NORM}} = 1.0$.

Taking the average value of the RMSE errors from Figure 3.15, it roughly reaches the value of $\sum_{i=1}^{n} \frac{\text{RMSE}_i}{n} \sim -2.6$, while in Figure 3.16, the value is $\sum_{i=1}^{n} \frac{\text{RMSE}_i}{n} \sim -2.4$, for χ_{12} equal to 0.9 and 5.0, respectively.
These results indicate that the fit is still not sufficiently precise. As mentioned earlier, the correlation between the data only reaches two decimal places, resulting in a loss of accuracy at lower orders.

3.3.2 Second attempt

In the following framework, it is useful to reuse the previous fitting attempt. As we have observed, combining a square root function with a linear equation seems to be the most logical approach. However, what if the uncertainty close to one arises because the square root is not as precise as expected? In such a case, we shall perform a correction in the power of that term, as follows:

$$y = \alpha(1-x) + (1-\alpha)(1-x)^{\frac{1}{2}-\gamma_0}. \tag{3.45}$$

Where γ_0 is just a shift parameter. Therefore, our curve fit has two parameters, α and γ_0. This last variable also serves to provide information on how far from the squared root behavior the correct data could be located.

In Figure 3.17 one can observe how perfectly the red and blue curves match each other. A clear hint that the change performed in the exponent helped to increase the precision. Also, this new framework improves the RMSE to a value of -3.07; however, it can be even better as it will be explained in the third attempt.

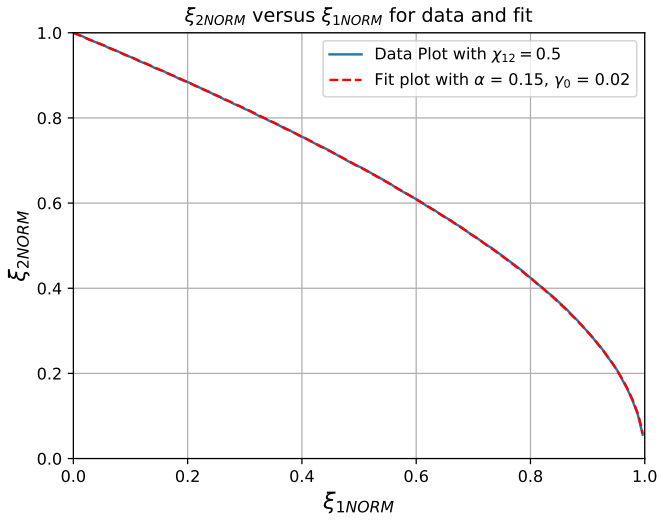

(a) $\xi_{2\text{NORM}}$ vs $\xi_{1\text{NORM}}$ for a fixed $\chi_{12} = 0.5$, alongside the corresponding fit for this χ_{12}.

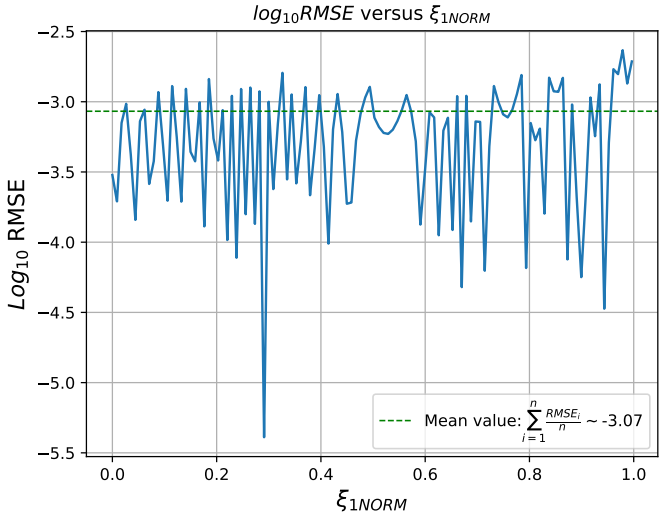

(b) Logarithmic root mean squared error with respect to $\xi_{1\text{NORM}}$. Its mean value is roughly -3.07.

Figure 3.17: Combined visualizations of data fitting and error analysis when $\chi_{12} = 0.5$.

3.3.3 Third attempt

If the influence of γ_0 is weighted in $(1-x)^{\frac{1}{2}}$, it would also be natural to consider it in $(1-x)$.

Similarly, the average error in the previous case falls within the barely acceptable range. Here, we propose a fit that gains generality and introduces a regularization factor for both terms.

$$y_{(x)} = \alpha(1-x)^{\frac{1}{\gamma_0}} + (1-\alpha)(1-x)^{\frac{1}{2}\gamma_0}. \tag{3.46}$$

Suggesting that the factor $\frac{1}{\gamma_0}$ is associated with the term $(1-x)^1$, while the factor γ_0 is applied to the term $(1-x)^{\frac{1}{2}}$. One is the reciprocal of the other, ensuring that in regimes dominated by linear behavior, γ_0 approaches one from the right, while in regions where the curve due to a square root dominates, γ_0 approaches one from the left.
It is advantageous to mention that this choice will become the definitive fit, primarily due to achieving the lowest RMSE across all curves associated with the different choices of χ_{12}.
In Figure 3.18, one can appreciate that the fit for the χ_{12} curve is practically identical to the real data. Additionally, in Figure 3.18b, the logarithmic RMSE calculation and the averaging of all points reveal an outstanding precision of three decimal places between the ξ_{2NORM} data and the fit $y_{(x)}$.

In a more linear-like regime, such as the case with $\chi_{12} = 2.0$ illustrated in Figure 3.19, a combination of both behaviors: linear and curved emerges, and the fit reasonably matches the ξ_{2NORM} data. Similarly to the previous case, the mean value of the logarithmic RMSE reaches ~ -3.39, indicating that the precision achieved is highly satisfactory.

When $\chi_{12} = 4.8$, $\chi_{12} = 6.0$ and $\chi_{12} = 14.0$, as shown in Figures 3.20, 3.21 and 3.22, it is observed a similar behavior with the exception that the linear trend now begins to dominate almost entirely. The fit performs well once again, with the RMSE remaining below ~ -3.3. However, at this point, slight peaks appear for $Log_{10}RMSE$ when ξ_{1NORM} values are near to one, being this a very recurring feature of the fit, as we have seen before. For example, it also appears in the previous cases for other χ_{12} curves.

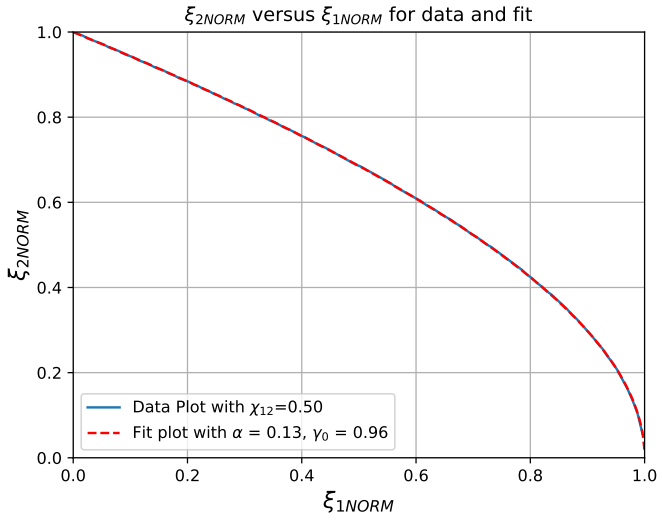

(a) $\xi_{2\mathrm{NORM}}$ vs $\xi_{1\mathrm{NORM}}$ for a fixed $\chi_{12} = 0.5$, alongside the corresponding fit for this χ_{12}.

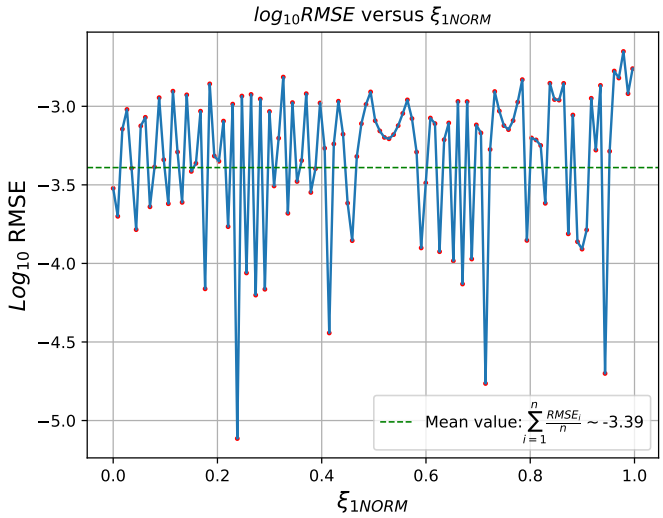

(b) Logarithmic root mean squared error with respect to $\xi_{1\mathrm{NORM}}$. Worth to mention that the mean value achieved is -3.39 in log scale.

Figure 3.18: Combined visualizations of data fitting and error analysis when $\chi_{12} = 0.5$.

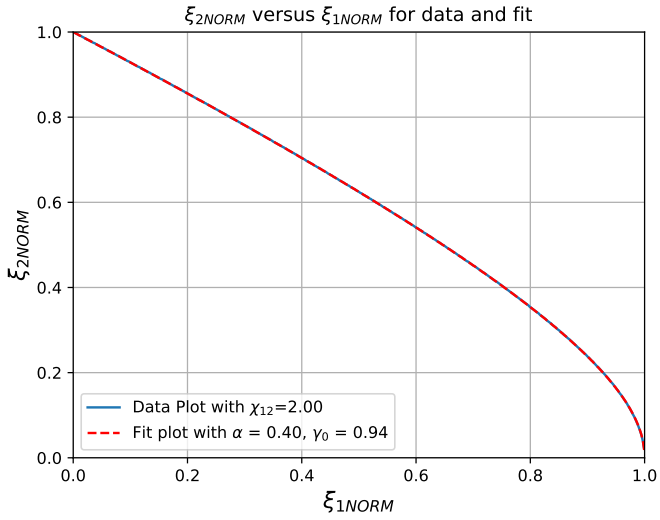

(a) $\xi_{2\mathrm{NORM}}$ vs $\xi_{1\mathrm{NORM}}$ for $\chi_{12} = 2.0$, with the empirical data in blue and the fitted curve in red.

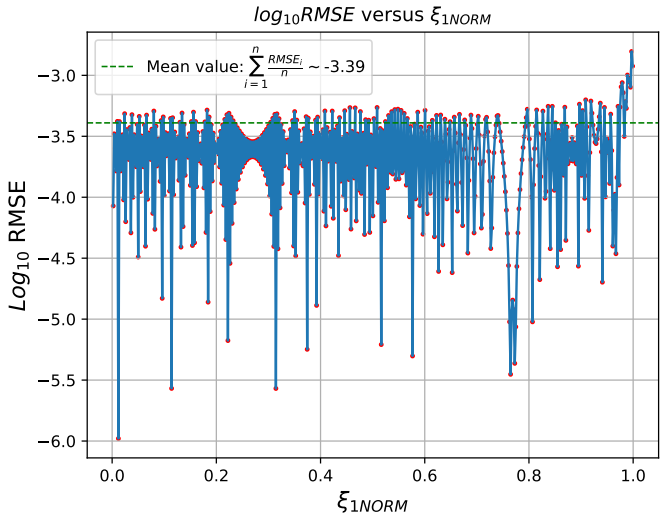

(b) Logarithmic root mean squared error with respect to $\xi_{1\mathrm{NORM}}$. Notably, the mean value attained is -3.39 in log scale.

Figure 3.19: Combined visualizations of data fitting and error analysis for $\chi_{12} = 2.0$.

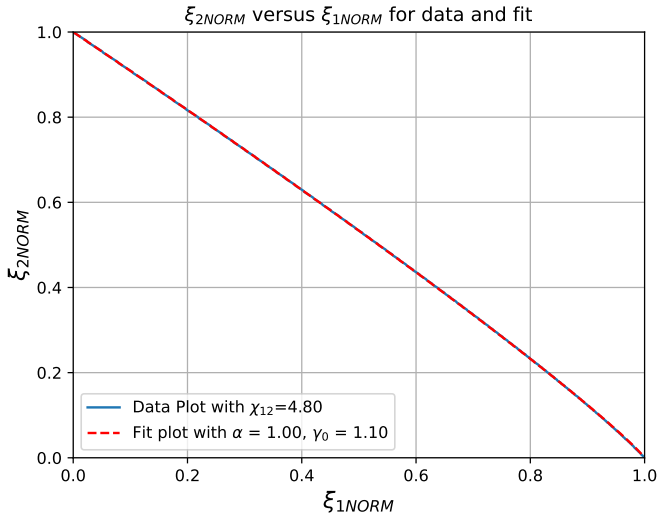

(a) $\xi_{2\text{NORM}}$ vs $\xi_{1\text{NORM}}$ for a fixed $\chi_{12} = 4.8$, alongside the corresponding fit for this χ_{12}.

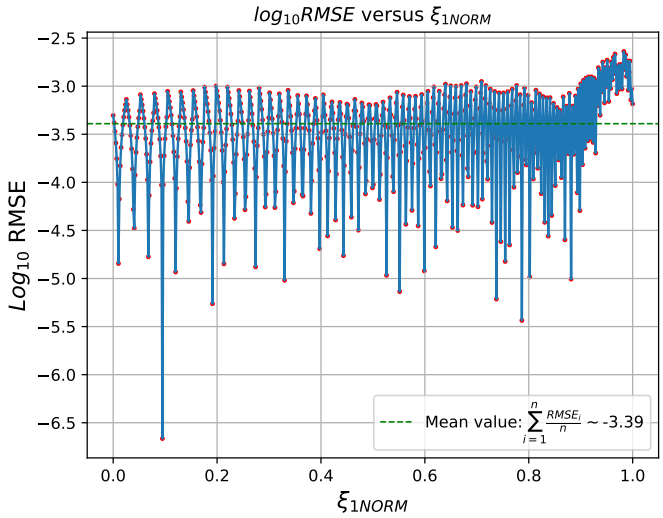

(b) Logarithmic root mean squared error with respect to $\xi_{1\text{NORM}}$, with a mean value of -3.39 in log scale, exhibiting a peak around (1.0, -3.0).

Figure 3.20: Combined visualizations of data fitting and error analysis.

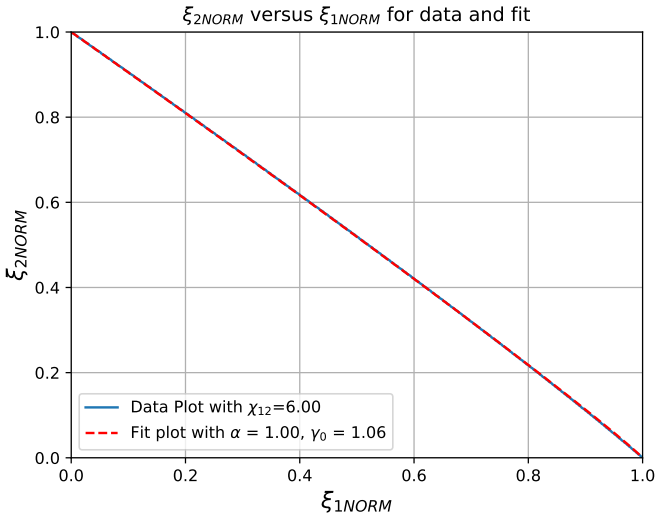

(a) Comparison of $\xi_{2\mathrm{NORM}}$ vs $\xi_{1\mathrm{NORM}}$ for $\chi_{12} = 6.0$, with the empirical data in blue and the fitted curve in red. These practically coincide.

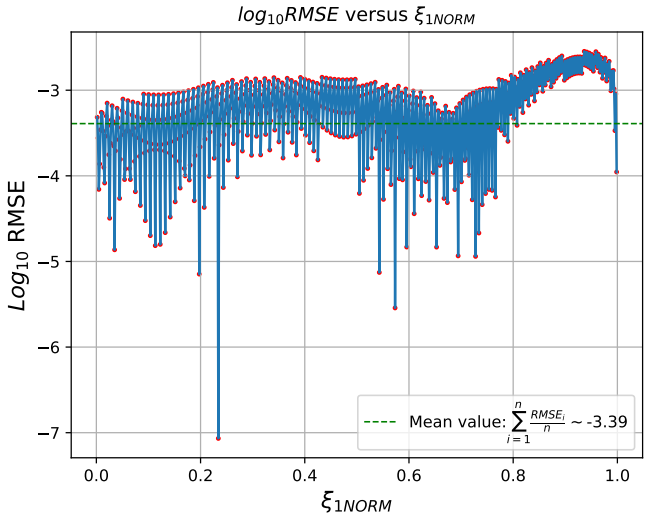

(b) Logarithmic root mean squared error with respect to $\xi_{1\mathrm{NORM}}$. Worth to mention that the mean value achieved is -3.39 in log scale.

Figure 3.21: Combined visualizations of data fitting and error analysis.

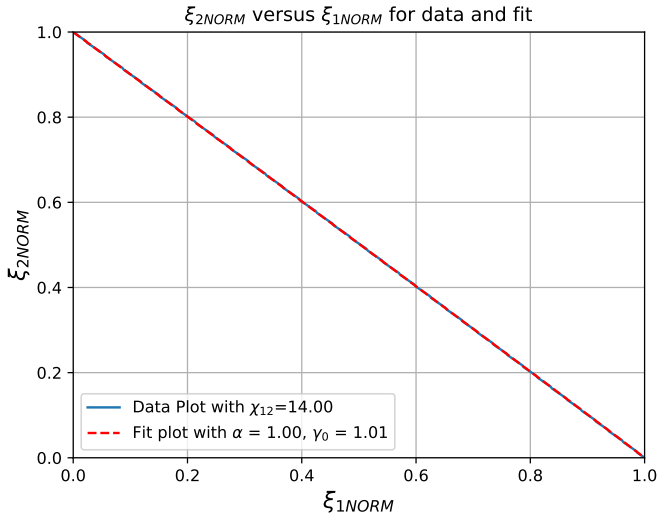

(a) $\xi_{2\text{NORM}}$ vs $\xi_{1\text{NORM}}$ for a fixed $\chi_{12} = 14$, alongside the corresponding fit for this χ_{12}.

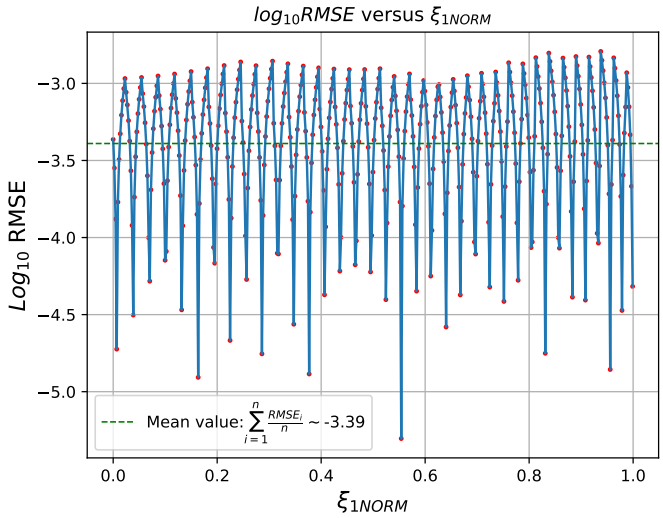

(b) Logarithmic root mean squared error with respect to $\xi_{1\text{NORM}}$. Worth to mention that the mean value achieved is -3.39 in log scale.

Figure 3.22: Combined visualizations of data fitting and error analysis.

In Figure 3.23, the Standard Deviation for each χ_{12} is illustrated, providing insight into how far the chosen curve fit deviates from the sample data. For the initial

values along the X-axis, most of the fitted data remains close to their mean value, achieving an accuracy of up to three decimal places. This highlights the effectiveness of the proposed fit, reaching an outstanding precision for $\chi_{12} = 2.0$ with a standard deviation of approximately $\sigma \sim 0.000322$.
On the other hand, for $\chi_{12} = \{0.9, 5.3, 6.0, 7.0, 8.0, 35.0\}$, the deviation is slightly higher. A plausible explanation for this effect in the range of $\chi_{12} = [5.3 - 8.0]$ could be the observed increase in the RMSE near the normalized value of $\xi_{1NORM} \sim 1.0$, as shown in Figure 3.21 among others. It is worth noting that this effect is consistently present in almost all RMSE plots and becomes more prominent within the aforementioned range.

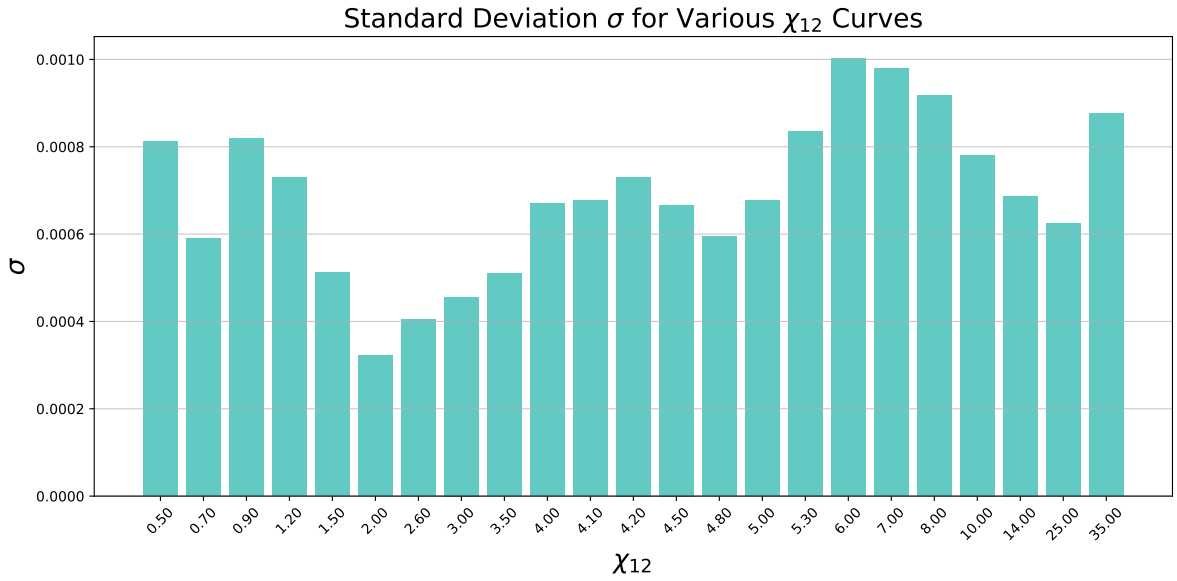

Figure 3.23: Standard Deviation for every sampled χ_{12}.

Another strong indicator that the proposed curve fitting is the correct one is the close relationship between the fitting coefficients, α and γ_0, when plotted against χ_{12}, as shown in Figure 3.24. Initially, in the range $\chi_{12} = [0, 5]$, a sustained "almost linear" growth of α is observed, while in the same range, γ_0 exhibits a behavior similar to a quadratic curve. Later, both parameters harmonize and stabilize at 1, which is naturally related to the fact that they represent a percentage—100%.

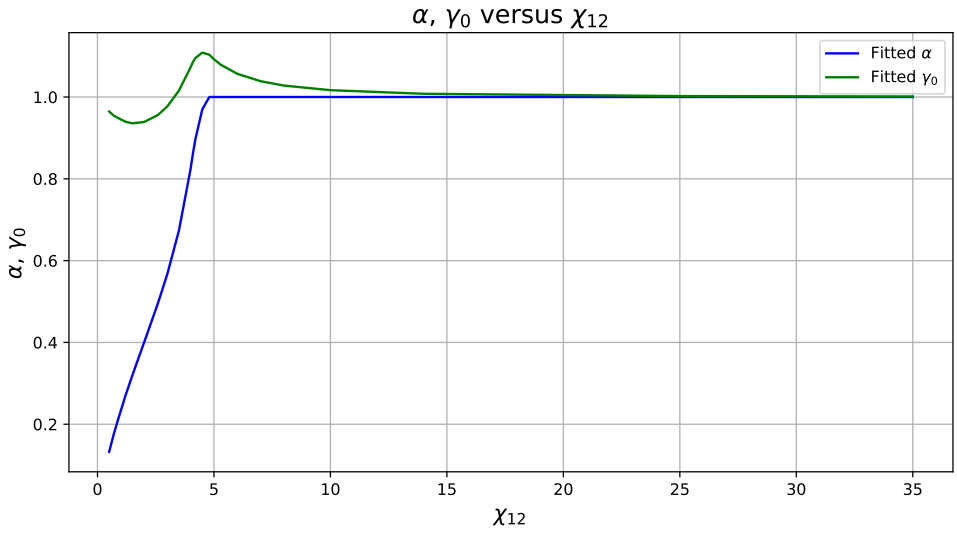

Figure 3.24: Continuous plot of the coefficients, α and γ_0 respect to χ_{12}.

The success of the fitting is attributed to the influence of the parameters α and γ_0, as they enable the immediate identification of the curve associated with a specific χ_{12} when plotting ξ_2 versus ξ_1. This is particularly relevant in the lower region of such curves, where only BFB configurations arise. Furthermore, thanks to the proposed fit:

$$y_{(x)} = \alpha(1-x)^{\frac{1}{\gamma_0}} + (1-\alpha)(1-x)^{\frac{1}{2}\gamma_0}, \tag{3.47}$$

it is possible to determine any positive-definite scalar potential (BFB) for values of χ_{12} ranging from $\chi_{12} = 0.0$ up to at least $\chi_{12} = 35$, and possibly even larger values.

Chapter 4

Differences between two frameworks

In this chapter, we will study the same generic potential for two real scalar fields that we previously analyzed. However, we will now express it in a different notation, specifically the one used in "*Vacuum Stability of a General Scalar Potential of a Few Fields*" [1]. The purpose of this comparison is to determine whether our approach is more or less restrictive than those described in the available literature on the subject. The complete expression for this scalar potential is:

$$V = \lambda_{40}\phi_1^4 + \lambda_{31}\phi_1^3\phi_2 + \lambda_{22}\phi_1^2\phi_2^2 + \lambda_{13}\phi_1\phi_2^3 + \lambda_{04}\phi_2^4. \tag{4.1}$$

This equation is the same as potential 3.3, with the distinction that here λ_{11} corresponds to λ_{40}, λ_{22} to λ_{04}, λ_{12} is $\lambda_{22}/2$, and finally, κ_{12} and κ_{21} correspond to λ_{31} and λ_{13}, respectively. If we rearrange the terms, we obtain a copositivity matrix added to the asymmetric interaction terms, resulting in:

$$V = \begin{pmatrix}\phi_1^2 & \phi_2^2\end{pmatrix}\begin{pmatrix}\lambda_{40} & \frac{\lambda_{22}}{2} \\ \frac{\lambda_{22}}{2} & \lambda_{04}\end{pmatrix}\begin{pmatrix}\phi_1^2 \\ \phi_2^2\end{pmatrix} + \lambda_{31}\phi_1^3\phi_2 + \lambda_{13}\phi_1\phi_2^3. \tag{4.2}$$

This structure closely resembles that found in equation 3.4.
Returning to equation 4.1, note that it can be normalized by ϕ_2^4, yielding the following reduced expression:

$$\frac{V}{\phi_2^4} = \lambda_{40}\frac{\phi_1^4}{\phi_2^4} + \lambda_{31}\frac{\phi_1^3\phi_2}{\phi_2^4} + \lambda_{22}\frac{\phi_1^2\phi_2^2}{\phi_2^4} + \lambda_{13}\frac{\phi_1\phi_2^3}{\phi_2^4} + \lambda_{04}\frac{\phi_2^4}{\phi_2^4}. \tag{4.3}$$

Since ϕ_2^4 is a positive quantity, we only need to ensure that the reduced expression is positive definite. Moreover, we rename the ratio ϕ_1/ϕ_2 as x, and by making the corresponding substitution, we obtain:

$$\frac{V}{\phi_2^4} = \lambda_{40}x^4 + \lambda_{31}x^3 + \lambda_{22}x^2 + \lambda_{13}x + \lambda_{04}. \tag{4.4}$$

Now the potential is more compact, and the problem has been reduced to one that depends only on a single variable. In fact, this is equivalent to dealing with a polynomial problem. For instance, assume that the reduced scalar potential is equivalent to:

$$P = a_4x^4 + a_3x^3 + a_2x^2 + a_1x + a_0. \tag{4.5}$$

To establish that polynomial 4.5 is positive definite, it is necessary to warrant that it has no real roots and that $a_4 > 0$ alongside $a_0 > 0$. Furthermore, the condition that guarantees the absence of real roots requires the discriminant D to be positive [37]:

$$\begin{aligned} D =& 256a_0^3a_4^3 - 4a_1^3a_3^3 - 27a_0^2a_3^4 + 16a_0a_4^2a_4 - 6a_0a_2^2a_3a_4 - 27a_1^4a_2^2 - 192a_0a_1a_3a_4^2 \\ & - 4a_2^3(a_0a_3^2 + a_1^2a_4) + 18a_2(a_1a_3 + 8a_0a_4)(a_0a_3^2 + a_1^2a_4) \\ & + a_2^2(a_1^2a_3 - 80a_0a_1a_3a_4 - 128a_0^2a_4^2). \end{aligned} \tag{4.6}$$

Additionally, the polynomials of its coefficients, Q and R defined as [38, 37]:

$$Q = 8a_2a_4 - 3a_3^2, \quad R = 64a_0a_4^3 + 16a_2a_3^2a_4 - 16a_4^2(a_2^2 + a_1a_3) - 3a_3^4, \tag{4.7}$$

they also ought to be greater than zero. Specifically, in the case of the scalar potential, replacing the corresponding couplings results in the conditions

$$\begin{aligned} D =& 256\lambda_{40}^3\lambda_{04}^3 - 4\lambda_{31}^3\lambda_{13}^3 - 27\lambda_{31}^4\lambda_{04}^2 + 16\lambda_{40}\lambda_{22}^4\lambda_{04} - 6\lambda_{40}\lambda_{31}^2\lambda_{04}\lambda_{13}^2 \\ & - 27\lambda_{40}^2\lambda_{13}^4 - 192\lambda_{40}^2\lambda_{31}\lambda_{04}^2\lambda_{13} - 4\lambda_{22}^3(\lambda_{31}^2\lambda_{04} + \lambda_{40}\lambda_{13}^2) \\ & + 18\lambda_{22}(8\lambda_{40}\lambda_{04} + \lambda_{31}\lambda_{13})(\lambda_{31}^2\lambda_{04} + \lambda_{40}\lambda_{13}^2) \\ & + \lambda_{22}^2(\lambda_{31}^2\lambda_{13}^2 - 80\lambda_{40}\lambda_{31}\lambda_{04}\lambda_{13} - 128\lambda_{40}^2\lambda_{04}^2), \end{aligned} \tag{4.8}$$

$$Q = 8\lambda_{40}\lambda_{22} - 3\lambda_{31}, \tag{4.9}$$

$$R = 64\lambda_{40}^3\lambda_{04} + 16\lambda_{40}\lambda_{22}\lambda_{31}^2 - 16\lambda_{40}^2(\lambda_{22}^2 + \lambda_{31}\lambda_{13}) - 3\lambda_{31}^4, \tag{4.10}$$

along with $\lambda_{40} > 0$ and $\lambda_{04} > 0$. In summary, vacuum stability for this scalar potential is guaranteed as long as the following constraints hold:

$$\lambda_{40} > 0, \quad \lambda_{04} > 0, \quad D > 0 \wedge (Q > 0 \vee R > 0). \tag{4.11}$$

Besides, the potential 4.1 can also be expressed in terms of our theoretical framework by using the transformation to polar coordinates.

$$\Phi = \begin{pmatrix} \phi_1 \\ \phi_2 \end{pmatrix} \to \begin{pmatrix} r\cos\theta \\ r\sin\theta \end{pmatrix}. \tag{4.12}$$

Along with the conversion of couplings given by:

$$\lambda_{13} \to \xi_{12}(\lambda_{40}^3\lambda_{04})^{\frac{1}{4}}, \tag{4.13}$$

$$\lambda_{31} \to \xi_{21}(\lambda_{40}\lambda_{04}^3)^{\frac{1}{4}}, \tag{4.14}$$

$$\lambda_{22} \to 2\delta_{12}(\lambda_{40}\lambda_{04})^{\frac{1}{2}}. \tag{4.15}$$

For sure, maintaining the past notation for ξ_{12}, ξ_{21}, and δ_{12}, which is:

$$\xi_{12} \to \xi_1 + \xi_2, \tag{4.16}$$

$$\xi_{21} \to \xi_1 - \xi_2, \tag{4.17}$$

$$\delta_{12} \to -1 + \chi_{12}. \tag{4.18}$$

The converted potential will receive the name of V_{kan} after Kristjan (The author of '*Vacuum Stability of a General Scalar Potential of a Few Fields*"). Replacing back in equation 4.1 and normalizing by the quartic radial term, the result is:

$$\begin{aligned} V_{kan} = \frac{V}{r^4} =& \cos^4\theta\lambda_{04} + (1-\cos^2\theta)^2\lambda_{40} - 2(-1+\chi_{12})\cos^2\theta(1-\cos^2\theta)\sqrt{\lambda_{04}\lambda_{40}} \\ &- \cos\theta(1-\cos^2\theta)^{3/2}(\lambda_{04}^3\lambda_{40})^{1/4}\, sgn^3(\xi_1-\xi_2) \\ &+ \cos^3\theta\sqrt{1-\cos^2\theta}(\lambda_{04}\lambda_{40}^3)^{1/4}\, sgn(\xi_1+\xi_2). \end{aligned} \tag{4.19}$$

Where the sign sgn is ± 1.
Indeed, this potential should be exactly the same as the one we found in equation 3.31, except that here the degrees of freedom of λ_{40} and λ_{04} are preserved explicitly, while in the other case they are hidden in diagonal scaling.
Regardless, both potentials should exhibit the same behavior for a given parameter configuration. Even so, as we will explore in the next section, this does not always hold true.

4.0.1 Scalar potentials Results and discussion

As stated at the beginning, this section compares the two normalized scalar potentials.
Primarily, a brute-force type code was developed to scan both scalar potentials and their constraints. This allows identifying the regions where each potential is or is not BFB, which can be visualized in the coupling space of ξ_1 and ξ_2, as shown in Figure 4.1. On the other hand, Table 4.1 presents the two potentials under consideration. One explicitly depends on the couplings λ_{04} and λ_{40}, corresponding to $V_{Kan.Norm}$, whereas in V_{NORM}, the information about the diagonal couplings has been concealed and reduced through diagonal scaling.

Potential	**Expression**
Kannike	$V_{Kan.NORM} = \frac{V}{r^4} = \cos^4\theta\lambda_{04} + (1-\cos^2\theta)^2\lambda_{40}$ $-2(-1+\chi_{12})\cos^2\theta(1-\cos^2\theta)\sqrt{\lambda_{04}\lambda_{40}}$ $-\cos\theta(1-\cos^2\theta)^{3/2}(\lambda_{04}^3\lambda_{40})^{1/4}\, sgn^3(\xi_1-\xi_2)$ $+\cos^3\theta\sqrt{1-\cos^2\theta}(\lambda_{04}\lambda_{40}^3)^{1/4}\, sgn(\xi_1+\xi_2).$
Our	$V_{NORM} = \frac{V}{r^4} = 4\cos^2\theta - 4\cos^4\theta - \frac{\xi_1}{2} + \xi_1\cos^2\theta$ $+sgn\cos\theta\sqrt{1-\cos^2\theta}\,\xi_2$ $-2sgn\cos^3\theta\sqrt{1-\cos^2\theta}\,\xi_2$ $+\frac{\chi_{12}}{2} - 2\cos^2\theta\chi_{12} + 2\chi_{12}\cos^4\theta.$

Table 4.1: The normalized potentials from Kannike and the developed in this work.

Concretely, we shall analyze a specific comparison case. Table 4.2 presents a sample of the parameters defining the potentials for a fixed χ_{12} value, set at $\chi_{12} = 2.6$. Additionally, these normalized scalar potentials are represented by either 1 or -1, indicating whether they are BFB. The value 1 means that the potential remains positive, regardless of its magnitude, while -1 indicates that it becomes negative, also independently of its magnitude.

λ_{04}	λ_{40}	ξ_1	ξ_2	χ_{12}	V_{kanike}	V_{norm}
0.00100	0.00100	0.000000	2.461538	2.6	1	1
2.00075	2.00075	0.000000	2.461538	2.6	1	1
4.00050	2.00075	0.000000	2.461538	2.6	1	1
2.00075	2.00075	0.000000	2.461538	2.6	1	1
4.00050	2.00050	0.000000	2.461538	2.6	1	1
⋮	⋮	⋮	⋮	⋮	⋮	⋮
8.00000	2.00075	3.076923	3.076923	2.6	1	-1
6.00025	2.00075	3.076923	3.076923	2.6	1	-1
8.00000	2.00075	3.076923	3.076923	2.6	1	-1
6.00025	2.00075	3.076923	3.692308	2.6	1	-1
8.00000	2.00075	3.076923	3.692308	2.6	1	-1

Table 4.2: Table of values for λ_{04}, λ_{40}, ξ_1, ξ_2, and $\chi_{12} = 2.6$, along with the corresponding potentials V_{kanike} and V_{norm}.

In Table 4.2, it is essential to clarify that the corresponding values of λ_{04} and λ_{40} are exclusively associated with the potential $V_{Kan.NORM}$. On the other hand, in Figure 4.1, a scatter plot was generated for the values of ξ_2 versus ξ_1, which may or may not be BFB, distinguishing three main regions. The red points indicate combinations that, according to $V_{Kan.NORM}$, are not bounded from below. Meanwhile, scatter points with a small light blue dot inside represent values that are not BFB according to V_{NORM}. Otherwise, scatter points with a tiny yellow dot inside correspond to values that are indeed BFB.

In summary, the entire blue region is valid for $V_{Kan.NORM}$, whereas the potential V_{NORM} suggests that this is only partially true, as the theoretically consistent region lies below the exclusion curve for $\chi_{12} = 2.6$. Nevertheless, caution must be exercised since λ_{40} and λ_{04} remain unconstrained, suggesting that a slightly more restrictive mixing might exist for a given $V_{Kan.NORM}$. Nonetheless, this "hypothetical region" would only approach the blue exclusion curve without reaching it.

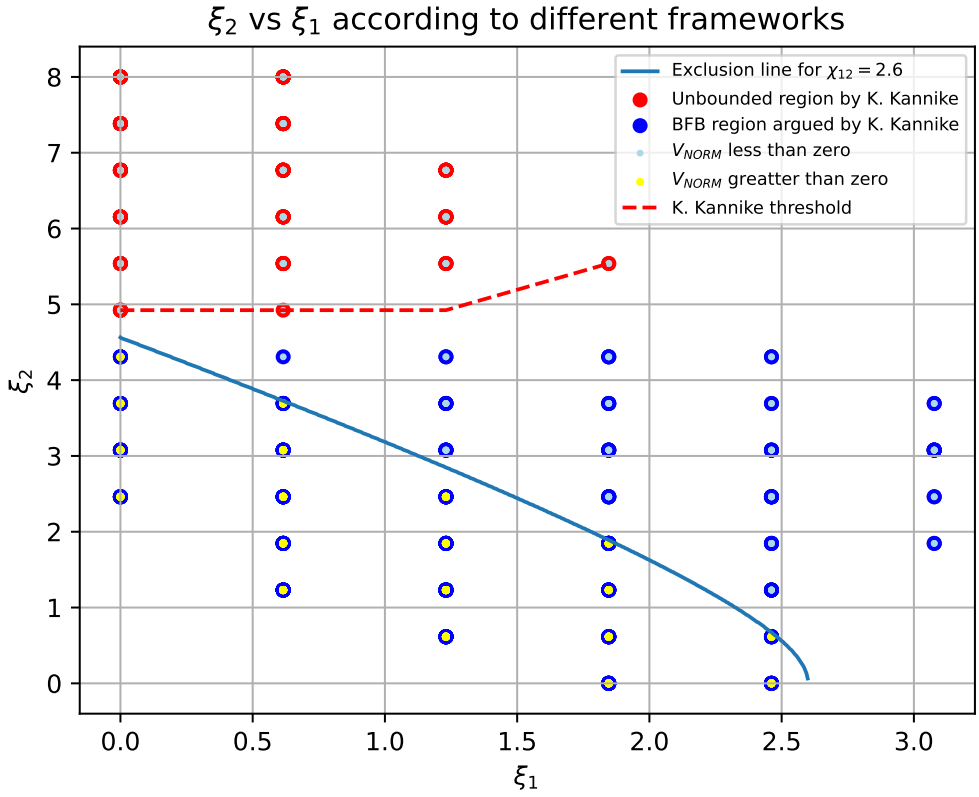

Figure 4.1: ξ_2 versus ξ_1, where red points are unbounded while blue points are BFB. Additionally, we identify two curves: a dashed red curve and a solid blue curve, which indicate the BFB threshold for $V_{Kan.NORM}$ and V_{NORM}, respectively. Maintaining a fixed $\chi_{12} = 2.6$

The profile presented in Figure 4.1 follows the expected trend. Still, it is crucial to emphasize that, regardless of color (red or blue), each point represents a scalar potential. In this case, we only have 413 samples, and to infer more details or even generalize the results, a larger dataset is required. This lack of data is evident even in the red dashed threshold, where a smoother curve would be expected.

4.0.2 Selected cases, $\chi_{12} = \{0.5, 0.7, 0.9, 2.0\}$

The results presented below are highly reliable in the sense that, to determine the exclusion zones, the scan was performed over more than 8 million possible configurations for $\chi_{12} = 0.5$, while 14 million were analyzed for $\chi_{12} = 0.7$. Similarly, $\sim$2

million and 14 million samples were considered for $\chi_{12} = 0.9$ and $\chi_{12} = 2.0$, respectively. This was done for both BFB cases and non-physical cases. Tables 4.3, 4.4, 4.5, and 4.6 provide sample values for the respective quantities under study.

λ_{04}	λ_{40}	ξ_1	ξ_2	χ_{12}	$V_{kanneki}$	V_{norm}
0.001000	0.001000	0.000000	1.014388	0.5	1	1
0.081798	0.081798	0.000000	1.014388	0.5	1	1
0.162596	0.162596	0.000000	1.014388	0.5	1	1
0.243394	0.162596	0.000000	1.014388	0.5	1	1
0.162596	0.243394	0.000000	1.014388	0.5	1	1
⋮	⋮	⋮	⋮	⋮	⋮	⋮
7.838404	1.859354	0.820144	0.712230	0.5	1	-1
7.919202	1.859354	0.820144	0.712230	0.5	1	-1
8.000000	1.859354	0.820144	0.712230	0.5	1	-1
7.919202	1.940152	0.820144	0.712230	0.5	1	-1
8.000000	1.940152	0.820144	0.712230	0.5	1	-1

Table 4.3: Table for the normalized potentials $V_{Kanneki}$ and V_{norm} along with $\xi_{1,2}$. For a fixed $\chi_{12} = 0.5$ with different positive values of λ_{04} and λ_{40}.

λ_{04}	λ_{40}	ξ_1	ξ_2	χ_{12}	V_{kanike}	V_{norm}
0.001000	0.001000	0.000000	1.187050	0.7	1	1
0.081798	0.081798	0.000000	1.187050	0.7	1	1
0.162596	0.081798	0.000000	1.187050	0.7	1	1
0.081798	0.162596	0.000000	1.187050	0.7	1	1
0.162596	0.162596	0.000000	1.187050	0.7	1	1
⋮	⋮	⋮	⋮	⋮	⋮	⋮
8.000000	1.619960	1.122302	0.928058	0.7	1	-1
7.757606	1.697758	1.122302	0.928058	0.7	1	-1
7.838404	1.697758	1.122302	0.928058	0.7	1	-1
7.919202	1.697758	1.122302	0.928058	0.7	1	-1
8.000000	1.697758	1.122302	0.928058	0.7	1	-1

Table 4.4: Table of values for λ_{04}, λ_{40}, ξ_1, ξ_2, and $\chi_{12} = 0.7$, along with the corresponding potentials V_{kanike} and V_{norm}.

λ_{04}	λ_{40}	ξ_1	ξ_2	χ_{12}	V_{kanike}	V_{norm}
0.001000	0.001000	0.000000	1.367089	0.9	1	1
0.164245	0.164245	0.000000	1.367089	0.9	1	1
0.327490	0.164245	0.000000	1.367089	0.9	1	1
0.164245	0.327490	0.000000	1.367089	0.9	1	1
0.327490	0.327490	0.000000	1.367089	0.9	1	1
⋮	⋮	⋮	⋮	⋮	⋮	⋮
7.510265	1.796694	1.405063	1.177215	0.9	1	-1
7.673510	1.796694	1.405063	1.177215	0.9	1	-1
7.836755	1.796694	1.405063	1.177215	0.9	1	-1
8.000000	1.796694	1.405063	1.177215	0.9	1	-1
8.000000	1.959939	1.405063	1.177215	0.9	1	-1

Table 4.5: Table of values for λ_{04}, λ_{40}, ξ_1, ξ_2, and $\chi_{12} = 0.9$, along with the corresponding potentials V_{kanike} and V_{norm}.

λ_{04}	λ_{40}	ξ_1	ξ_2	χ_{12}	V_{kanike}	V_{norm}
0.001000	0.001000	0.000000	2.020202	2.0	1	1
0.081798	0.081798	0.000000	2.020202	2.0	1	1
0.162596	0.081798	0.000000	2.020202	2.0	1	1
0.081798	0.162596	0.000000	2.020202	2.0	1	1
0.162596	0.162596	0.000000	2.020202	2.0	1	1
⋮	⋮	⋮	⋮	⋮	⋮	⋮
8.000000	1.778556	2.878788	2.222222	2.0	1	-1
7.757606	1.859354	2.878788	2.222222	2.0	1	-1
7.838404	1.859354	2.878788	2.222222	2.0	1	-1
7.919202	1.859354	2.878788	2.222222	2.0	1	-1
8.000000	1.859354	2.878788	2.222222	2.0	1	-1

Table 4.6: Table of values for λ_{04}, λ_{40}, ξ_1, ξ_2, and $\chi_{12} = 2.0$, along with the corresponding potentials V_{kanike} and V_{norm}.

Using the data from these tables, we plotted ξ_2 versus ξ_1 to examine in detail the BFB regions identified by each potential. These regions are displayed in Figures 4.2 and 4.3, where three distinct zones are observed in each plot. For both cases, these zones lead to the same conclusions. Region I corresponds to a completely discarded sector, meaning it is physically impossible. Region II, on the other hand,

has an uncertain nature but, in principle, is entirely excluded according to our newly derived bounds. Finally, Region III represents the configurations of ξ_1 and ξ_2 that always result in a BFB potential.

For $\chi_{12} = \{0.5, 0.7\}$

In Figure 4.2a, when viewed from left to right, an initial rise in the red dashed curve (Kannike threshold) is noticeable. This curve then remains uniform until it reaches approximately $\sim (0.4, 2.0)$, where local maxima and minima appear once again.
On the other hand, Figure 4.2b also exhibits a similar behavior from left to right, but in this case, it can be observed that the peak of the red dashed line is significantly smaller. Additionally, the slope of this curve systematically increases until it stabilizes around the point $\sim (0.6, 2.5)$. For both cases, we argue that the only BFB zone corresponds to Region III, while we claim that the other two regions are completely discarded since they don't match with the positiveness of the normalized diagonally scaled scalar potential.

For $\chi_{12} = \{0.9, 2.0\}$

In the case shown in Figure 4.3a, corresponding to the scenario with $\chi_{12} = 0.9$, we observe that the red dashed exclusion curve, which arises from the constraints of $V_{Kan.NORM}$, exhibits a slight and sustained increase in slope, reducing the allowed space for Region I. However, in contrast, Region II expands; though, like Region I, it remains unbounded from below according to our framework. Meanwhile, the exclusion curve associated with V_{NORM} is broad, smooth, and homogeneous, defining the entire stability zone, which corresponds to Region III.
Similarly, for $\chi_{12} = 2.0$ in Figure 4.3b, it is also evident how the red curve steadily ascends, thereby shrinking Region I while expanding Region II. Nevertheless, once again, it is observed that Region III is bounded from below and is described by the solid blue exclusion curve. Its behavior is continuous and smooth, allowing it to be modeled through the proposed fit presented in the previous chapter.

Regarding the red dashed curves associated with the constraints of $V_{Kan.NORM}$, it is noteworthy that their behavior does not seem to exhibit any periodicity or pattern, suggesting that there is no straightforward way to find a smooth curve fit for them in terms of our guiding parameters, ξ_1, ξ_2, and χ_{12}. This observation makes sense when considering that their parameter space is determined by simultaneously satisfying the conditions given in 4.11.

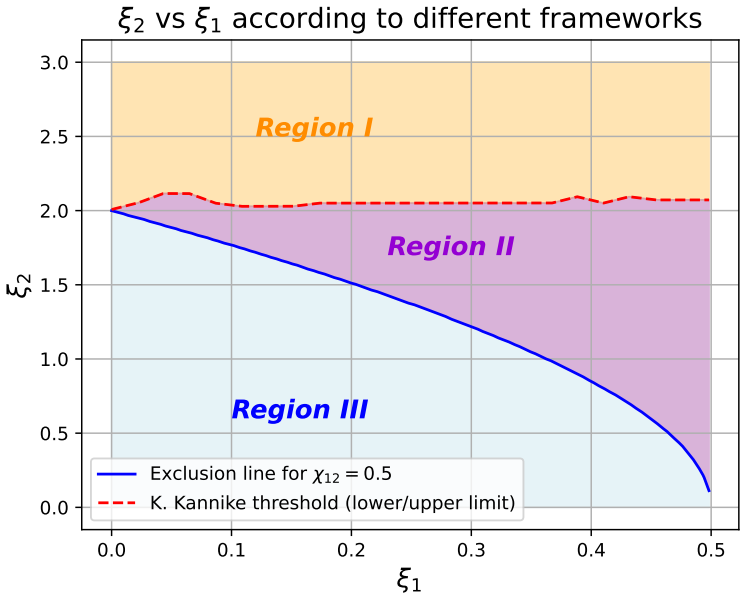

(a) Allowed and excluded ξ_2-ξ_1 parameter space for both potentials given $\chi_{12} = 0.5$.

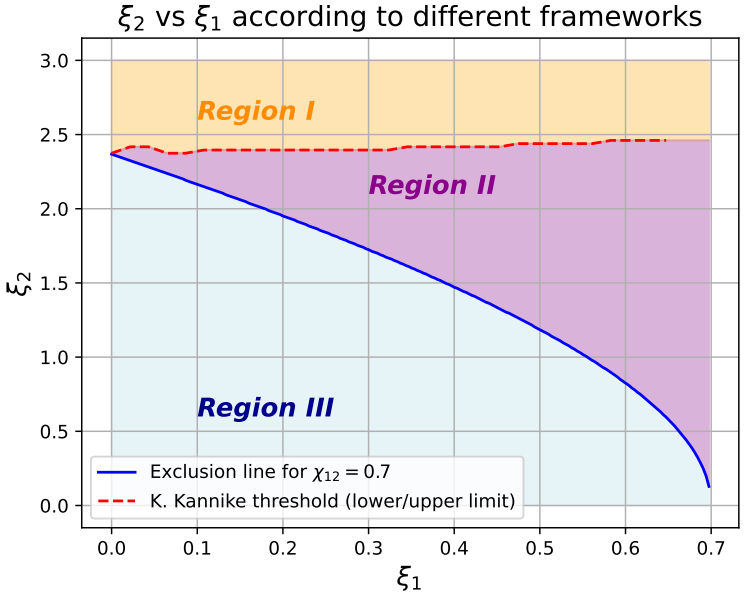

(b) Allowed and excluded parameter space for ξ_2-ξ_1 with $\chi_{12} = 0.7$.

Figure 4.2: In both figures, Region III corresponds to the only sector where configurations are BFB.

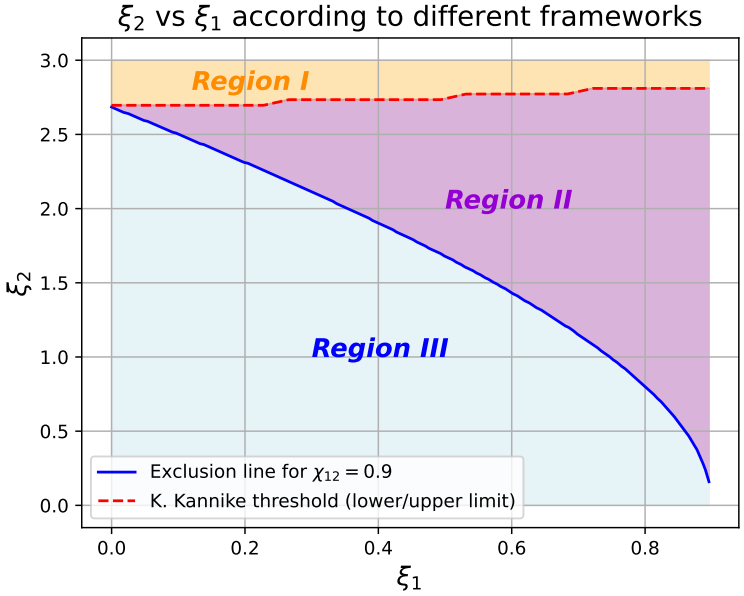

(a) Allowed and excluded ξ_2-ξ_1 parameter space for $\chi_{12} = 0.9$.

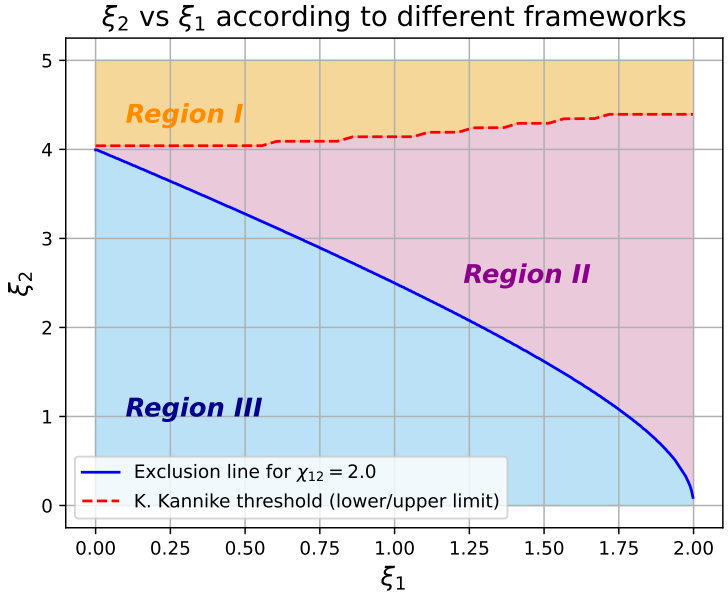

(b) Allowed and excluded ξ_2-ξ_1 parameter space for $\chi_{12} = 2.0$.

Figure 4.3: In both figures, the three regions are defined by the exclusion curves of Kannike and V_{NORM}. Only Region III is BFB.

4.0.3 Discussion

We have demonstrated that the same scalar potentials describe different regions that may or may not be BFB. On the one hand, the approach developed in this thesis is significantly more precise and restrictive than the conditions provided in 4.11.

In Figures 4.4a, 4.4b, 4.5a, and 4.5b, we observe potentials of the Region III, where for exactly the same values of ξ_1, ξ_2, and χ_{12}, as well as λ_{40} and λ_{04}, the results differ between $V_{Kan.Norm}$ and V_{NORM}. For instance, in Figure 4.4a, both potentials satisfy the BFB condition for $\chi_{12} = 0.5$, with the specific values $\xi_1 = 0.02$, $\xi_2 = 1.06$, $\lambda_{40} = 2.67$, and $\lambda_{04} = 5.09$. While both potentials remain positive, the orange potential exhibits a steeper divergence. A similar behavior is observed in Figure 4.4b for $\chi_{12} = 0.7$, where once again, the orange potential scales more rapidly. In both cases, there are two intersection points where both potentials acquire the same value of V.

On the other hand, in Figure 4.5a for $\chi_{12} = 0.9$, with $\xi_1 = 0.49$, $\xi_2 = 0.08$, $\lambda_{40} = 2.12$, and $\lambda_{04} = 6.69$, we observe a pseudo-saddle point in the orange potential, along with two intersections with the normalized blue potential. Meanwhile, in Figure 4.5b for $\chi_{12} = 2.0$, the orange potential exhibits a more oscillatory appearance. In this case, there are no intersections between the two potentials.

Finally, in the scalar potentials shown in Figures 4.6, two cases belonging to the so-called Region II are identified. Specifically, the normalized potentials V_{NORM} (solid blue line) in Figures 4.6a and 4.6b take negative values, indicating that they are not positive definite and, consequently, are not bounded from below according to the polynomial constraints 4.11. In contrast, the orange potentials, $V_{Kan.NORM}$, satisfy the boundedness from below condition within this theoretical framework.

At first glance, it is not entirely clear why these differences arise; yet, they open a range of possibilities. One hypothesis is that the diagonal scaling performed in V_{NORM} modifies the growth rate of the potential, implying that as the parameter values increase, both potentials grow at different rates. This effect would become more pronounced for very large values, suggesting a highly divergent behavior between the two frameworks. Another related possibility is that, in the polynomial approach 4.11, the parameters λ_{40} and λ_{04} remain free, whereas in the diagonally scaled model, they are constrained by specific parameterizations. This could indirectly alter part of the behavior of the scalar potential.

Another possibility is that the polynomial criterion 4.11, which requires $D > 0$ along with $Q > 0 \vee R > 0$, may not be the most stringent constraint. Instead, there might be an underlying parameter leakage that better predicts the appropriate phenomenology to ensure a potential where $V > 0$. This "leakage" could stem from the fact that the criterion relies solely on the discriminant and the coefficients, along with the conditions $\lambda_{40} > 0$ and $\lambda_{04} > 0$. While these conditions may be necessary, they might not be sufficient.

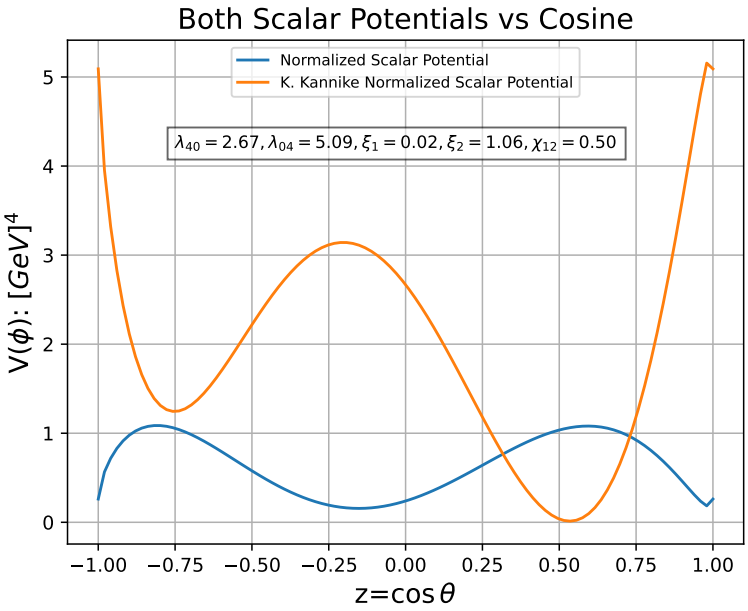

(a) Both Potentials maintaining fixed λ_{40} and λ_{04} as well as ξ_1, ξ_2 and $\chi_{12} = 0.5$.

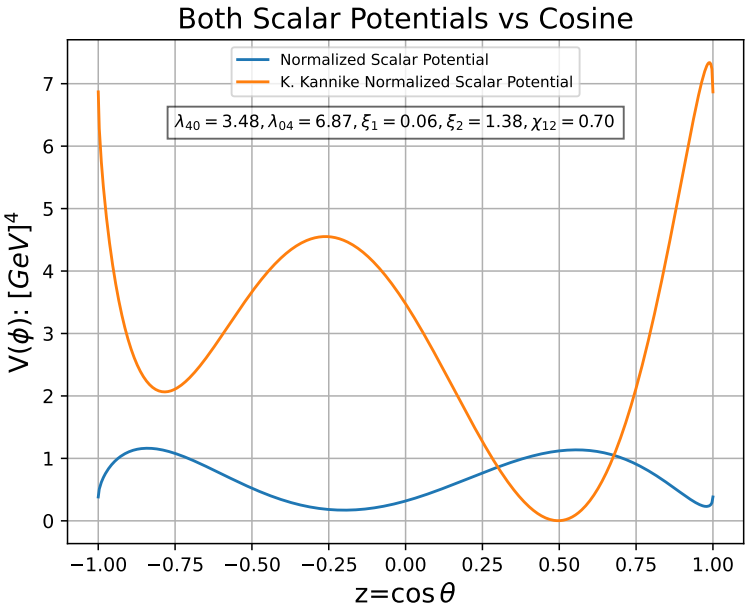

(b) Potentials for $\chi_{12} = 0.7$ along with the fixed parameters λ_{40}, λ_{04}, ξ_1 and ξ_2.

Figure 4.4: Combined potentials plots with the parameters described in the labels.

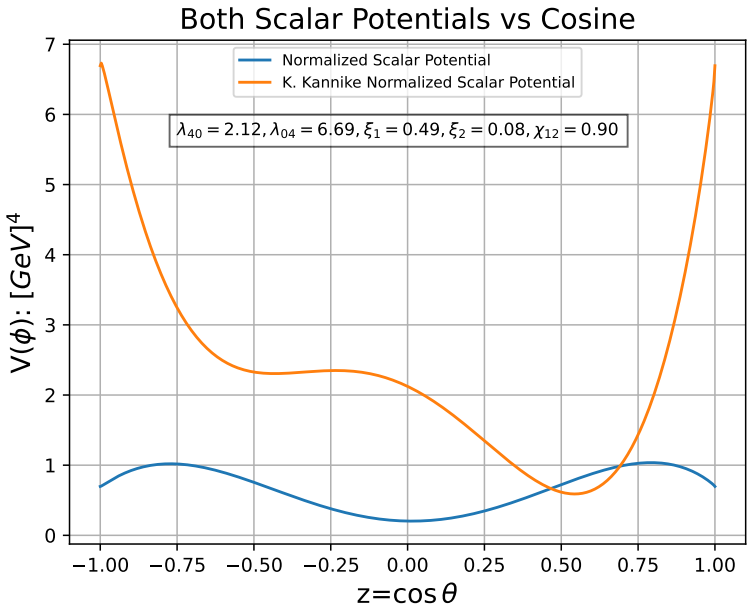

(a) Potentials with $\chi_{12} = 0.9$ and the above values (label panel) of ξ_1, ξ_2, λ_{40} and λ_{04}.

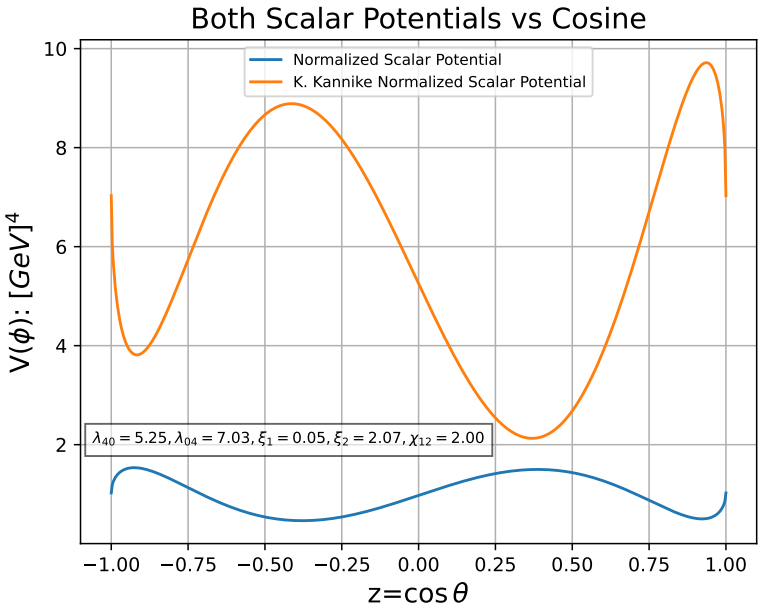

(b) Potentials with $\chi_{12} = 2.0$ and the fixed parameters λ_{40}, λ_{04}, ξ_1, ξ_2.

Figure 4.5: Combined visualization of four potentials with parameter values in the labels.

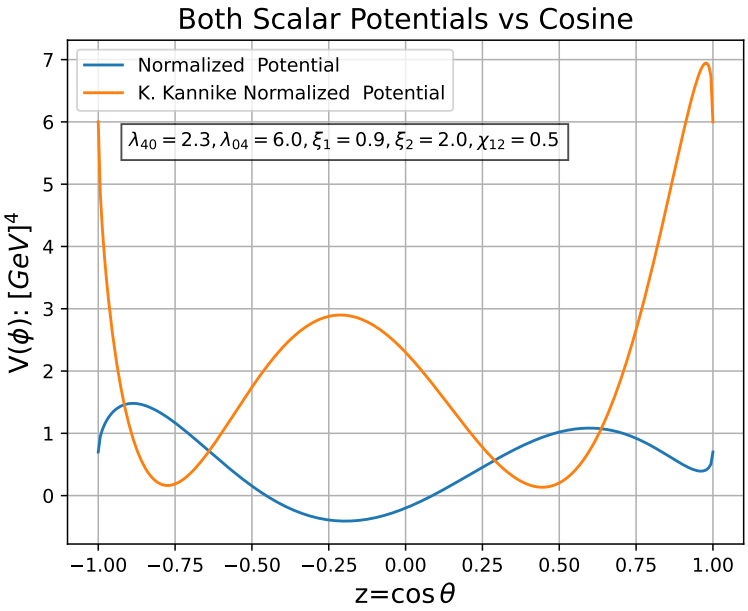

(a) Normalized scalar potentials. One is BFB while the other not for same configuration.

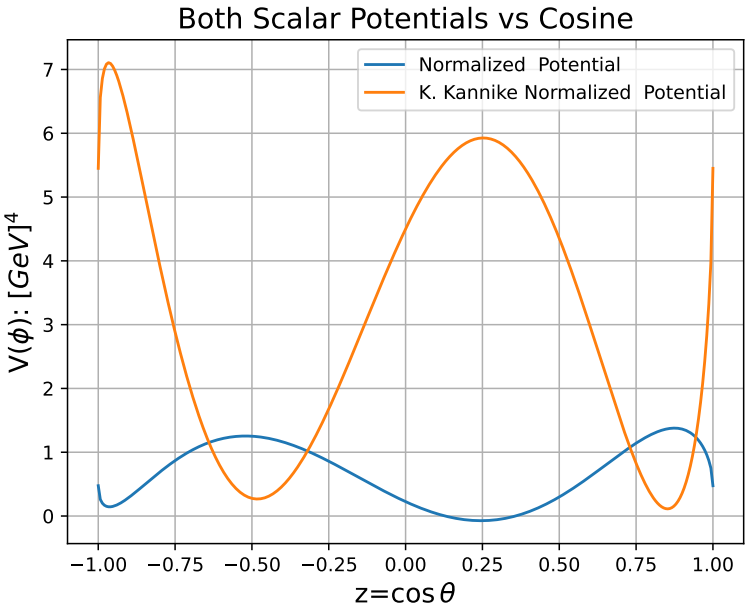

(b) Scalar potentials with parameters, $\lambda_{04} = 5.45$, $\lambda_{40} = 4.5$,$\xi_1 = 0.25$, $\xi_2 = 2.2$ and $\chi_{12} = 0.7$.

Figure 4.6: Combined visualization of two potentials unbounded from below.

Chapter 5

Conclusions

An extensive numerical scan was conducted, allowing us to analyze the stability and exclusion regions in terms of the parameters ξ_1, ξ_2, and χ_{12}. It was found that they follow predictable trends, such as a square root dependence in some cases. Furthermore, thanks to this analysis, we successfully addressed how the interactions of the form: $\phi_1\phi_2^3$,$\phi_1^3\phi_2$ can affect the regions that produce a stable vacuum configuration. Something that is not easily studied under other paradigms.

Moreover, we were able to contrast and compare the results obtained with previous bounds available in the literature, and preliminarily, our constraints appear to be more restrictive than the pre-existing ones.

In summary, a successfully developed theoretical-computational approach for the two real scalar fields model has been achieved, providing remarkable precision in distinguishing between bounded-from-below (BFB) scenarios and those that are not. Additionally, exploring the diagonal scaling executed in the fields has brought significant advantages. Nevertheless, it has to be handled carefully, ensuring that no information is lost in its implementation through a detailed analysis of how scalar potentials grow toward positive infinity under two different frameworks.

The computational optimization achieved with this approach is significant. Previously, identifying a curve defined by χ_{12} that delineated a bounded-from-below region required an exhaustive search across the entire parameter space. However, with the developed techniques, it is now possible to find configurations that yield BFB potentials in just a matter of minutes. Moreover, this method can, in principle, be applied

to any value of χ_{12}, increasing the confidence level within the range $\chi_{12} \in [0, 35]$.

In the future, it is expected to extend this study to models with more than two scalar fields. Additionally, it is feasible to explore how additional couplings might affect the BFB conditions, for instance, in BSM models.

Without a doubt, it is worth mentioning that the objective set last semester was also successfully achieved: to enlighten a methodology for characterizing vacuum stability in a simple model, such as the two real scalar fields framework. These new results constitute ongoing research that we aim to refine further, with the eventual goal of publication.

Bibliography

[1] K. Kannike, *Vacuum stability of a general scalar potential of a few fields*, *Eur. Phys. J. C* **76** (2016) 324, [1603.02680].

[2] S. T. Love, *The role of symmetry in the development of the standard model*, *Philosophical Transactions of the Royal Society A: Mathematical, Physical and Engineering Sciences* **382** (2024) 20240042.

[3] M. Gomez-Bock, M. Mondragon, M. Muhlleitner, R. Noriega-Papaqui, I. Pedraza, M. Spira et al., *Rompimiento de la simetría electrodébil y la física del higgs: Conceptos básicos*, *arXiv preprint hep-ph/0509077* (2005) .

[4] D. Restrepo, *Teoría clásica de campos. el lagrangiano del modelo estándar*, 2017.

[5] G. Hiller, T. Höhne, D. F. Litim and T. Steudtner, *Vacuum stability in the standard model and beyond*, *Physical Review D* **110** (2024) 115017, [2401.08811].

[6] E. A. R. Rojas, *The higgs boson at lhc and the vacuum stability of the standard model*, *arXiv preprint* (2015) , [1511.03651].

[7] M. E. Peskin and D. V. Schroeder, *An Introduction to Quantum Field Theory*. Addison-Wesley, 1995.

[8] A. Messiah, *Quantum Mechanics*. North-Holland Publishing Company, Amsterdam, 1961.

[9] R. W. Cottle, G. J. Habetler and C. E. Lemke, *On classes of copositive matrices*, *Linear Algebra and its Applications* **3** (1970) 103–119.

[10] C. Collaboration, *Observation of a new boson at a mass of 125 gev with the cms experiment at the lhc*, *Physics Letters B* **716** (2012) 30–61.

[11] A. Collaboration, *A detailed map of higgs boson interactions by the atlas experiment ten years after the discovery*, *Nature* **607** (2022) 52–59, [2207.00092].

[12] C. Grojean, *Beyond the standard higgs after the 125 gev higgs discovery*, *Philosophical Transactions of the Royal Society A: Mathematical, Physical and Engineering Sciences* **373** (2015) 20140042.

[13] G. Moultaka and M. C. Peyranère, *Vacuum stability conditions for higgs potentials with $su(2)_l$ triplets*, *Physical Review D* **103** (2021) 115006, [2012.13947].

[14] J. Chakrabortty, P. Konar and T. Mondal, *Copositive criteria and boundedness of the scalar potential*, *Physical Review D* **89** (2014) 095008, [1311.5666].

[15] R. N. Mohapatra and G. Senjanović, *Neutrino masses and mixings in gauge models with spontaneous parity violation*, *Physical Review D* **23** (1981) 165–180.

[16] J. Gluza, M. Kordiaczyńska and T. Srivastava, *Discriminating the htm and mlrsm models in collider studies via doubly charged higgs boson pair production and the subsequent leptonic decays*, *Chinese Physics C* **45** (2021) 073113.

[17] J. Chakrabortty, P. Konar and T. Mondal, *Copositive criteria and boundedness of the scalar potential*, *Physical Review D* **89** (2014) 095008, [1311.5666].

[18] R. M. Fonseca, *Boundedness from below of su(n) potentials*, 2110.08290.

[19] M. Abud and G. Sartori, *The geometry of orbit space and natural minima of higgs potentials*, *Physics Letters B* **104** (1981) 147–152.

[20] M. D. Schwartz, *Quantum Field Theory and the Standard Model*. Cambridge University Press, 2014.

[21] A. Das, *Field Theory: A Path Integral Approach*. World Scientific, Singapore, 1993.

[22] J. Körner, A. Arnold, C. Klein and J. M. Melenk, *Optimally truncated wkb approximation for the highly oscillatory stationary 1d schrödinger equation*, *arXiv preprint* (2023) , [2310.00955].

[23] W. N. Cottingham and D. A. Greenwood, *An Introduction to the Standard Model of Particle Physics*. Cambridge University Press, 2nd ed., 2007.

[24] G. L. Kane, *Modern Elementary Particle Physics: Explaining and Extending the Standard Model*. Cambridge University Press, 2017.

[25] A. Cayley, *A memoir on the theory of matrices*, *Philosophical Transactions of the Royal Society of London* **148** (1858) 17–37.

[26] G. T. Gilbert, *Positive definite matrices and sylvester's criterion*, *The American Mathematical Monthly* **98** (1991) 44–46.

[27] W. Kaplan, *A test for copositive matrices*, *Linear Algebra and its Applications* **313** (2000) 203–206.

[28] R. A. Horn and C. R. Johnson, *Matrix Analysis*. Cambridge University Press, 2nd ed., 2013.

[29] K. D. Ikramov, *Conditionally definite matrices*, *Journal of Mathematical Sciences* **98** (2000) 1–50.

[30] D. o. M. Purdue University, *Ma301: An introduction to proof through real analysis (chapter 2: Inequalities)*, 2007.

[31] G. H. Hardy, J. E. Littlewood and G. Pólya, *Inequalities*. Cambridge University Press, 2nd ed., 1952.

[32] L. Golland, *Karl menger and taxicab geometry*, *Mathematics Magazine* **63** (1990) 326–327.

[33] G. C. Branco, P. M. Ferreira, L. Lavoura, M. N. Rebelo, M. Sher and J. P. Silva, *Theory and phenomenology of two-higgs-doublet models*, *Physics Reports* **516** (2012) 1–102.

[34] G. H. Hardy, J. E. Littlewood and G. Pólya, *Inequalities*. Cambridge University Press, 2nd ed., 1952.

[35] M. Gustafsson, *The inert doublet model and its phenomenology*, in *Proceedings of Science*, 2011.

[36] Z. Allen-Zhu, Y. Li, R. Oliveira and A. Wigderson, *Much faster algorithms for matrix scaling*, *arXiv preprint arXiv:1704.02315* (2017) .

[37] E. L. Rees, *Graphical discussion of the roots of a quartic equation*, *The American Mathematical Monthly* **29** (1922) 51–55.

[38] D. Lazard, *Quantifier elimination: Optimal solution for two classical examples*, *Journal of Symbolic Computation* **5** (1988) 261–266.

Appendix 1

In order to solve equation 1.8, it is necessary to consider some very helpful tools. At this stage, it is important to rename some notations from relativity and field theory. A contravariant coordinate in the Bjorken-Drell convention [21] can be expressed as:

$$x^{\mu} = (x^0, \vec{x}) \tag{5.1}$$

$$x_{\mu} = \eta_{\mu\nu} x^{\nu} = (x^0, -\vec{x}) \tag{5.2}$$

The covariant and contravariant metric have diagonal form with the signatures:

$$\eta^{\mu\nu} = (+, -, -, -), \tag{5.3}$$

$$\eta_{\mu\nu} = (+, -, -, -). \tag{5.4}$$

While the invariant length is given by:

$$x^2 = x^{\mu} x_{\mu} = \eta^{\mu\nu} x_{\mu} x^{\nu} = \eta_{\mu\nu} x^{\mu} x^{\nu} = x_0^2 - \vec{x}^2 \tag{5.5}$$

Whereas x_0 is usually recognized as the temporal coordinate, when μ is regarded to $\mu = 0, 1, 2, 3$. Which corresponds to a 3+1 dimensional field theory [21].
Equivalently for the gradients:

$$\partial_{\mu} = \frac{\partial}{\partial x^{\mu}} = (+\frac{\partial}{\partial x^0}, +\frac{\partial}{\partial x^1}, +\frac{\partial}{\partial x^2}, +\frac{\partial}{\partial x^3}) \tag{5.6}$$

In Minkowski space, specifically in rectangular coordinates the spatial-temporal covariant derivative is:

$$\partial_{\mu} = (\frac{\partial}{\partial t}, \vec{\nabla}), \tag{5.7}$$

similarly for ∂^{μ}:

$$\partial^{\mu} = (\frac{\partial}{\partial t}, -\vec{\nabla}). \tag{5.8}$$

With the above tools we can get a better approach to the energy-momentum tensor, hence:

$$T^{\mu\nu} = \partial^\mu \phi^* \partial^\nu \phi + \partial^\mu \phi \partial^\nu \phi^* - g^{\mu\nu} g^{\alpha\beta} \partial_\alpha \phi^* \partial_\beta \phi + g^{\mu\nu} m^2 \phi^* \phi, \tag{5.9}$$

expanding the third term:

$$\sum_{\alpha,\beta} g^{\mu\nu} g^{\alpha\beta} \partial_\alpha \phi^* \partial_\beta \phi. \tag{5.10}$$

This is simply equal to:

$$= \frac{\partial \phi^*}{\partial x^0} \frac{\partial \phi}{\partial x^0} + \sum_{i=1}^{3} \frac{\partial \phi^*}{\partial x^i} \frac{\partial \phi}{\partial x^i} \tag{5.11}$$

$$= + \frac{\partial \phi^*}{\partial x_0} \cdot + \frac{\partial \phi}{\partial x^0} - \frac{\partial \phi^*}{\partial x_1} \cdot + \frac{\partial \phi}{\partial x^1} - \frac{\partial \phi^*}{\partial x_2} \cdot + \frac{\partial \phi}{\partial x^2} - \frac{\partial \phi^*}{\partial x_3} \cdot + \frac{\partial \phi}{\partial x^3} \tag{5.12}$$

$$= \partial_0 \phi^* \partial_0 \phi - \vec{\nabla} \phi^* \cdot \vec{\nabla} \phi. \tag{5.13}$$

Appendix 2

Using the definition of a complex scalar field and getting its derivatives, we shall do:

$$\partial^0\phi^\star = \partial_0 \int \frac{d^3p}{(2\pi)^3}\frac{1}{\sqrt{2\omega_p}}\left(a_p^\dagger e^{ipx} + b_p e^{-ipx}\right),$$
$$\partial^0\phi^\star = \int \frac{d^3p}{(2\pi)^3}\frac{ip_0}{\sqrt{2\omega_p}}\left(a_p^\dagger e^{ipx} - b_p e^{-ipx}\right), \tag{5.14}$$

while:

$$\partial^0\phi = \partial_0 \int \frac{d^3p}{(2\pi)^3}\frac{1}{\sqrt{2\omega_p}}\left(a_p e^{-ipx} + b_p^\dagger e^{ipx}\right),$$
$$\partial^0\phi = \int \frac{d^3p}{(2\pi)^3}\frac{-ip_0}{\sqrt{2\omega_p}}\left(a_p e^{-ipx} - b_p^\dagger e^{ipx}\right). \tag{5.15}$$

Multiplying:

$$\partial^0\phi^*\partial^0\phi = \int\int \frac{d^3p}{(2\pi)^3}\frac{d^3q}{(2\pi)^3}\frac{-i^2p_0q_0}{\sqrt{4\omega_p\omega_q}}\left(a_p^\dagger e^{ipx} - b_p e^{-ipx}\right)\left(a_q e^{-iqx} - b_q^\dagger e^{iqx}\right) \tag{5.16}$$
$$= \int\int \frac{d^3p}{(2\pi)^3}\frac{d^3q}{(2\pi)^3}\frac{-i^2p_0q_0}{\sqrt{4\omega_p\omega_q}}\Big(a_p^\dagger a_q e^{ipx}e^{-iqx} - a_p^\dagger b_q^\dagger e^{ipx}e^{iqx} - b_p a_q e^{-ipx}e^{-iqx}$$
$$+ b_p b_q^\dagger e^{-ipx}e^{iqx}\Big) \tag{5.17}$$

But p_0, q_0 are just $p_0 = \omega_p$ and $q_0 = \omega_q$; therefore:

$$= \int\int \frac{d^3p}{(2\pi)^3}\frac{d^3q}{(2\pi)^3}\frac{\omega_p\omega_q}{\sqrt{4\omega_p\omega_q}}(a_p^\dagger a_q e^{i(p-q)\cdot x} - a_p^\dagger b_q^\dagger e^{i(p+q)\cdot x} - b_p a_q e^{-i(p+q)\cdot x} + b_p b_q^\dagger e^{i(q-p)\cdot x}) \tag{5.18}$$

it can be already replaced in the energy integral, giving it space to the second quantization trick in order to solve it:

$$E_{\partial_0\phi\partial^0\phi} = \int\int \frac{d^3p}{(2\pi)^3}\frac{d^3q}{(2\pi)^3}\frac{\omega_p\omega_q}{\sqrt{4\omega_p\omega_q}}\int d^3x(a_p^\dagger a_q e^{i(p-q)\cdot x} - a_p^\dagger b_q^\dagger e^{i(p+q)\cdot x} - b_p a_q e^{-i(p+q)\cdot x} + \\ + b_p b_q^\dagger e^{i(q-p)\cdot x}) \tag{5.19}$$

Now we aim to reproduce the second energy term. It is associated to $\vec{\nabla}\phi^*\cdot\vec{\nabla}\phi$. First, compute $\vec{\nabla}\phi^*$:

$$\vec{\nabla}\phi^\star(x) = \partial_\mu\int\frac{d^3p}{(2\pi)^3}\frac{1}{\sqrt{2\omega_p}}\left(a_p^\dagger e^{ip_\mu x^\mu} + b_p e^{-ip_\mu x^\mu}\right),$$
$$\vec{\nabla}\phi^\star(x) = \int\frac{d^3p}{(2\pi)^3}\frac{ip_\mu}{\sqrt{2\omega_p}}\left(a_p^\dagger e^{ip_\mu x^\mu} - b_p e^{-ip_\mu x^\mu}\right). \tag{5.20}$$

Now, proceeding with $\vec{\nabla}\phi$:

$$\vec{\nabla}\phi(x) = \partial_\mu\int\frac{d^3p}{(2\pi)^3}\frac{1}{\sqrt{2\omega_p}}\left(a_p e^{-ip_\mu x^\mu} + b_p^\dagger e^{ip_\mu x^\mu}\right),$$
$$\vec{\nabla}\phi(x) = \int\frac{d^3p}{(2\pi)^3}\frac{-ip_\mu}{\sqrt{2\omega_p}}\left(a_p e^{-ip_\mu x^\mu} - b_p^\dagger e^{ip_\mu x^\mu}\right). \tag{5.21}$$

Finally multiplying both terms:

$$\vec{\nabla}\phi^\star\vec{\nabla}\phi = \int\int\frac{d^3p}{(2\pi)^3}\frac{d^3q}{(2\pi)^3}\frac{ip_\mu}{\sqrt{2\omega_p}}\frac{-iq_\nu}{\sqrt{2\omega_q}}(a_p^\dagger e^{ip_\mu x^\mu} - b_p e^{-ip_\mu x^\mu})\left(a_p e^{-ip_\nu x^\nu} - b_p^\dagger e^{ip_\nu x^\nu}\right), \tag{5.22}$$

$$\vec{\nabla}\phi^\star\vec{\nabla}\phi = \int\int\frac{d^3p}{(2\pi)^3}\frac{d^3q}{(2\pi)^3}\frac{p_\mu q_\nu}{\sqrt{4\omega_p\omega_q}}(a_p^\dagger a_q e^{i(p-q)\cdot x} - a_p^\dagger b_q^\dagger e^{i(p+q)\cdot x} - b_p a_q e^{-i(p+q)\cdot x} + \\ + b_p b_q^\dagger e^{i(q-p)\cdot x}). \tag{5.23}$$

and the corresponding energy integral:

$$E_{\vec{\nabla}\phi^\star\vec{\nabla}\phi} = \int\int\frac{d^3p}{(2\pi)^3}\frac{d^3q}{(2\pi)^3}\frac{p_\mu q_\nu}{\sqrt{4\omega_p\omega_q}}\int d^3x(a_p^\dagger a_q e^{i(p-q)\cdot x} - a_p^\dagger b_q^\dagger e^{i(p+q)\cdot x} - b_p a_q e^{-i(p+q)\cdot x}$$

$$+ b_p b_q^\dagger e^{i(q-p)\cdot x}), \tag{5.24}$$

$$E_{\vec{\nabla}\phi^\star\vec{\nabla}\phi} = \int\int \frac{d^3p}{(2\pi)^3}\frac{d^3q}{(2\pi)^3}\frac{p_\mu q_\nu}{\sqrt{4\omega_p\omega_q}}(a_p^\dagger a_q\delta_{(p-q)}(2\pi)^3 - a_p^\dagger b_q^\dagger\delta_{(p+q)}(2\pi)^3 - b_p a_q\delta_{(p+q)}(2\pi)^3 + b_p b_q^\dagger\delta_{(q-p)}(2\pi)^3). \tag{5.25}$$

Ultimately, the term $m^2\phi^*\phi$ is needed:

$$\begin{aligned} m^2\phi^*\phi = m^2\phi^\star\phi &= \int \frac{d^3p}{(2\pi)^3}\frac{1}{\sqrt{2\omega_p}}\left(a_p^\dagger e^{ipx} + b_p e^{-ipx}\right)\int \frac{d^3q}{(2\pi)^3}\frac{1}{\sqrt{2\omega_q}}\left(a_q e^{-iqx} + b_q^\dagger e^{iqx}+\right), \\ &= m^2\int\int \frac{d^3pd^3q}{(2\pi)^3(2\pi)^3\sqrt{4\omega_p\omega_q}}(a_p^\dagger a_q e^{i(p-q)x} + a_p^\dagger b_q e^{i(p+q)x}+ \\ &\quad + b_p a_q e^{-i(p+q)x} + b_p b_q^\dagger e^{-i(p-q)x}). \end{aligned} \tag{5.26}$$

And the energy integral is:

$$E_{m^2\phi^*\phi} = m^2\int\int \frac{d^3pd^3q}{(2\pi)^3(2\pi)^3\sqrt{4\omega_p\omega_q}}\int d^3x(a_p^\dagger a_q e^{i(p-q)x} + a_p^\dagger b_q e^{i(p+q)x}+ + b_p a_q e^{-i(p+q)x} + b_p b_q^\dagger e^{-i(p-q)x}), \tag{5.27}$$

Appendix 3

The full solutions resulting from the minimization of potential $V_{NORM,\xi_1=0}$ are:

$$V_{\mathrm{NORM},\xi_1=0}\left(-\frac{1}{2}\sqrt{2-\sqrt{2-\frac{2|-2+\chi_{12}|}{\sqrt{\xi_2^2+(-2+\chi_{12})^2}}}},1\right)$$
$$\text{if } -1 \leq -\frac{1}{2}\Re\left[\sqrt{2-\sqrt{2-\frac{2|-2+\chi_{12}|}{\sqrt{\xi_2^2+(-2+\chi_{12})^2}}}}\right] \leq 1,$$
$$\text{and } \frac{1}{4}\left(2-\Re\left[\sqrt{2-\frac{2|-2+\chi_{12}|}{\sqrt{\xi_2^2+(-2+\chi_{12})^2}}}\right]\right) \geq 0, \tag{5.28}$$
$$\infty \quad \text{otherwise}$$

$$V_{\mathrm{NORM},\xi_1=0}\left(\frac{1}{2}\sqrt{2-\sqrt{2-\frac{2|-2+\chi_{12}|}{\sqrt{\xi_2^2+(-2+\chi_{12})^2}}}},1\right)$$
$$\text{if } -1 \leq \frac{1}{2}\Re\left[\sqrt{2-\sqrt{2-\frac{2|-2+\chi_{12}|}{\sqrt{\xi_2^2+(-2+\chi_{12})^2}}}}\right] \leq 1,$$
$$\text{and } \frac{1}{4}\left(2-\Re\left[\sqrt{2-\frac{2|-2+\chi_{12}|}{\sqrt{\xi_2^2+(-2+\chi_{12})^2}}}\right]\right) \geq 0, \tag{5.29}$$
$$\infty \quad \text{otherwise}$$

$$V_{\mathrm{NORM},\xi_1=0}\left(-\frac{1}{2}\sqrt{2+\sqrt{2-\frac{2|-2+\chi_{12}|}{\sqrt{\xi_2^2+(-2+\chi_{12})^2}}}},1\right)$$
$$\text{if } -1 \leq -\frac{1}{2}\Re\left[\sqrt{2+\sqrt{2-\frac{2|-2+\chi_{12}|}{\sqrt{\xi_2^2+(-2+\chi_{12})^2}}}}\right] \leq 1,$$
$$\text{and } \frac{1}{4}\left(2+\Re\left[\sqrt{2-\frac{2|-2+\chi_{12}|}{\sqrt{\xi_2^2+(-2+\chi_{12})^2}}}\right]\right) \geq 0, \tag{5.30}$$
$$\infty \quad \text{otherwise}$$

$$V_{\mathrm{NORM},\xi_1=0}\left(\frac{1}{2}\sqrt{2+\sqrt{2-\frac{2|-2+\chi_{12}|}{\sqrt{\xi_2^2+(-2+\chi_{12})^2}}}},1\right)$$
$$\text{if } -1 \leq \frac{1}{2}\Re\left[\sqrt{2+\sqrt{2-\frac{2|-2+\chi_{12}|}{\sqrt{\xi_2^2+(-2+\chi_{12})^2}}}}\right] \leq 1,$$
$$\text{and } \frac{1}{4}\left(2+\Re\left[\sqrt{2-\frac{2|-2+\chi_{12}|}{\sqrt{\xi_2^2+(-2+\chi_{12})^2}}}\right]\right) \geq 0, \tag{5.31}$$
$$\infty \quad \text{otherwise}$$

$$\chi_{12}/2, \quad 1 \tag{5.32}$$